NASA TECHNICAL NOTE

NASA TN D-2887

NASA TN D-2887

EXPERIMENTAL STUDY OF WIND-TUNNEL WALL EFFECTS AND WALL CORRECTIONS FOR A GENERAL-RESEARCH V/STOL TILT-WING MODEL WITH FLAP

by Kalman J. Grunwald

Langley Research Center

Langley Station, Hampton, Va.

NATIONAL AERONAUTICS AND SPACE ADMINISTRATION • WASHINGTON, D. C. • JULY 1965

NASA TN D-2887

EXPERIMENTAL STUDY OF WIND-TUNNEL WALL EFFECTS AND WALL CORRECTIONS FOR A GENERAL-RESEARCH V/STOL TILT-WING MODEL WITH FLAP

By Kalman J. Grunwald

Langley Research Center
Langley Station, Hampton, Va.

NATIONAL AERONAUTICS AND SPACE ADMINISTRATION

For sale by the Clearinghouse for Federal Scientific and Technical Information
Springfield, Virginia 22151 – Price $4.00

CONTENTS

EXPERIMENTAL STUDY OF WIND-TUNNEL WALL EFFECTS AND WALL CORRECTIONS FOR A GENERAL-RESEARCH V/STOL TILT-WING MODEL WITH FLAP

By Kalman J. Grunwald
Langley Research Center

SUMMARY

The wall-effects investigation conducted in the Langley 300-MPH 7- by 10-foot tunnel, the 17-foot test section in this 7- by 10-foot tunnel, and the Langley full-scale tunnel (30- by 60-foot tunnel) on a tilt-wing configuration (with neither fuselage nor tail) showed small wall effects on the force data. The application of a wall correction theory (which accounts for wake deflection) to the force data from the 7- by 10-foot tunnel resulted in large corrections to angle of attack and dynamic pressure. However, when these corrections were applied to the data obtained with this particular model, they compensated one another in such a manner that the resulting data varied only slightly from the original test data.

This compensating effect appears to be unique for the configuration used in this investigation. In prior work on other models (buried-fan configurations) large noncompensating wall effects were evident in the basic data.

Wall effects on pitching moment (flaps on) were large, particularly for data taken in the 7- by 10-foot tunnel. The wall correction theory corrected the pitching-moment data for wall effects on this tailless configuration.

For tail-on configurations (such as fan-in-wing configurations) the theory did not adequately correct for the wall effects on pitching moment. This inadequacy is believed to be due to the linear wake assumed in the theory. This assumption of linear wake is not critical in determining the wall-induced upwash at the primary lifting element; however, the interference velocities in the region of the tail would differ substantially for assumptions of curved and straight-line wakes.

INTRODUCTION

The development of V/STOL aircraft has reached the stage where operational rather than test-bed-type aircraft are being designed and developed; however, the intelligent design of an operational aircraft requires an adequate

understanding of such limitations on wind-tunnel data as are imposed by wall effects and scale effects.

Wind-tunnel tests of V/STOL configurations in the speed range involved in transitions from hovering to normal flight require that models be tested under conditions where the downward deflected wake from the lifting element leaves the model at large angles (up to 90°) with respect to the free-stream direction. The velocity in this wake is typically much greater than the free-stream velocity. This high-speed wake at large angles to the flow influences and distorts the flow field at large distances from the model. However, at the tunnel walls the flow is constrained to be parallel to the walls, a condition which forces an artificial restriction on the flow field and thus affects the measured characteristics of the model.

A wind-tunnel wall correction theory (ref. 1) has been developed to approximate the highly deflected wake condition and is discussed briefly in appendix A. This theory is an extension of the classical wind-tunnel theory (ref. 2) in that it assumes a linear wake deflection from the model with no decay of wake velocity with distance from the model.

The purpose of the present investigation is twofold: first, to determine the magnitude of the wind-tunnel wall effects on configurations of the deflected-slipstream and tilt-wing type, where the wing is the primary lifting element through transition and, second, to determine the validity of applying the theory of reference 1 to correct data for wind-tunnel wall effects.

In order to investigate the magnitude of wall effects the same general-research wing model was tested in three wind-tunnel test facilities of different size: the Langley 300-MPH 7- by 10-foot tunnel, the 17-foot test section in this 7- by 10-foot tunnel, and the Langley full-scale tunnel (referred to herein as the 30- by 60-foot tunnel). The data from the tests in the 7- by 10-foot tunnel and the 17-foot test section were corrected by the method of reference 1 and compared with the data from the 30- by 60-foot tunnel (which represents nearly free-air conditions) in order to determine the validity of the wall correction theory of reference 1.

Some of the results from the present investigation have already been presented in reference 3, along with information on wall effects for fan-in-wing and fan-in-fuselage configurations. The wall effects on the fan-in-fuselage configuration are discussed fully in reference 4.

SYMBOLS

The positive sense of forces, moments, and angles is shown in figure 1.

A_m momentum area of lifting system, taken herein as $\frac{\pi(\text{Wing span})^2}{4}$, square feet

A_T cross-sectional area of wind-tunnel test section, square feet

B semiwidth of wind-tunnel test section, feet

b lateral distance from center of model to right-hand sidewall of tunnel (viewed from rear), also blade chord, feet

C_L lift coefficient, $\frac{L}{qS}$

C_m pitching-moment coefficient, $\frac{M_Y}{qS\bar{c}}$

C_T free-stream thrust coefficient, $\frac{T}{qS}$

$C_{T,S}$ slipstream thrust coefficient, $\frac{T}{q_S S}$

C_X longitudinal force coefficient, $\frac{F_X}{qS}$

$\bar{c}$ chord of model, feet

D total drag, pounds

D_i induced drag (due to lift), pounds

d propeller diameter, feet

F_X longitudinal force, pounds

H semiheight of wind tunnel, feet

h' blade thickness, feet

L lift, pounds

M_Y pitching moment, foot-pounds

n ratio of final induced velocities in far wake to initial induced velocities at model ($n = 2$ for tilt-wing configuration)

q free-stream dynamic pressure, pounds per square foot

q_S slipstream dynamic pressure, $q + \frac{T}{\frac{2\pi d^2}{4}}$, pounds per square foot

r/R	ratio of blade span station to total span
N_{Re}	Reynolds number of wing, based on slipstream velocity
S	wing area, square foot
T	propeller total thrust, pounds
Δu	total longitudinal interference velocity, positive rearward, feet per second
Δu_D	longitudinal interference velocity due to induced drag, positive rearward, feet per second
Δu_L	longitudinal interference velocity due to lift, positive rearward, feet per second
V	free-stream velocity, feet per second
Δw	total vertical interference velocity, positive upward, feet per second
Δw_D	vertical interference velocity due to induced drag, positive upward, feet per second
w_h	reference velocity, positive upward, $-\sqrt{\frac{L}{n\rho A_m}}$, feet per second
Δw_L	vertical interference velocity due to lift, positive upward, feet per second
w_o	mean or momentum-theory value of vertical induced velocity, positive upward, feet per second (ref. 1)
x,y,z	location of a point with respect to X, Y, and Z axes, respectively (x measured positive rearward, y measured positive to the right when viewed from rear, and z measured positive upward), feet (ref. 1)
x',y',z'	location of a point with respect to X', Y', and Z' axes, respectively (x' measured positive rearward, y' measured positive to the right when viewed from rear, and z' measured positive upward), feet (ref. 1)
X,Y,Z	Cartesian axes with origin at center of model
X',Y',Z'	Cartesian axes centered at center of wind tunnel
α	angle of attack, degrees

$\Delta\alpha$	correction to angle of attack for jet interference, degrees
δ_f	flap deflection, degrees
γ	ratio of wind-tunnel width to wind-tunnel height, $\frac{B}{H}$
δ	jet-boundary correction, or interference, factor (general)
$\delta_{u,D}$	interference factor for longitudinal interference velocity due to drag
$\delta_{u,L}$	interference factor for longitudinal interference velocity due to lift
$\delta_{w,D}$	interference factor for vertical interference velocity due to drag
$\delta_{w,L}$	interference factor for vertical interference velocity due to lift
ζ	ratio of wind-tunnel semiheight to height of model above tunnel floor
η	ratio of lateral distance between model center and right-hand side of wall (viewed from rear) to semiwidth of wind tunnel, $\frac{b}{B}$
ρ	mass density of air, slugs per cubic foot
σ	ratio of rotor diameter or total wing span to total wind-tunnel width
χ	wake skew angle, angle between Z-axis (negative direction) and wake center line, positive rearward, degrees

Subscripts:

c	corrected
un	uncorrected

MODEL AND APPARATUS

The tilt-wing model used for the wall-effects investigation is shown installed in the 17-foot test section (in the Langley 300-MPH 7- by 10-foot tunnel) in figure 2 and pertinent dimensions are presented in table I. A drawing of the model is presented in figure 3. The wing model had a 4.23-foot span, an 18-inch chord, and an NACA 0015 airfoil section. A flap having a 30-percent-chord full-span Clark Y airfoil section and set at 40° deflection (fig. 3) was used on the model during some of the tests. A $\frac{1}{8}$-inch transition

strip of No. 60 carborundum (0.012 mean grain diameter) was installed on the model at 8-percent chord as shown in figure 3. Each of the propellers, whose blade form curves are in figure 4, was 2 feet in diameter.

The model had no fuselage, but a 5-inch width at the center of the wing, from maximum thickness aft, was contoured to allow for the entrance of the sting and balance. The same support stings and readout equipment were used in each of the three test sections. The orientation of the model with respect to the tunnels is schematically represented in figure 5. The model was pitched in the yaw plane of the 17-foot test section and the Langley full-scale tunnel (referred to as the 30- by 60-foot tunnel) to allow a range of angles of attack to be recorded from 0° to 90° in one continuous run. However, because of the size of the 7- by 10-foot tunnel no complete angle-of-attack transition could be made without changing the sting configuration. Stings bent at angles of 40° to 70° were used in the 7- by 10-foot tunnel so that tests could be made at angles of attack as large as 90°. None of the changes in angle of attack resulted in any significant change in position of the model in the tunnel.

The model overall forces were measured on a six-component internal strain-gage balance. The pitching moments were transferred from the balance to the quarter-chord of the wing as indicated in figure 3. The model motors were also mounted on strain-gage beams to give readings of propeller thrust, normal force, torque, and pitching moment.

TESTS

When embarking on an investigation in an effort to determine the magnitude of wall effects where only small differences in the data may be found, a very systematic approach is necessary. Such an approach was attempted in this investigation. Power-on tests of the model were made for a range of angle of attack from 0° to 90° in 5° increments for nearly constant slipstream thrust coefficients of 0.50, 0.60, 0.72, 0.75, 0.80, 0.86, 0.90, 0.92, 0.93, 0.94, and 0.95 with the flaps on and off. The tests were conducted first in the 7- by 10-foot tunnel (in background in fig. 2). Then the model was moved directly to the 30- by 60-foot tunnel in which the tests were duplicated. Finally, the model was moved to the 17-foot test section of the 7- by 10-foot tunnel (fig. 2) where the tests were duplicated again.

The basic power-on tests were made with wing Reynolds numbers near 6.3×10^5, based on propeller slipstream velocity. Rotational speed of the propellers varied from 4500 rpm to nearly 6000 rpm in order to hold thrust constant.

EFFECT OF RATIO OF MODEL SIZE TO TUNNEL SIZE ON WALL EFFECTS

The parameter used to define model size for these tests is the model momentum area A_m. The model momentum area is the cross-sectional area of the wake leaving the lifting element of the model (ref. 1). For the tilt-wing and deflected-slipstream configuration, where the wing is the primary lifting element, A_m was assumed to be the area of the circle whose diameter is the span of the wing. At the very lowest speeds the propeller disk area would better represent the momentum area; however, computations indicated that for the range of speeds in this investigation, the momentum area based on the wing span would be the more desirable choice.

By testing the same tilt-wing wall-effects model in three test sections of different size the ratio of model size to tunnel size was varied in a systematic manner. The ratio of model momentum area to tunnel cross-sectional area $\frac{A_m}{A_T}$ was 0.18 for the model in the 7- by 10-foot tunnel, 0.047 for the model in the 17-foot test section, and 0.008 for the model in the 30- by 60-foot tunnel.

Because of the large ratio of tunnel size to model size, the 30- by 60-foot tunnel represents a facility nearly free of wall effects. The data from the tests in this tunnel were thus assumed to be completely free of wall effects. The 17-foot test section was chosen primarily because this facility is being used for VTOL and STOL testing and it was important that the wall effects be known. The 7- by 10-foot tunnel was chosen as the third test facility because it represented a condition where the ratio of model size to tunnel size (0.18) is so large that the data were expected to have very large wall effects.

RESULTS AND DISCUSSION

Experimental Wall Effects

Power-off data.- The power-off data, with propellers removed (flaps off and flaps on), from the tests in the three test facilities (7- by 10-foot tunnel, 17-foot test section, and 30- by 60-foot tunnel) at $N_{Re} = 6.3 \times 10^5$ are presented in figures 6 and 7. Agreement between the three sets of data was good, as would be expected (except for some excessive scatter in pitching moment in fig. 7). The theoretical power-off lift-curve slope as computed from reference 5 is 0.057 per degree and is in good agreement with the data in figure 6. The conventional wall correction theory (presented in ref. 6) applied to the lift-curve slope computes only a 3% correction to the data measured in the 7- by 10-foot test section.

The effects of Reynolds number on the characteristics of the wing are presented in figure 8 and the only significant effects occur at maximum lift coefficient as expected.

Power-on lift- and longitudinal-force data.- The basic uncorrected power-on lift-, longitudinal-force, and pitching-moment data from the tests in the three tunnels are presented for a number of nearly constant thrust coefficient in appendix B (figs. B1 and B2). These lift-, longitudinal-force, and pitching-moment coefficients were plotted as a function of thrust coefficient. From these plots, constant-thrust-coefficient cross plots of lift coefficient were made and are presented in figure 9 (flaps off) and figure 10 (flaps on), as a function of angle of attack and as lift—longitudinal-force polars at free-stream thrust coefficients of 4, 8, and 12 ($C_{T,S}$ = 0.80, 0.88, and 0.93, respectively).

The comparison of the lift and longitudinal force from the three tunnels, at constant thrust coefficient, indicated small wall effects.

Pitching-moment data.- The basic pitching-moment-coefficient data are presented in appendix B (fig. B1 for flaps off and fig. B2 for flaps on). The flaps-off pitching moments (fig. B1) were small in magnitude for each tunnel and indicated negligible differences when compared. However, there were large differences between the flaps-on pitching-moment data (fig. B2) from the three tunnels, an indication of the large effect of the tunnel walls. A more detailed discussion of the pitching-moment data and the implications of the large wall effects are included in the next section.

Procedure Used for Application of Wall Corrections

Reference 1 presents a linearized wind-tunnel wall correction theory to correct wind-tunnel data from VTOL-STOL configuration for wall effects. In this theoretical approach the wake of any generalized lifting system is considered to be represented by a semi-infinite string of point doublets whose axes are tilted at an angle related to the lift and drag of the model. This inclined wake gives rise to both longitudinal and vertical-jet boundary interference factors. The interference factors δ applicable to the present test in the three tunnels are presented in figure 11 and are taken from references 7, 8, 9, and 10.

The theory of reference 1 is strictly applicable only to vanishingly small models because it assumes that the lifting element can be represented by a point doublet. It is proposed in reference 1, however, that for those cases where the wing span is appreciable with respect to the tunnel width the wing can be represented by a number of lifting elements as shown schematically in figure 12, where three lifting elements have been chosen. In this three-point method the mutual interference effects of each element on the others were calculated as suggested by reference 1 for the 7- by 10-foot tunnel. The calculated correction factors are shown in figure 11. These factors have been applied to the data and the results are compared with similar results for the one-point method in figure 13. As can be seen, the difference between the data computed by the two methods is so small as to be considered negligible. The rest of the data in this paper was corrected by using the one-point method.

The method by which the correction factors were computed and applied to the data is presented in appendix A as well as in reference 1. Some suggestions

for shortening data-reduction-machine time when applying the corrections are also presented in appendix A.

Because of the large angle (skew angle χ in ref. 1) at which the wake leaves the lifting element, the tunnel walls cause longitudinal as well as vertical induced velocities at the model location. Thus both the angle of attack and the tunnel velocity (or dynamic pressure) must be corrected for wall effects.

Some typical angle-of-attack corrections $\Delta\alpha$ and dynamic-pressure corrections q_c/q as well as the skew angle χ associated with these corrections are presented in figure 14, for data from all three tunnels at free-stream thrust coefficients of approximately 13.5 and 6.0. As indicated in figure 14, the corrections for data from the 30- by 60-foot tunnel are essentially zero. This was true for all data from that tunnel; therefore, no tunnel wall corrections were applied to any data from the 30- by 60-foot tunnel and these data were considered to be a wall-interference-free base for comparisons with data from the 17-foot test section and the 7- by 10-foot tunnel.

Comparisons of Corrected Force Data

Data from 7- by 10-foot and 30- by 60-foot tunnels.- The data in figures 13 and 14 can be used to illustrate the method by which basic data are corrected and also the implications of the corrections.

Large changes in the lift-, the longitudinal-force, the pitching-moment, and the thrust coefficients occur when the $\Delta\alpha$ and q_c/q corrections (presented in fig. 14) for the 7- by 10-foot tunnel data are applied to the basic data in figure 13. The first impression imparted by these large changes in the data is that the corrections of reference 1 are obviously too large since it has already been shown that the wall effects for this tilt-wing model are small. However, this impression is erroneous because, although there are large changes in the forces and moments, there is also a large change in the thrust coefficient. In order to compare the net effect of the wall corrections the data must be compared at a constant corrected thrust coefficient. Therefore, the corrected data from the 7- by 10-foot test section were plotted as a function of thrust coefficient (figs. 15 and 16) and cross plots were made at constant thrust coefficient (figs. 17 and 18). The resulting comparisons with the data from the 30- by 60-foot tunnel showed only a small net wall effect. If large changes in the corrected thrust coefficients are expected at the beginning of the tests enough thrust-coefficient conditions should be chosen so that a cross plot similar to the one previously mentioned can be developed.

Although the net effect of applying corrections to the data taken in the 7- by 10-foot tunnel (figs. 17 and 18) indicated little change from the uncorrected curve to the corrected curve the corrections to angle of attack and dynamic pressure were very large (fig. 14). If only the angle-of-attack corrections had been applied to the data and the dynamic-pressure correction had not been applied, large differences would have existed between the corrected and uncorrected data. In order to illustrate this point the uncorrected data (7- by 10-foot tunnel) from figure 18 (flaps on) have been corrected in steps (fig. 19) to show the effect of applying only the angle-of-attack correction

and then applying the dynamic-pressure correction. It can be seen from the data in figure 19 that step changes of 10 to 15 percent occur in the lift coefficient when the corrections are applied separately.

The significant conclusion for the lift- and longitudinal-force-coefficient data is that the large α corrections computed by the method of reference 1 for this model compensate for the large q corrections and the overall net result is not significantly different from the original data. This compensating feature of the corrections appears to be peculiar to this configuration, as evidenced in figure 20 (taken from fig. 18(c) of ref. 4) where the lift corrections did not compensate one another for the buried-fan configurations.

Data from 17-foot test section and 30- by 60-foot tunnel.- A data comparison similar to that made for tests made in the 7- by 10-foot and 30- by 60-foot tunnels has also been made for tests made in the 17-foot test section and the 30- by 60-foot tunnel. A similar cross-plot procedure was used in reducing and correcting the data from tests in the 17-foot test section. The flaps-on data for a constant thrust coefficient are compared for the 17-foot test section and the 30- by 60-foot tunnel in figure 21. This comparison indicates higher lift coefficients in the 17-foot test section than in the 30- by 60-foot tunnel both before and after corrections.

This result may be due to the unusual shape of the test section. The wall correction theory is based on an infinite-length test section with the wake from the model flowing along the floor in a straight line to infinity. This assumption is not badly violated for most wind tunnels, such as the 7- by 10-foot and 30- by 60-foot tunnels; however, the 17-foot test section has a severely convergent section immediately behind the short 15-foot-long test section. This convergent section would cause a large change in the path of the real wake. Under these circumstances the assumptions about wake locations are severely violated. Thus, the theory of reference 1 would not be applicable for wind-tunnel test sections of this design.

From a practical consideration it can be seen that data from the 17-foot test section are in good enough agreement with correction-free data from the 30- by 60-foot tunnel to be considered usable.

Results of Wall Corrections Applied to Pitching Moment

The preceding discussion has generally been limited to the effects of wall corrections on lift and longitudinal force. It has been shown that by applying these large corrections to the force data from this particular model the net change in the data is small. Since the experimental wall effects were small to begin with, the corrected data are in good agreement with correction-free data. However, for the flaps-on pitching-moment data, large wall effects were encountered. By applying the theory of reference 1 to the data from the 7- by 10-foot and 30- by 60-foot tunnels, these wall effects were predicted and corrections made.

Typical constant-thrust-coefficient cross plots of the pitching-moment coefficient against angle of attack are presented in figure 22 (flaps off) and

figure 23 (flaps on). The lower part of each of these figures shows a comparison of the basic uncorrected data for the tests in the three test facilities and the upper part shows the corrected data.

The pitching-moment coefficients (flaps off) shown in figure 22 were very small and wall effects were not evident. With wall corrections applied to these data good agreement still remained. Large wall effects are, however, evident in the flaps-on data in figure 23 (particularly at thrust coefficients of 8 and 14); these wall effects are typical of all flaps-on data for the higher thrust coefficients.

For tail-on configurations (such as fan in wing, ref. 3) the theory did not adequately correct for the wall effects on pitching moment. This inadequacy is believed to be due to the linear-wake simplification in the theory as discussed in reference 3. This assumption of a linear wake is not critical in determining the wall-induced upwash at the primary lifting element; however, the interference velocities in the region of the tail would differ substantially for assumptions of curved and straight-line wakes.

Limitations of Theory of Reference 1

Although the general agreement between the corrected data for flaps on from the 7- by 10-foot tunnel and the free-air data (30- by 60-foot tunnel) was good, the corrected data indicated noticeably higher longitudinal-force coefficients at the highest angles of attack (lift—longitudinal-force polars of fig. 18). This is more clearly shown in figure 24(a) where longitudinal-force coefficient is plotted against angle of attack and the approximate angle of attack at which excessive overcorrection is considered to occur is indicated.

The angle-of-attack and dynamic-pressure corrections corresponding to the data of figure 24 are shown in figure 25. The angle-of-attack correction increases continuously with angle of attack whereas the dynamic-pressure correction q_c/q reaches a maximum at about the same angle of attack at which the corrected and free-air longitudinal-force-coefficient curves diverge significantly. The angle-of-attack correction and dynamic-pressure correction at which the correction theory appears to break down are presented in figure 26 along with the skew angle χ at which these occur. It should be noted that these boundaries apply strictly to this configuration and may be somewhat different for other configurations.

The flaps-off data of figure 24(b) do not indicate any theory overestimation; however, from the flaps-off data of figure 25 it can be seen that the point of maximum deviation for the dynamic-pressure correction was not reached.

The apparent theory breakdown may have come from the nature of the theory, that is, the assumption of a linear wake with no jet mixing. A curved-wake theory, with some air mixing of the slipstream and free stream assumed, has been attempted in reference 11. It is also possible that some of the simplifying assumptions used in applying the theory, such as using measured drag for

induced drag and assuming model momentum area to be the circle whose diameter is the wing span, may have caused some of the indicated differences.

CONCLUDING REMARKS

The wall-effects investigation conducted in the Langley 300-MPH 7- by 10-foot tunnel, the 17-foot test section in this 7- by 10-foot tunnel, and the Langley full-scale tunnel (30- by 60-foot tunnel) on a tilt-wing configuration (with neither fuselage nor tail) showed small wall effects on the force data. The application of a wall correction theory (which accounts for wake deflection) to the force data from the 7- by 10-foot tunnel and the 17-foot test section resulted in large corrections to angle of attack and dynamic pressure. However, when these corrections were applied to the data obtained with this particular model, they compensated one another in such a manner that the resulting data varied only slightly from the original test data. This compensating effect appears to be unique for the configuration used in this investigation. In prior work on other models (buried-fan configurations) large noncompensating wall effects were evident in the basic data.

Wall effects on pitching moment with the flaps on were large, particularly for data taken in the 7- by 10-foot tunnel. The wall correction theory corrected the pitching-moment data for wall effects on this tailless configuration.

For tail-on configurations (such as fan-in-wing configurations) the theory did not adequately correct the wall effects on pitching moment. This inadequacy is believed to be due to the linear wake assumed in the theory. This assumption of a linear wake is not critical in determining the wall-induced upwash at the primary lifting element; however, the interference velocities in the region of the tail would differ substantially for assumptions of curved and straight-line wakes.

Langley Research Center,
National Aeronautics and Space Administration,
Langley Station, Hampton, Va., March 9, 1965.

TABLE I

MODEL DIMENSIONS

Wing:	
Airfoil section	NACA 0015
Area, ft	6.34
Chord, ft	1.50
Span, ft	4.23
Propeller:	
Diameter, ft	2.00
Total disk area, sq ft	6.28
Flap:	
Airfoil section	Clark Y
Total area, sq ft	1.69
Chord, ft	0.45
Total span (center cutout excluded), ft	3.75

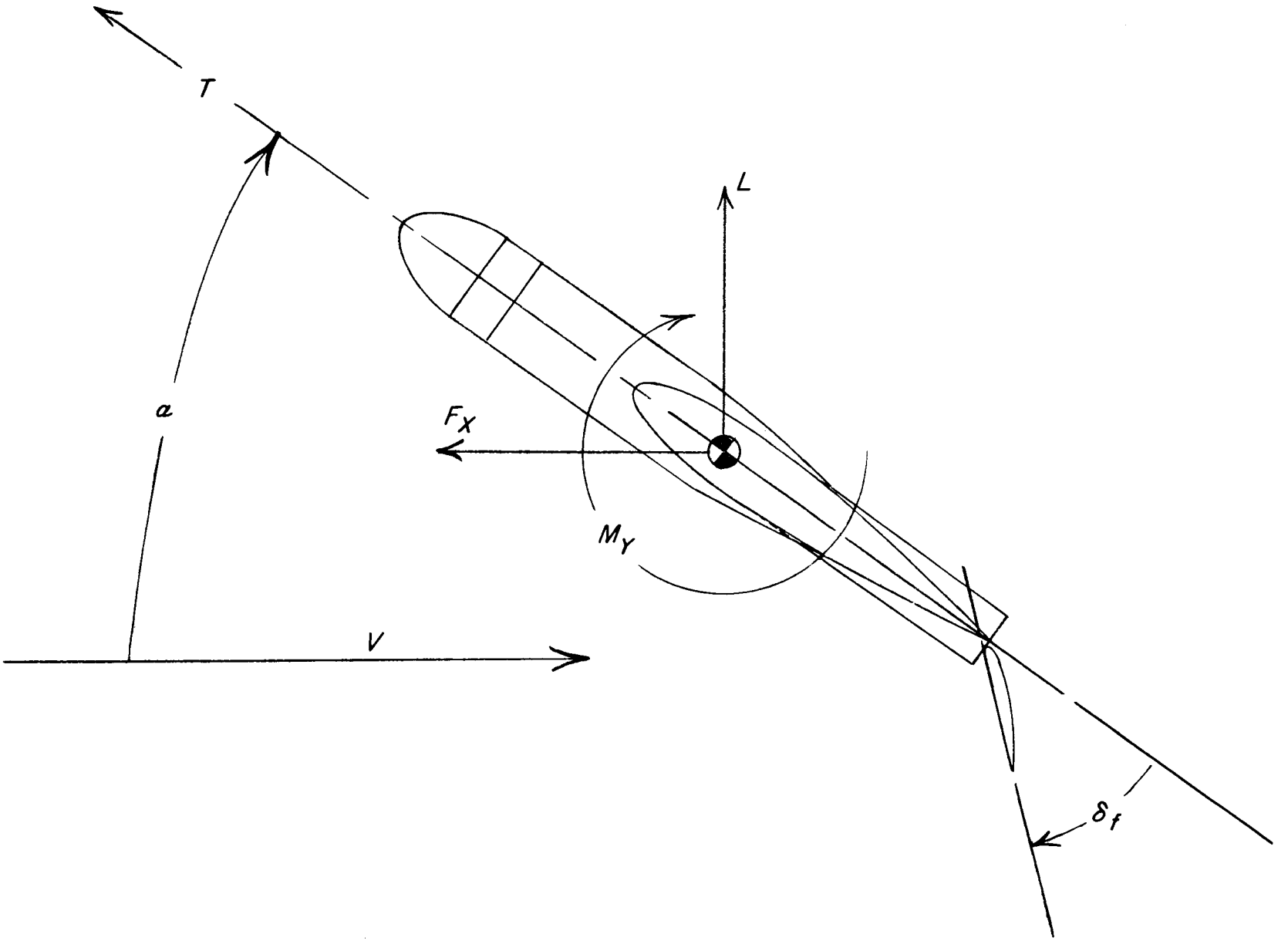

Figure 1.- Conventions used to define positive sense of forces, moments, and angles.

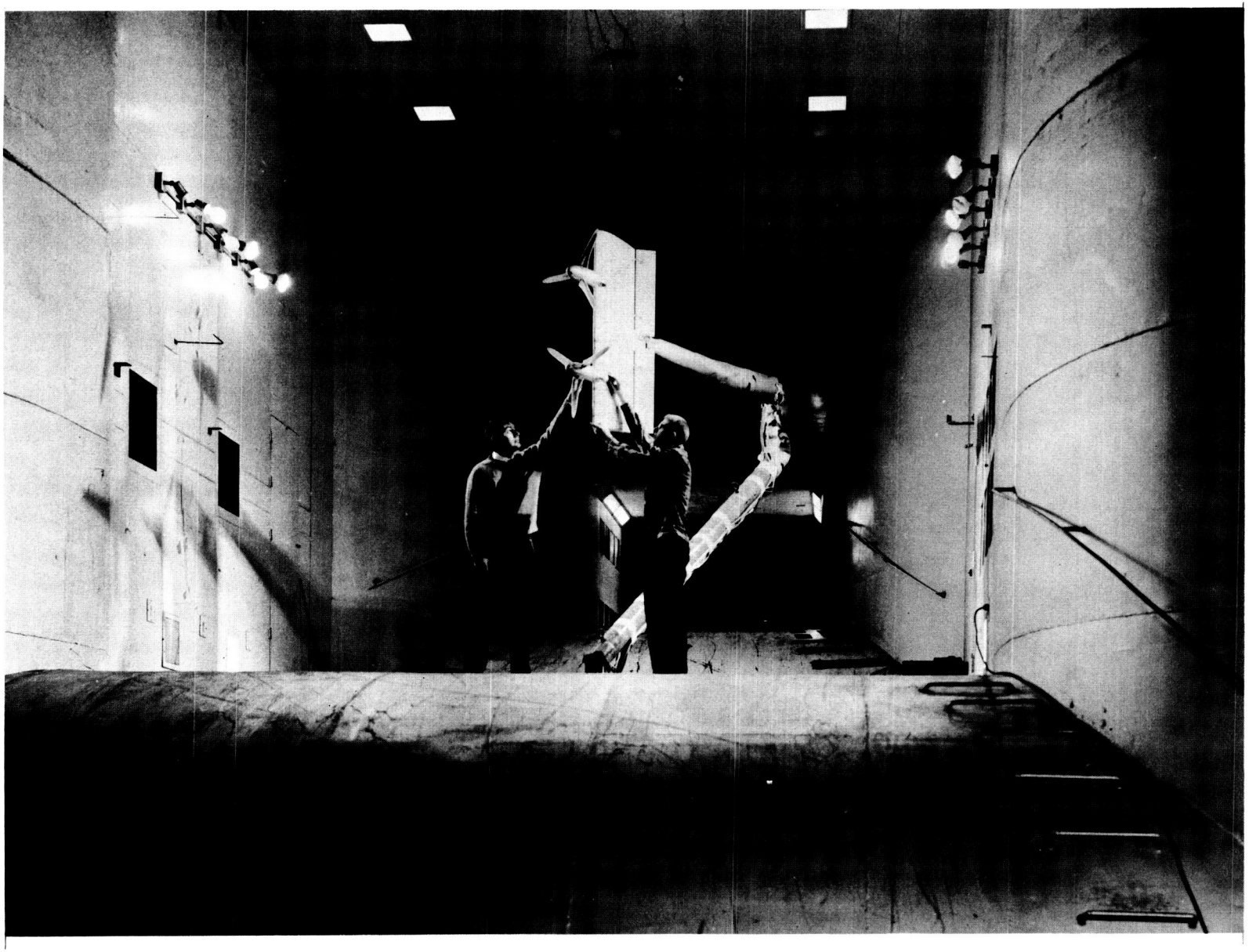

L-62-9430

Figure 2.- Photograph of model installation in 17-foot test section of Langley 300-MPH 7- by 10-foot tunnel.

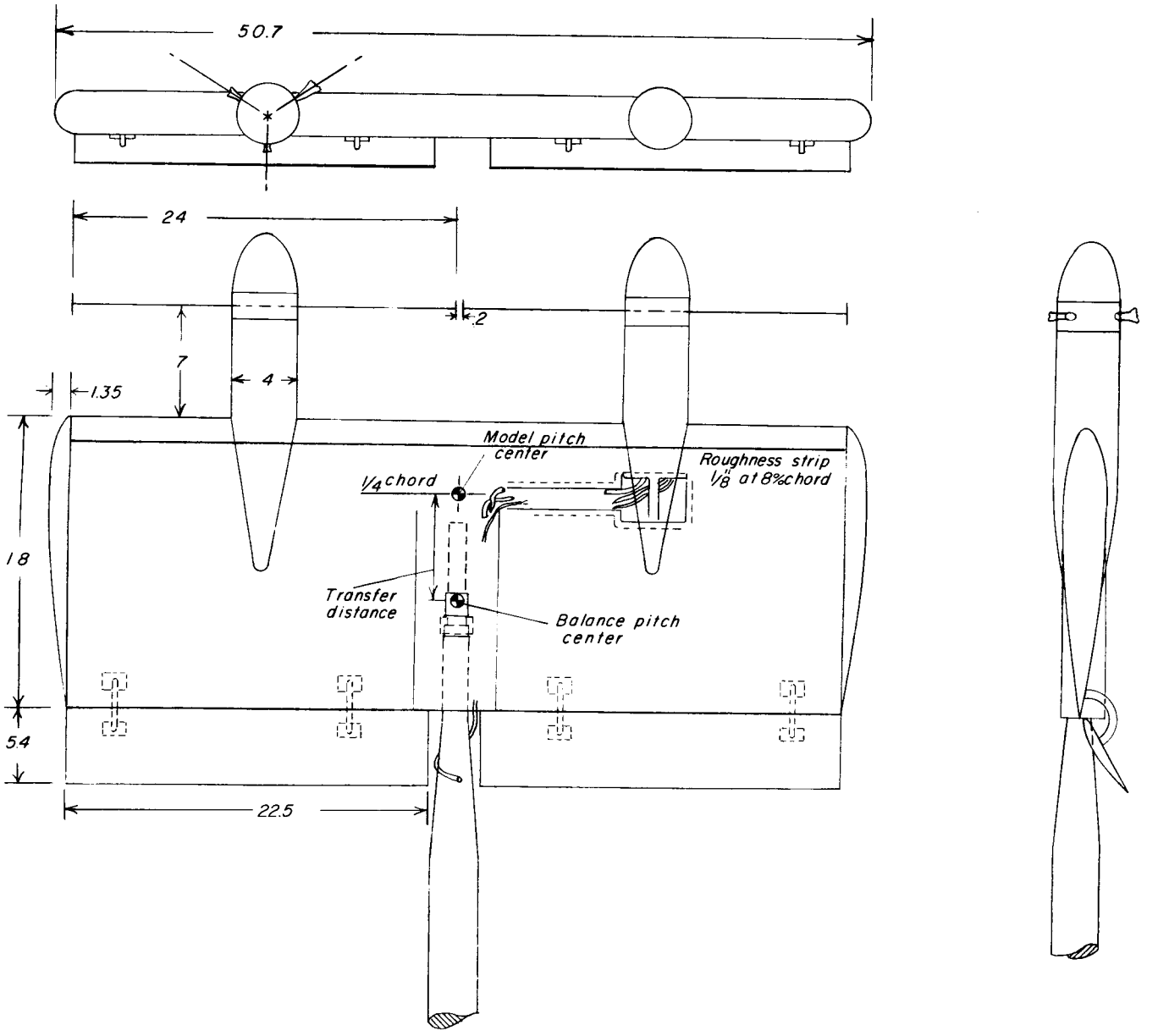

Figure 3.- Wall-effects model with flap. All dimensions are in inches.

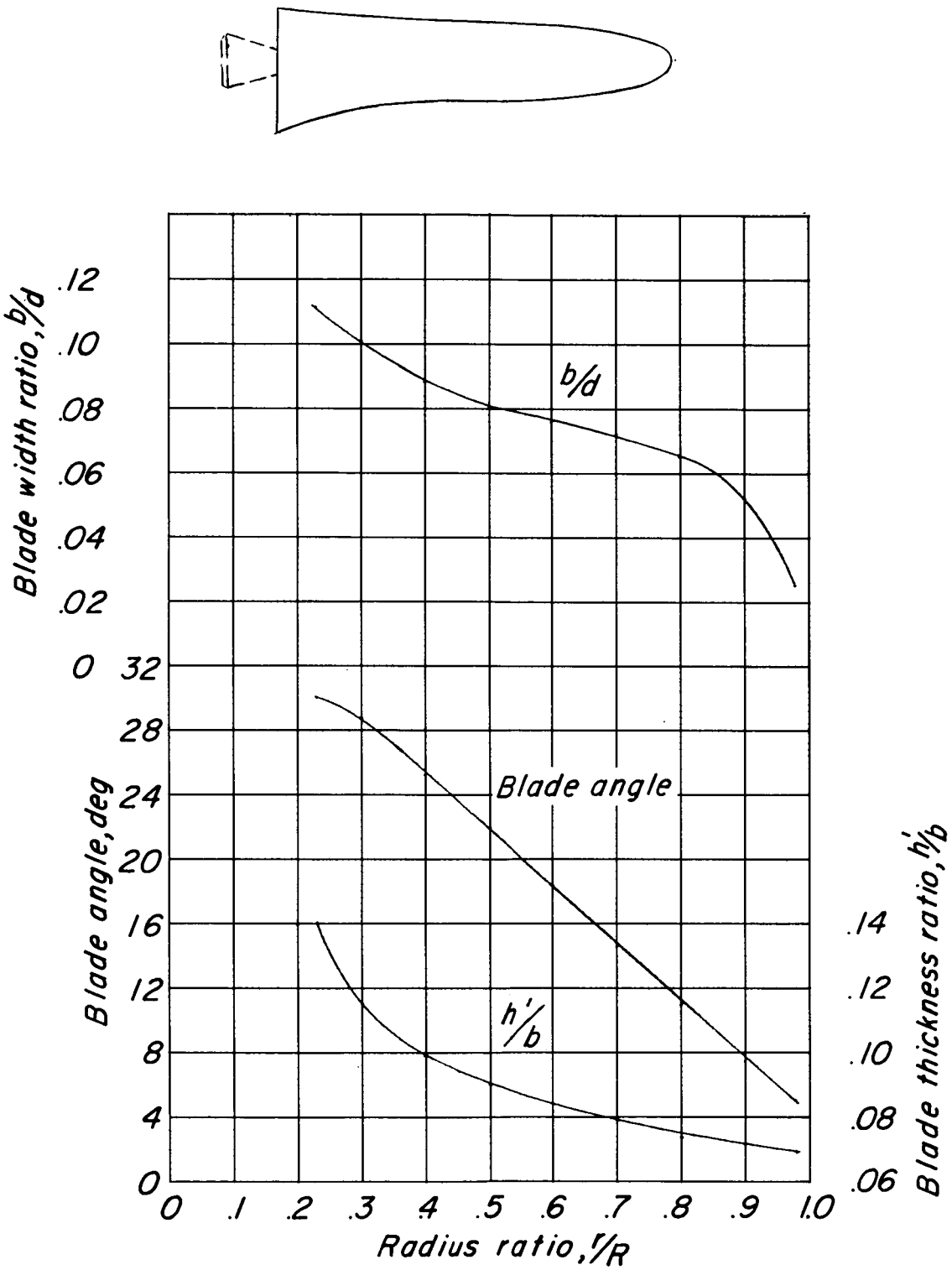

Figure 4.- Propeller blade form curves.

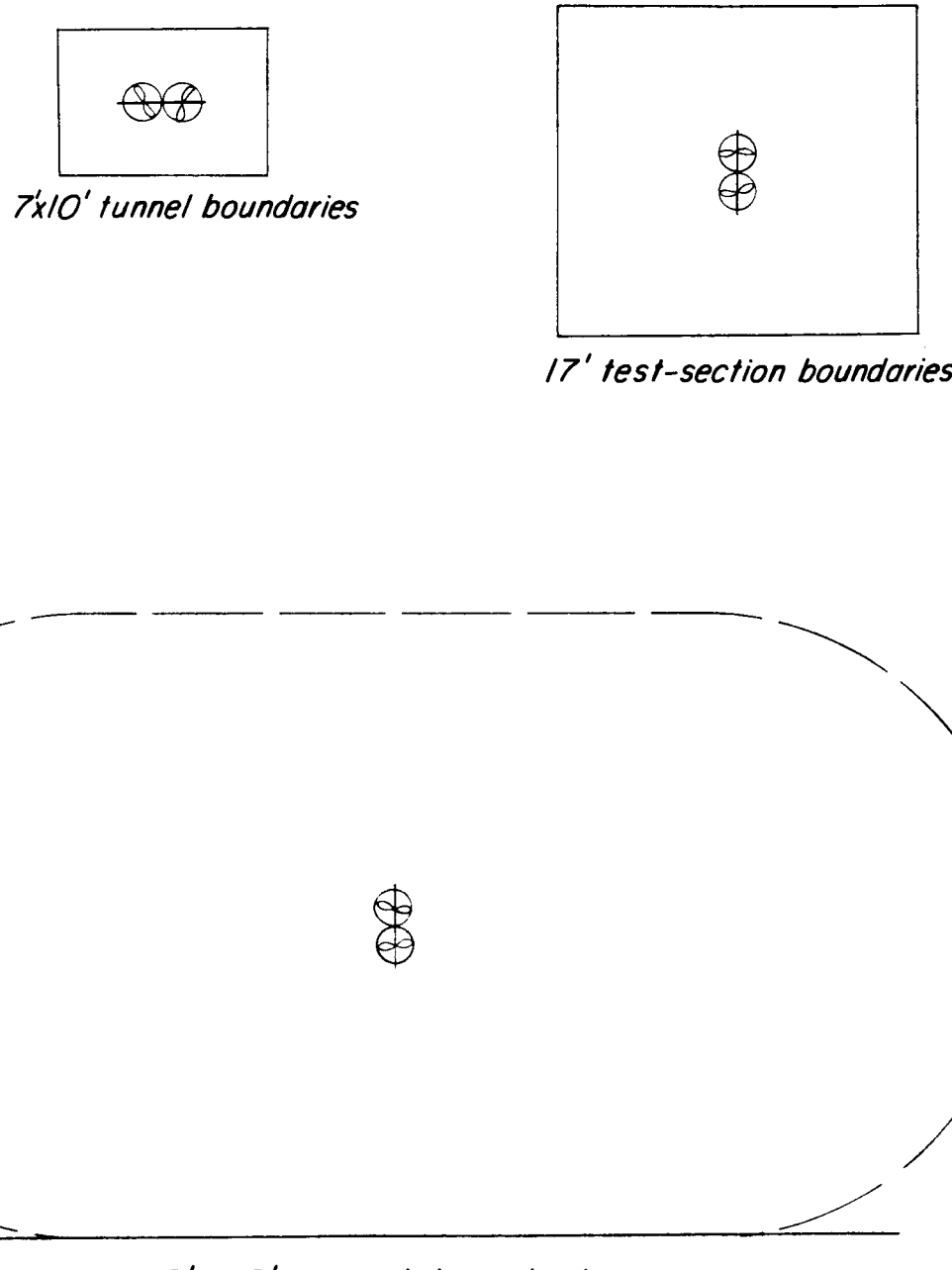

Figure 5.- Drawing indicating relative size and position of wall-effects model in Langley 7- by 10-foot 300-MPH tunnel, 17-foot test section of this 7- by 10-foot tunnel, and Langley full-scale tunnel (30- by 60-foot tunnel).

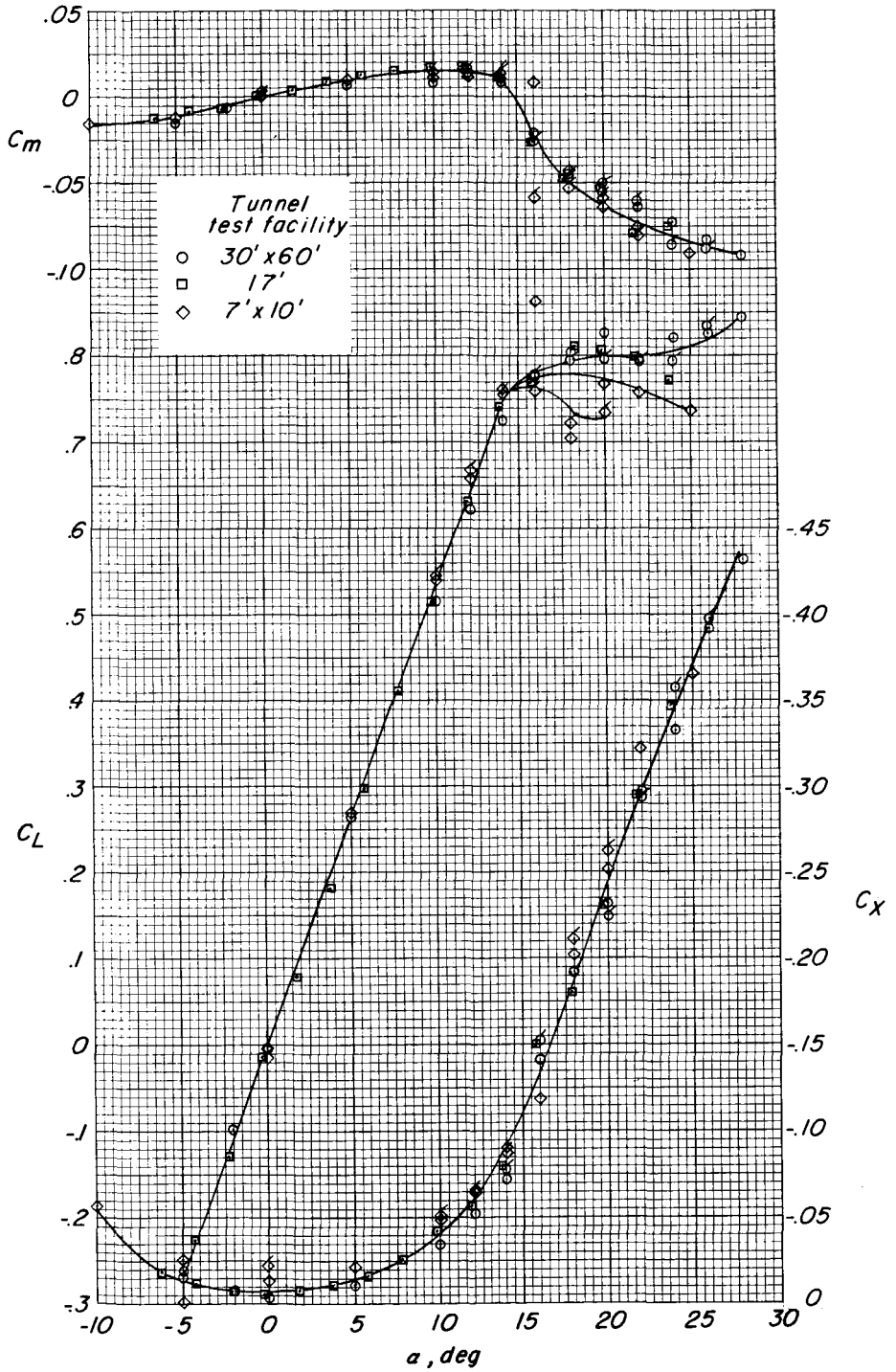

Figure 6.- Tunnel-size comparison of lift-, longitudinal-force, and pitching-moment coefficients as functions of angle of attack. Power off; flaps off; Reynolds number = 6.3×10^5. Flagged symbols denote repeat points.

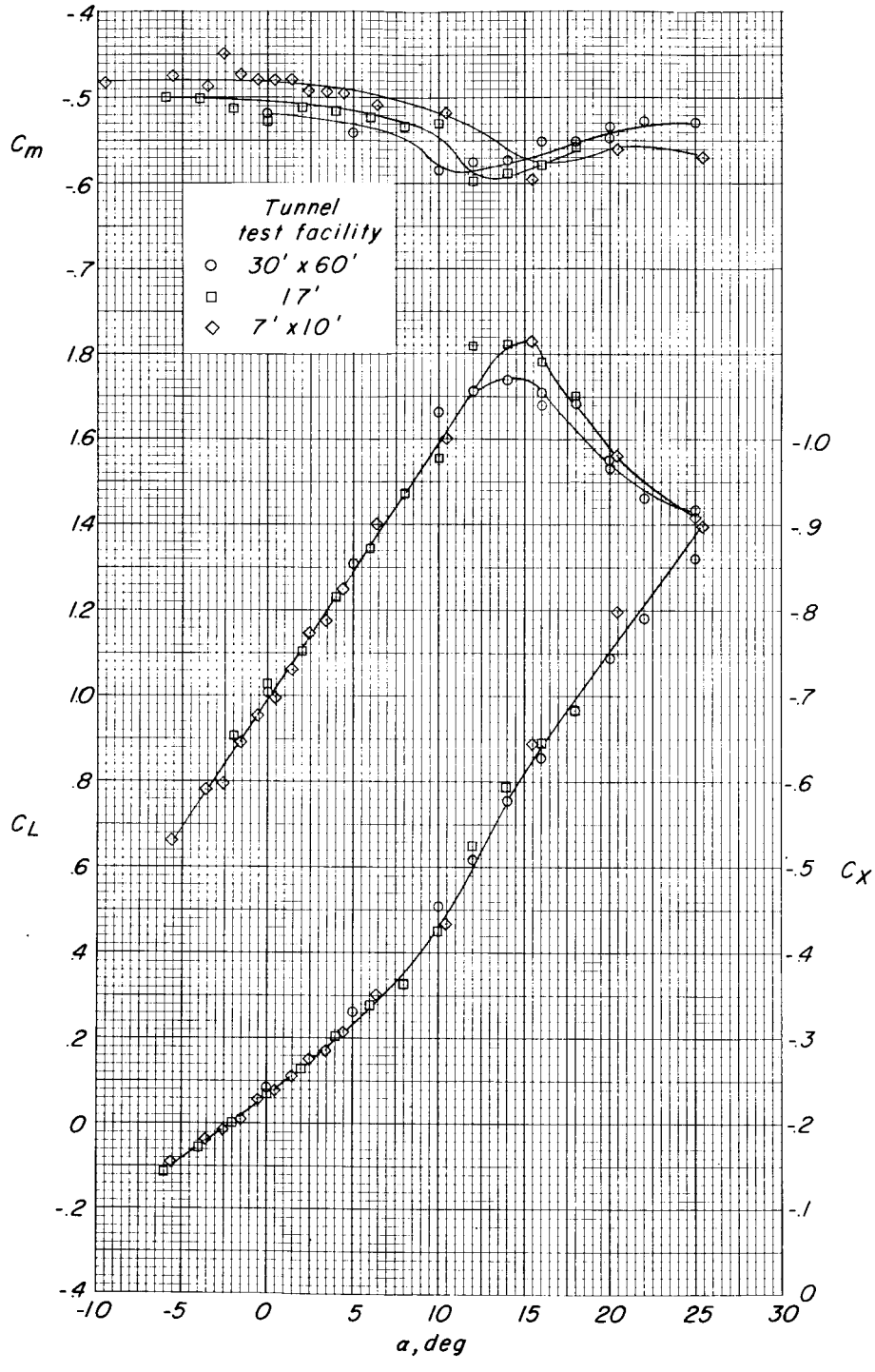

Figure 7.- Tunnel-size comparison of lift-, longitudinal-force, and pitching-moment coefficients as functions of angle of attack. Power off; flaps on (deflected 40°); Reynolds number = 6.3×10^5.

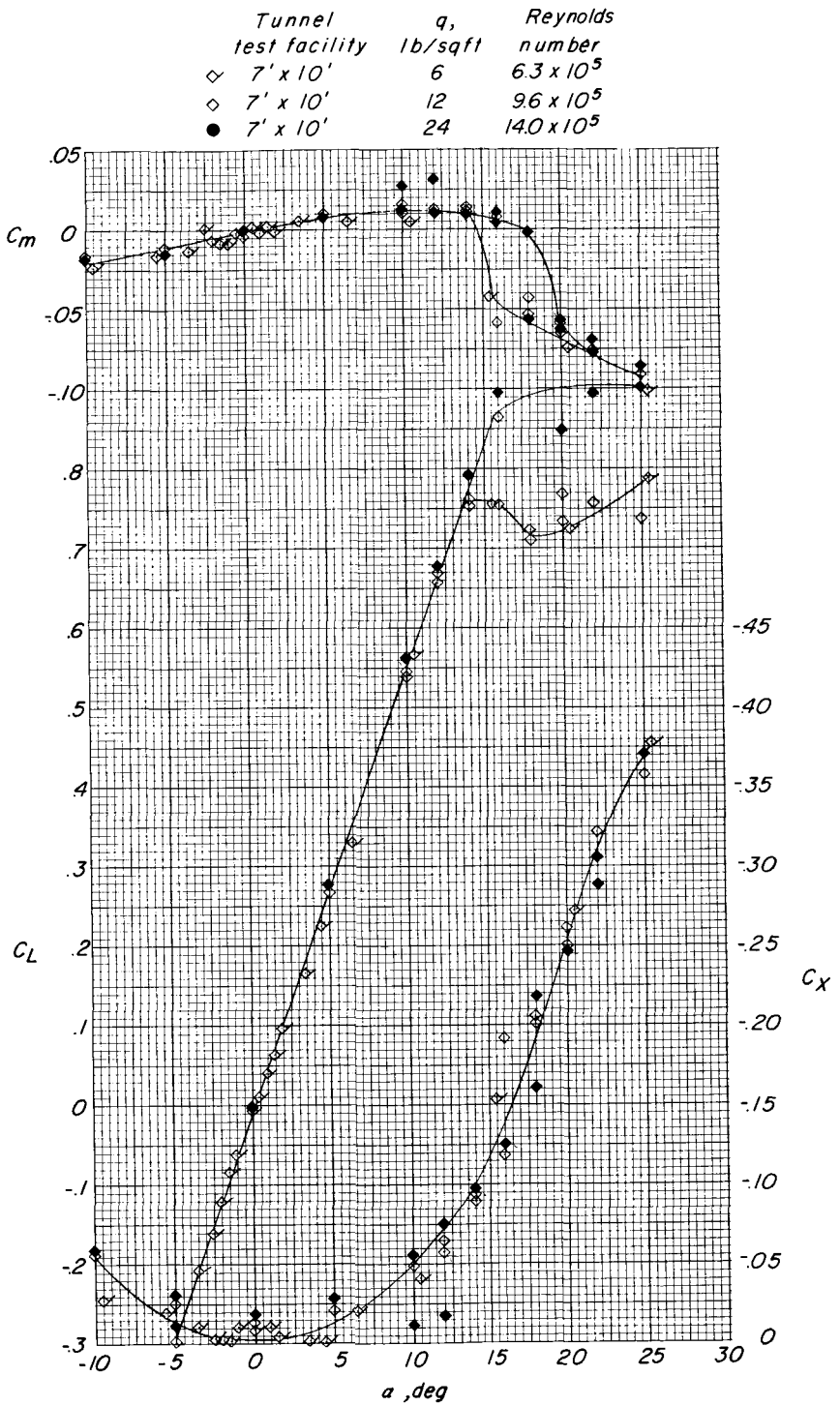

Figure 8.- Effect of Reynolds number on lift-, longitudinal-force, and pitching-moment coefficients as functions of angle of attack in 7- by 10-foot tunnel. Power off; flaps off. Flagged symbols denote repeat points.

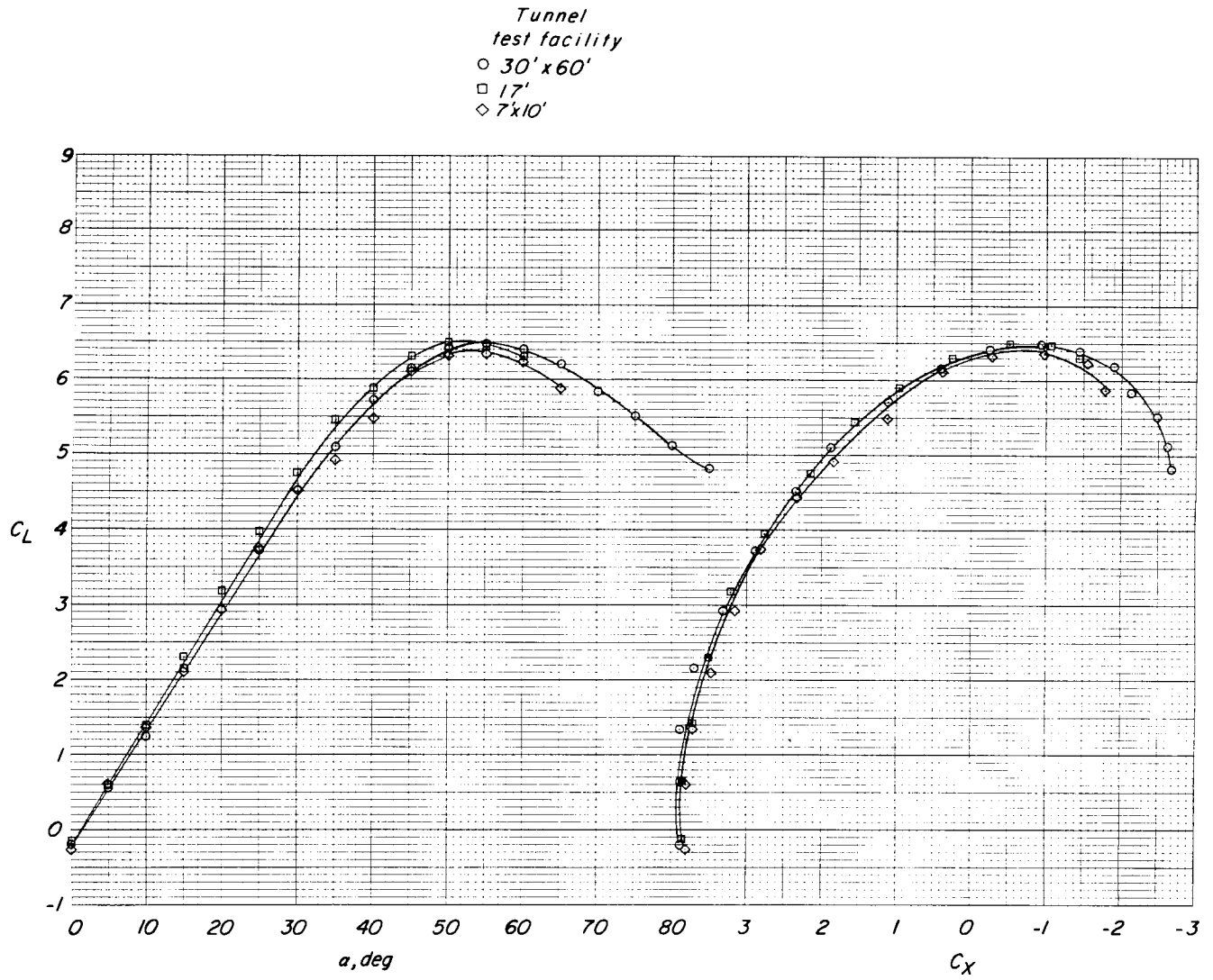

(a) $C_T = 4$; $C_{T,S} = 0.80$.

Figure 9.- Comparison of uncorrected data at constant thrust coefficient from 7- by 10-foot tunnel, 17-foot test section, and 30- by 60-foot tunnel. Flaps off.

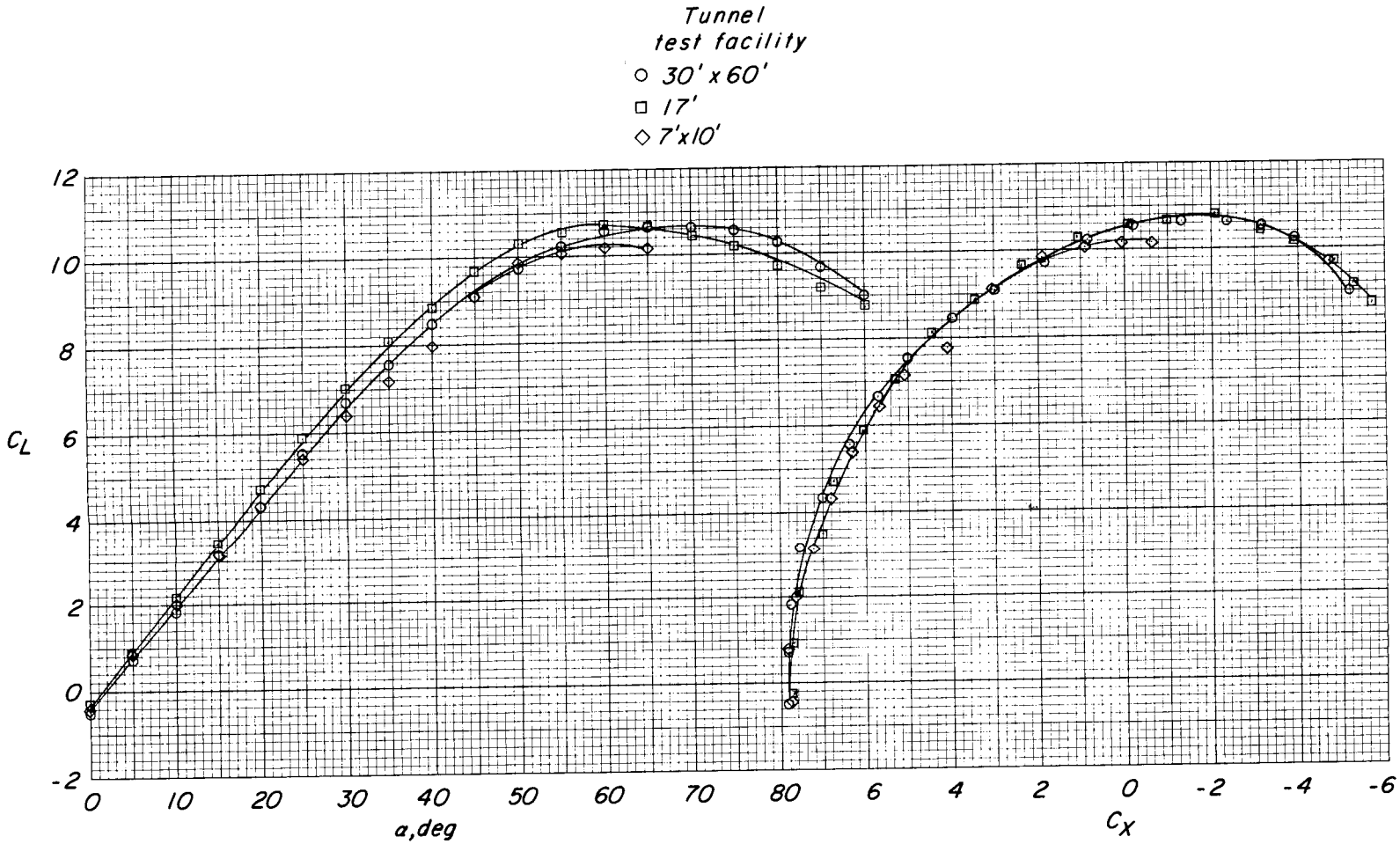

(b) $C_T = 8$; $C_{T,S} = 0.88$.

Figure 9.- Continued.

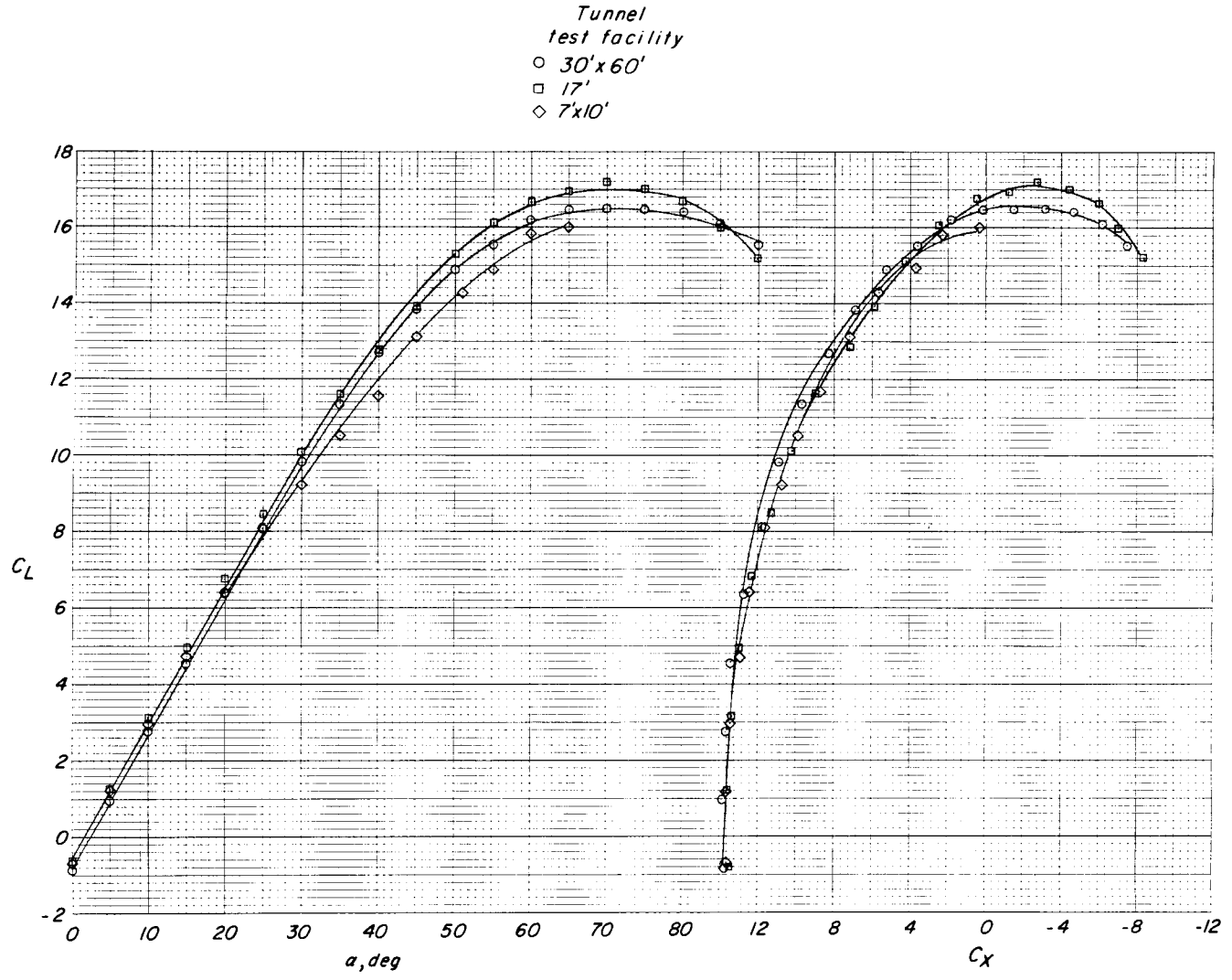

(c) $C_T = 14$; $C_{T,S} = 0.93$.

Figure 9.- Concluded.

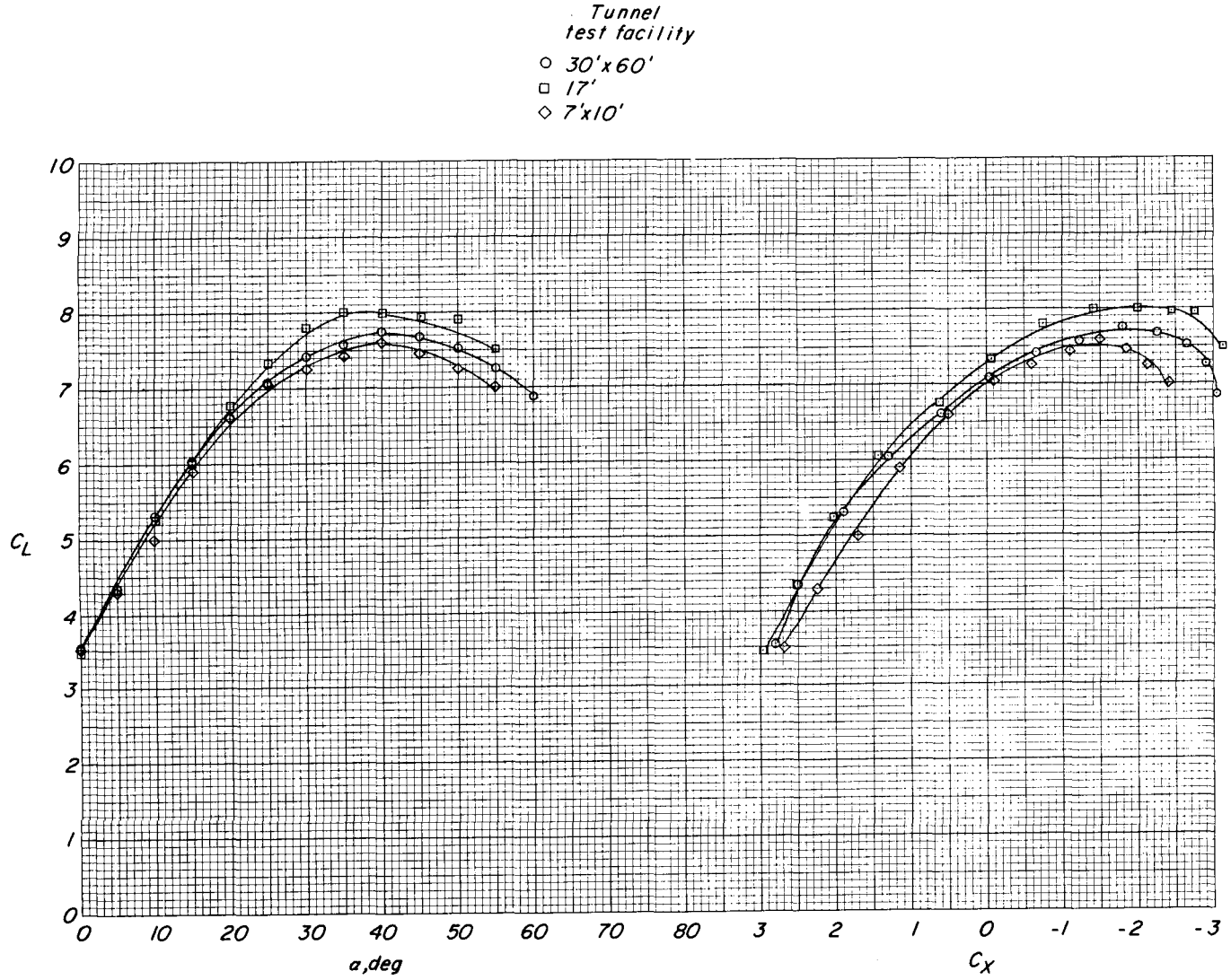

(a) $C_T = 4$; $C_{T,S} = 0.80$.

Figure 10.- Comparison of uncorrected data at constant thrust coefficient from 7- by 10-foot tunnel, 17-foot test section, and 30- by 60-foot tunnel. Flaps on (deflected 40°).

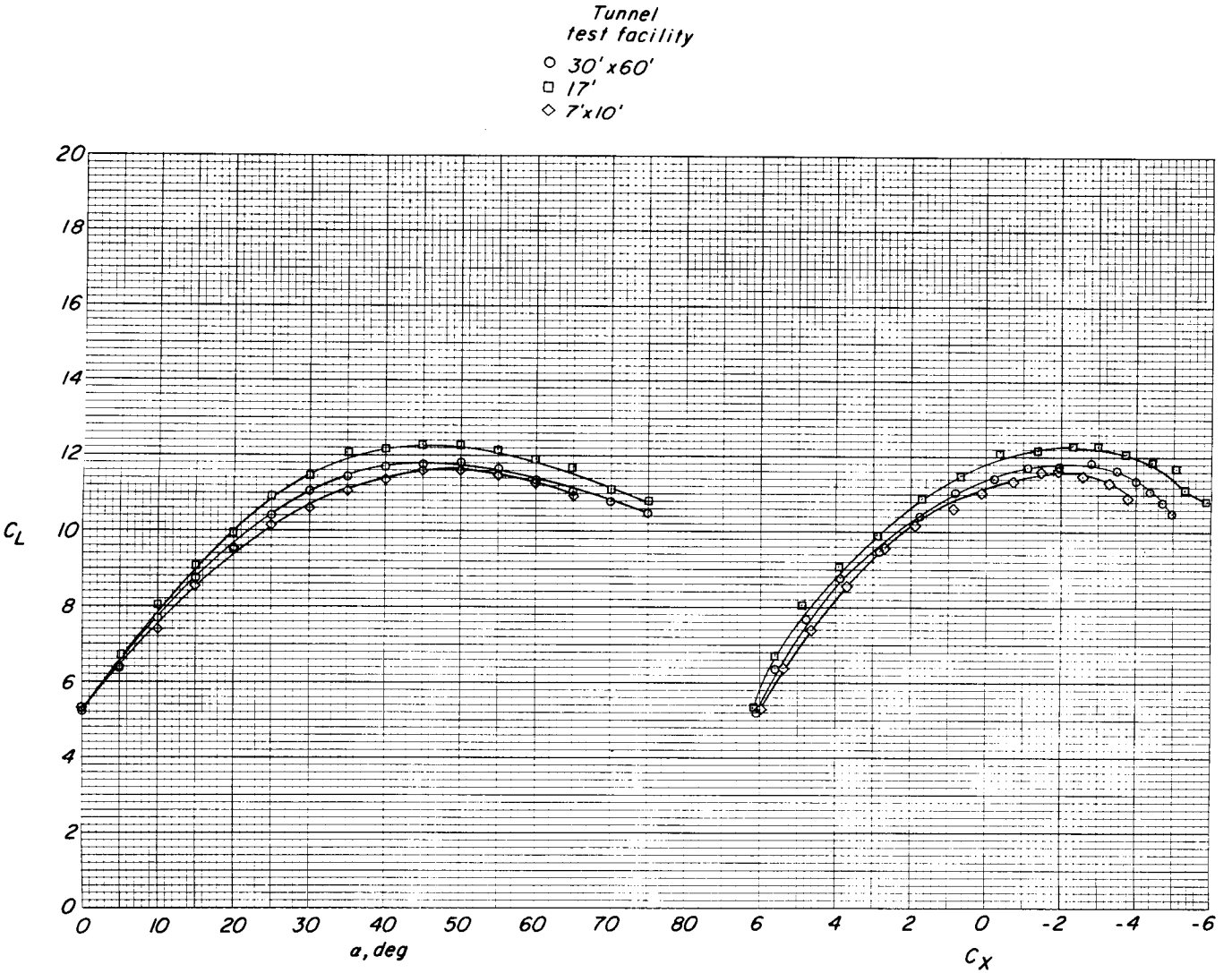

(b) $C_T = 8$; $C_{T,S} = 0.88$.

Figure 10.- Continued.

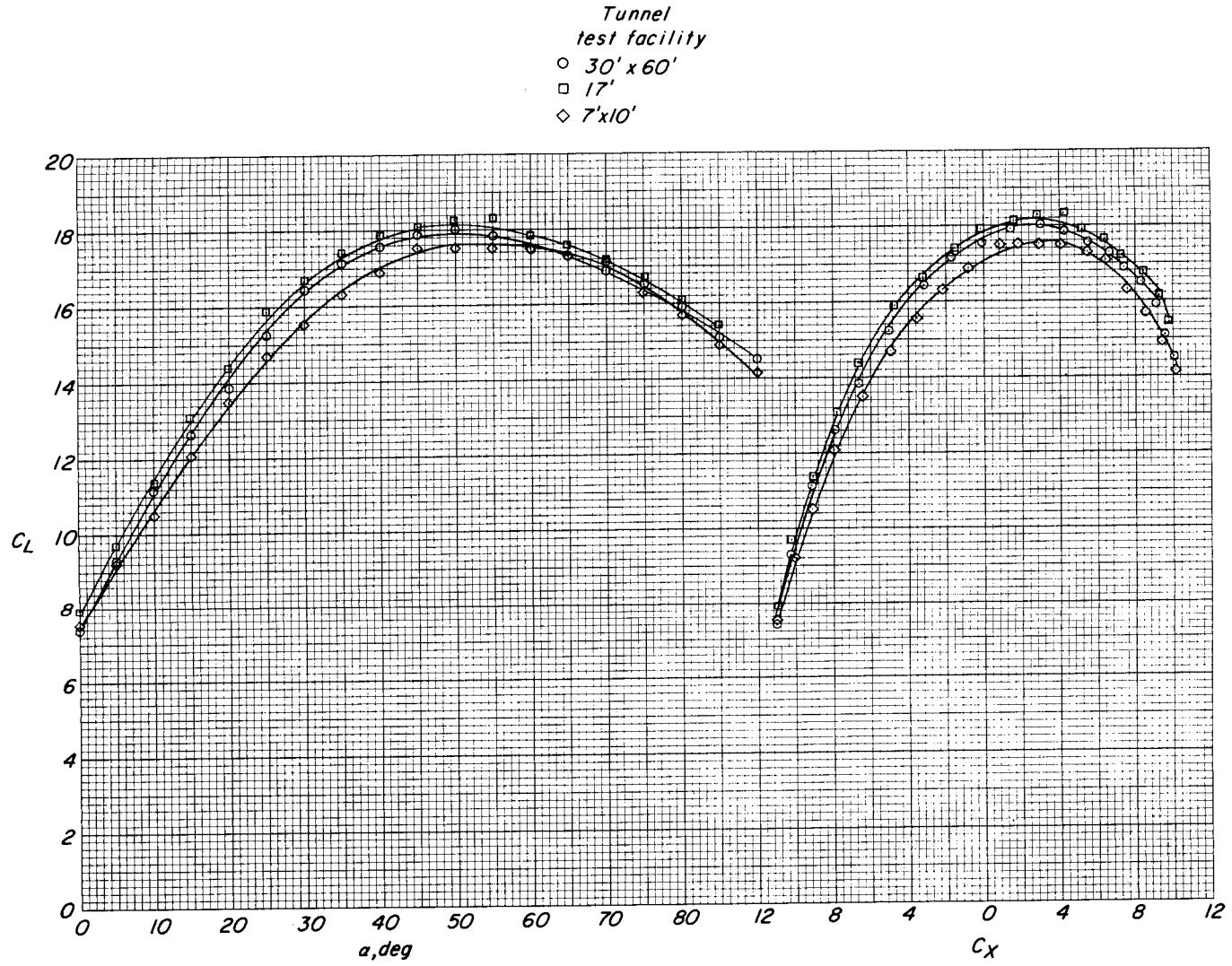

(c) $C_T = 14$; $C_{T,S} = 0.93$.

Figure 10.- Concluded.

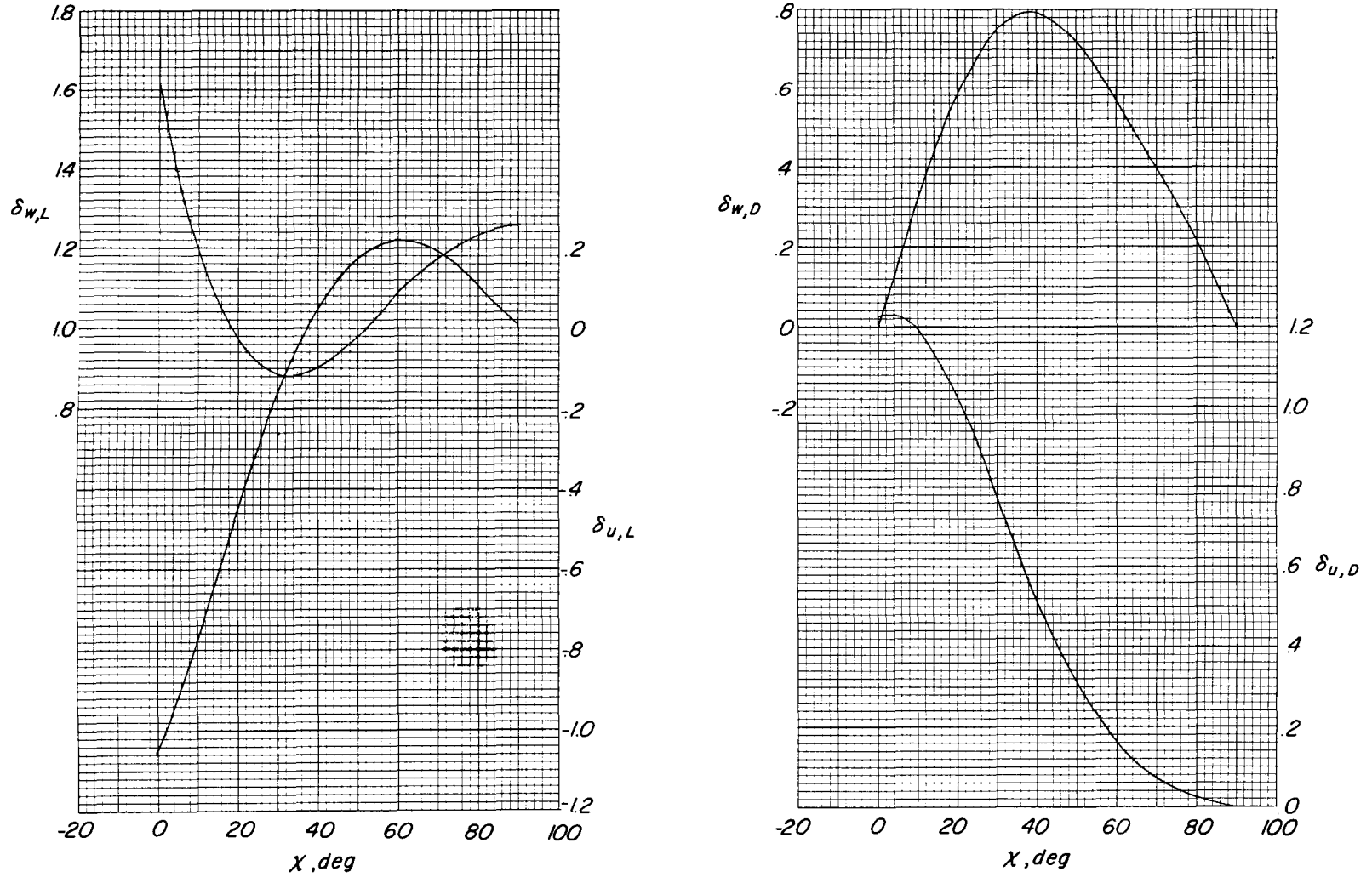

(a) For data from 30- by 60-foot tunnel (one-point method).

Figure 11.- Correction factors used to correct data for wall effects by method of reference 1.

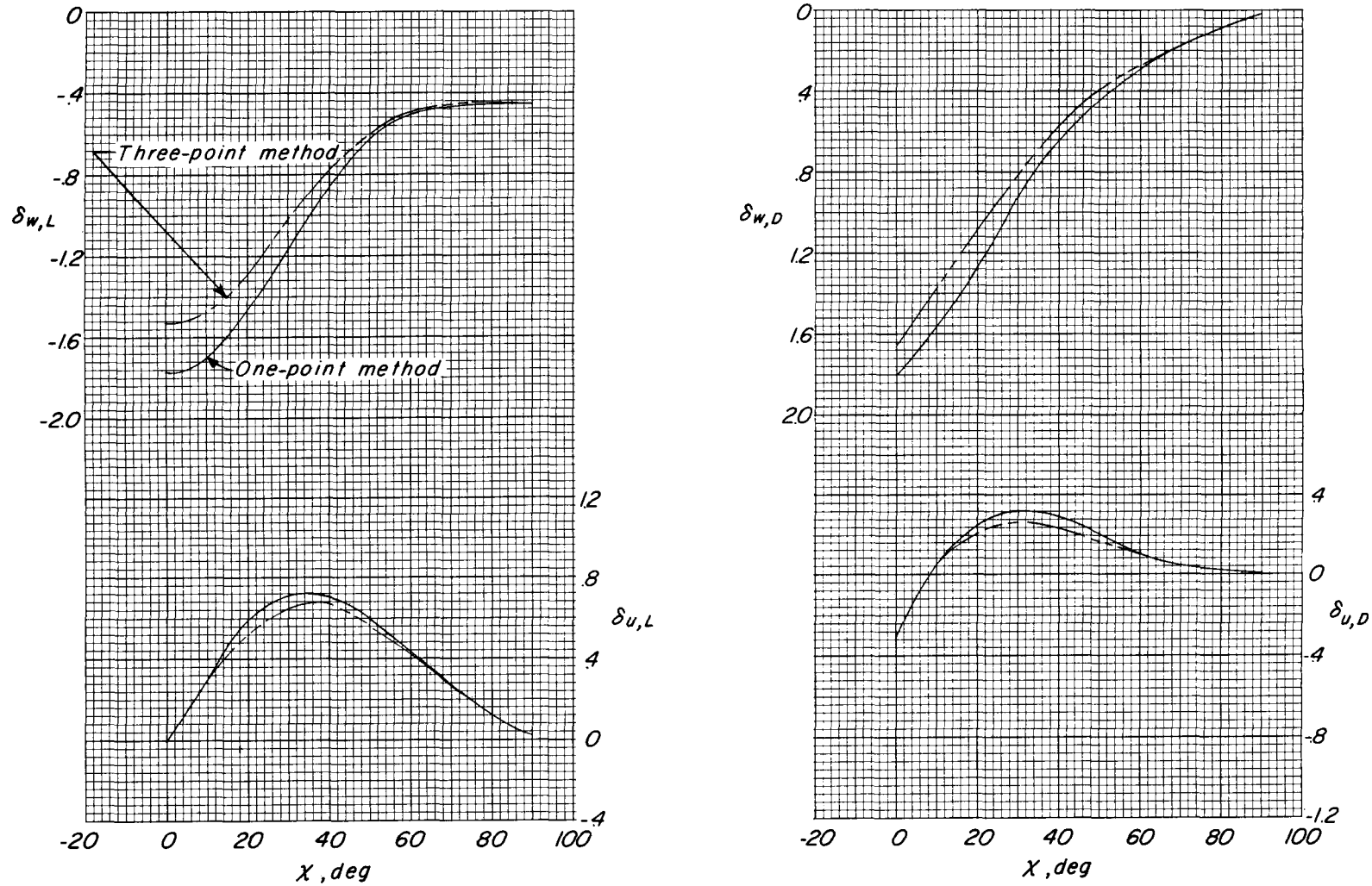

(b) For data from 7- by 10-foot tunnel (one-point and three-point methods).

Figure 11.- Continued.

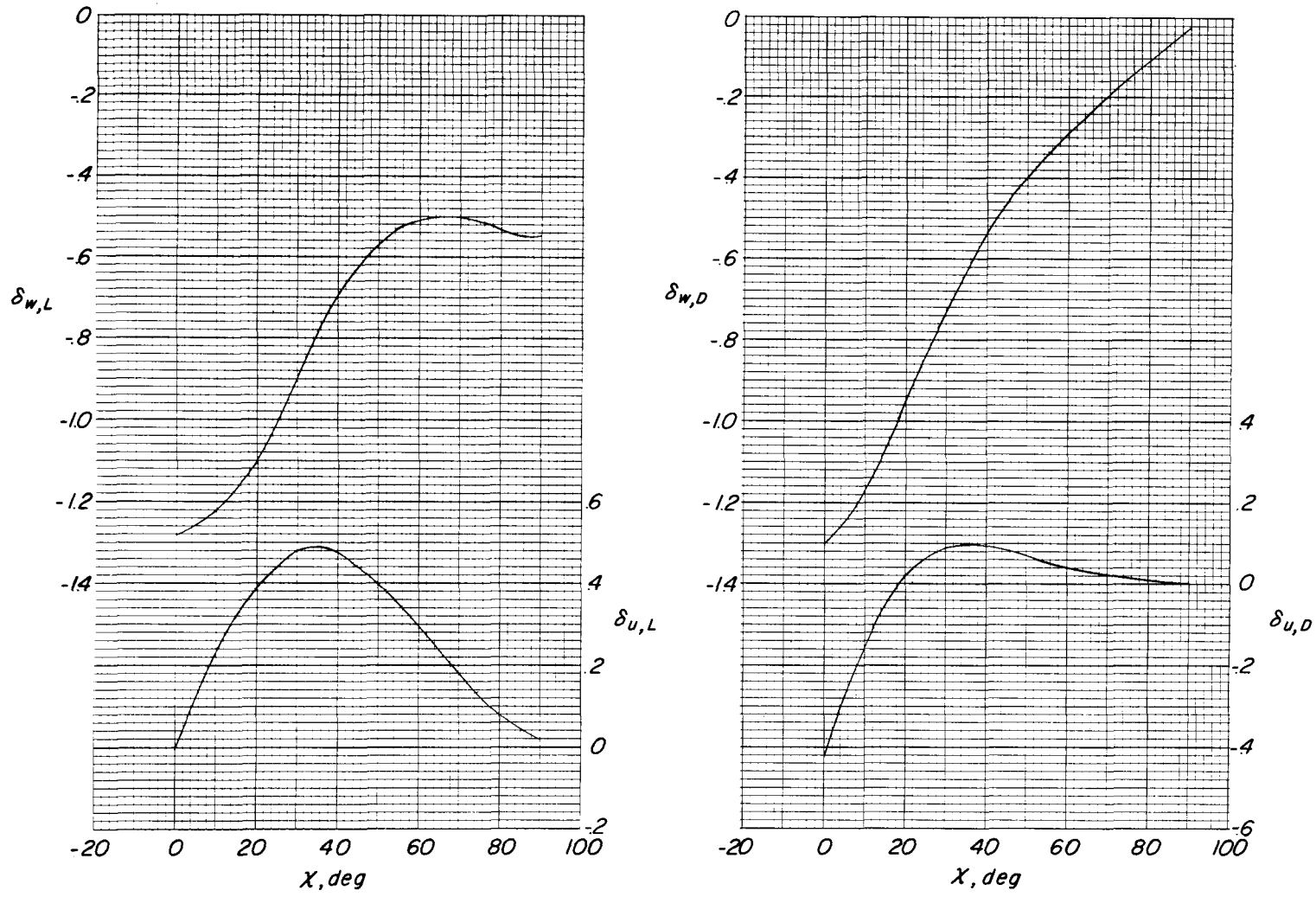

(c) For data from 17-foot test section (one-point method).

Figure 11.- Concluded.

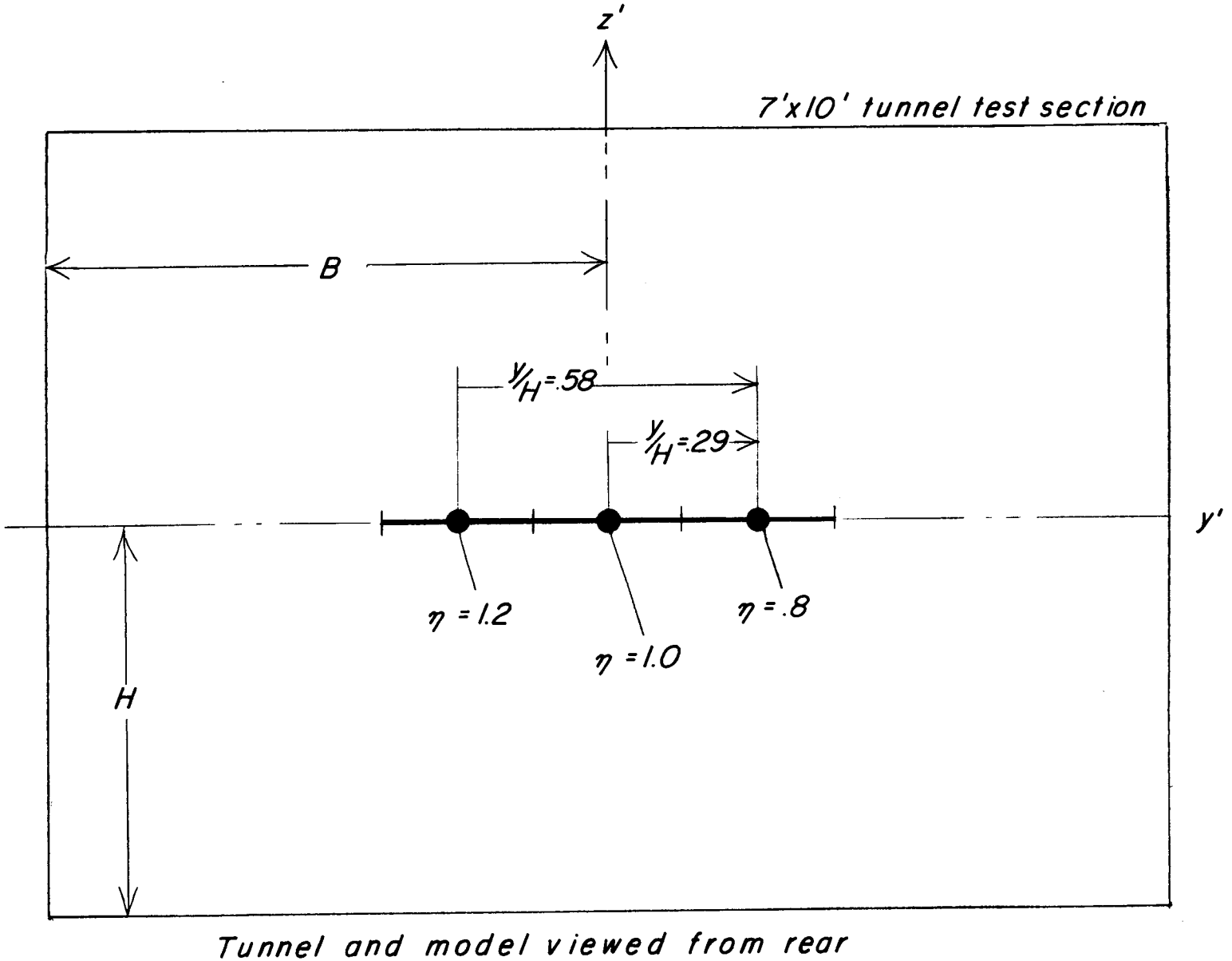

Figure 12.- Schematic representation of finite-span lifting element (three-point method). $\gamma = 1.5$; $\sigma = 0.4$; $\zeta = 1.0$.

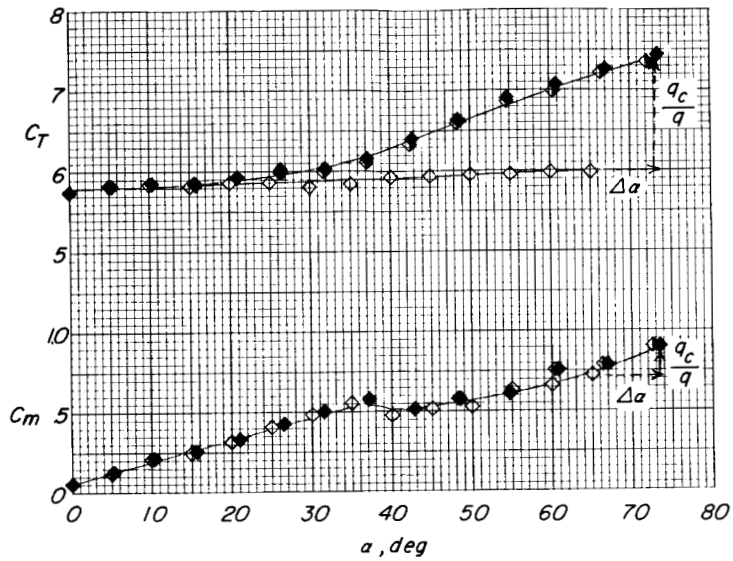

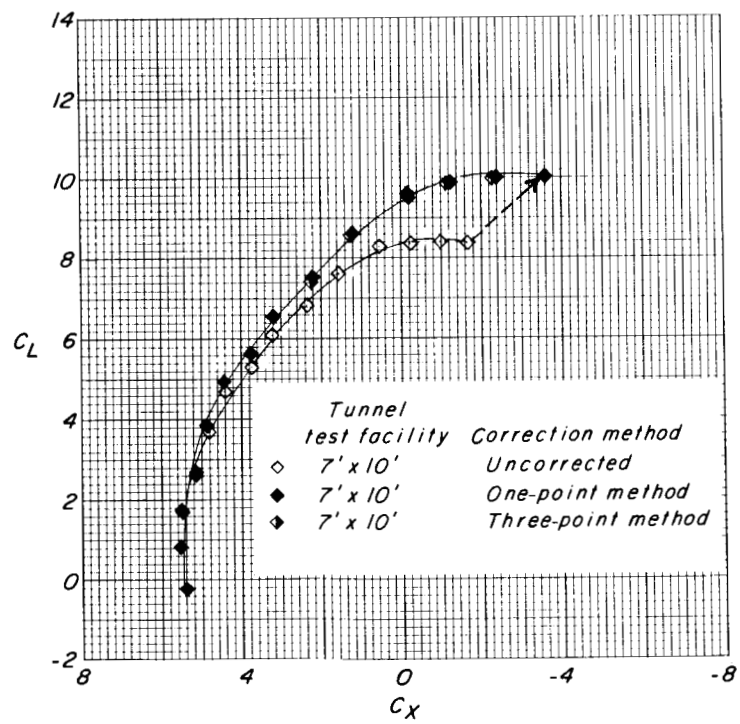

(a) $C_T \approx 6.0$; $C_{T,S} \approx 0.86$.

Figure 13.- Comparison of uncorrected data and data with $\Delta\alpha$ and q_c/q corrections applied (one- and three-point methods from ref. 1). Flaps off; 7- by 10-foot tunnel.

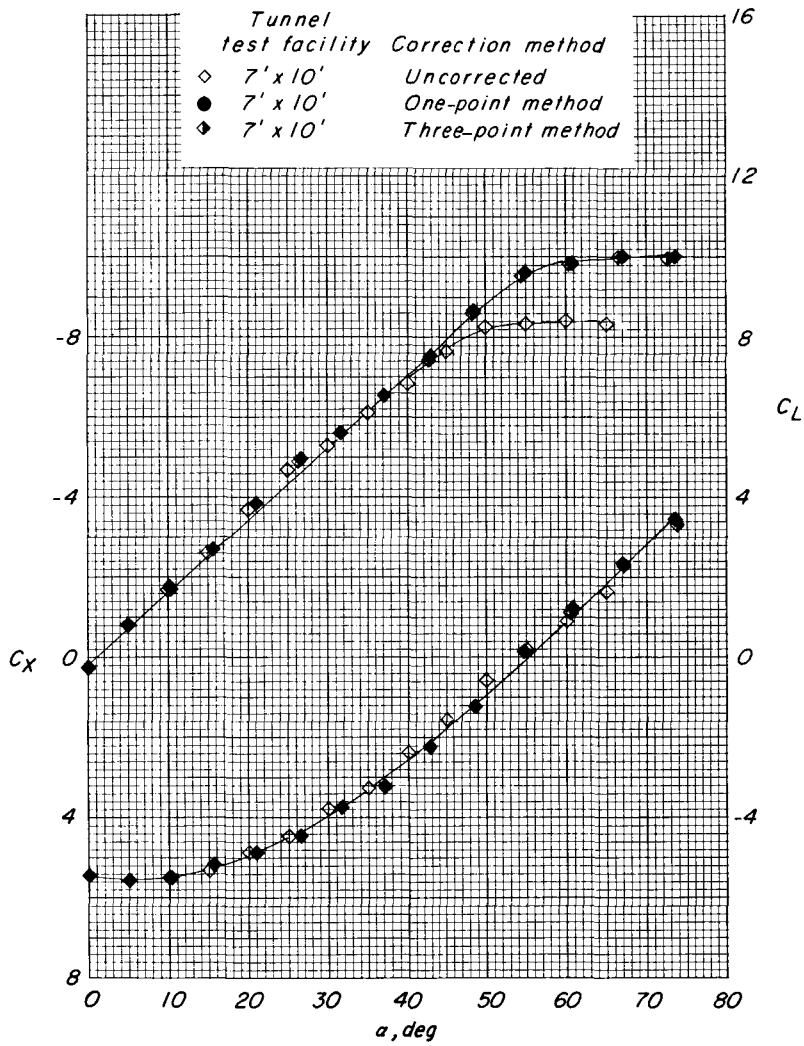

(a) Concluded.

Figure 13.- Continued.

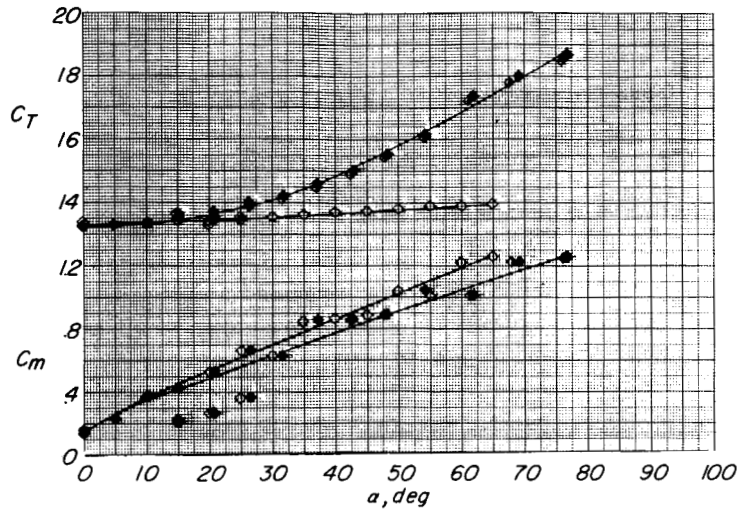

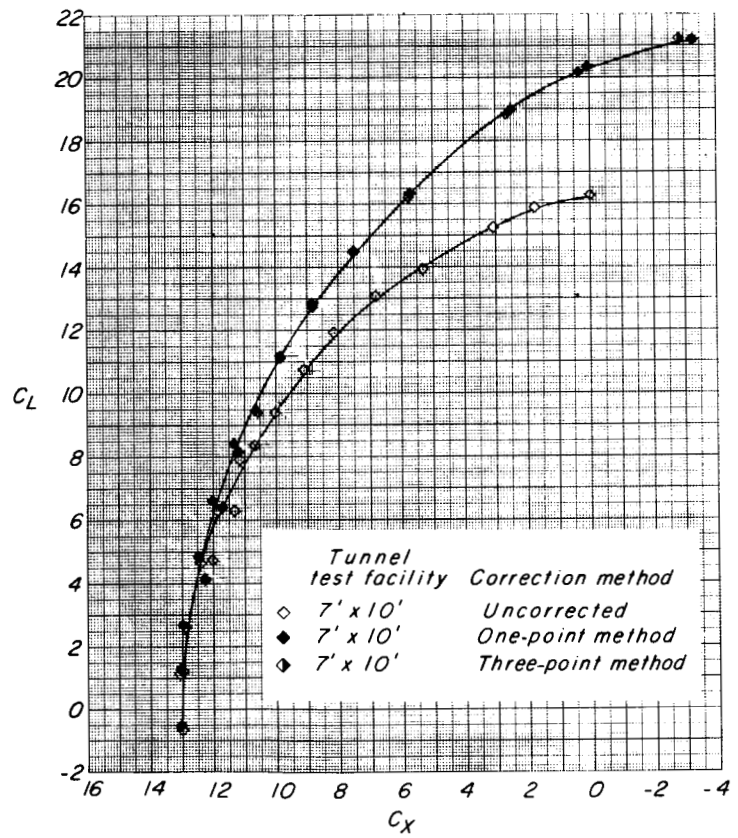

(b) $C_T \approx 13.5$; $C_{T,S} \approx 0.93$.

Figure 13.- Continued.

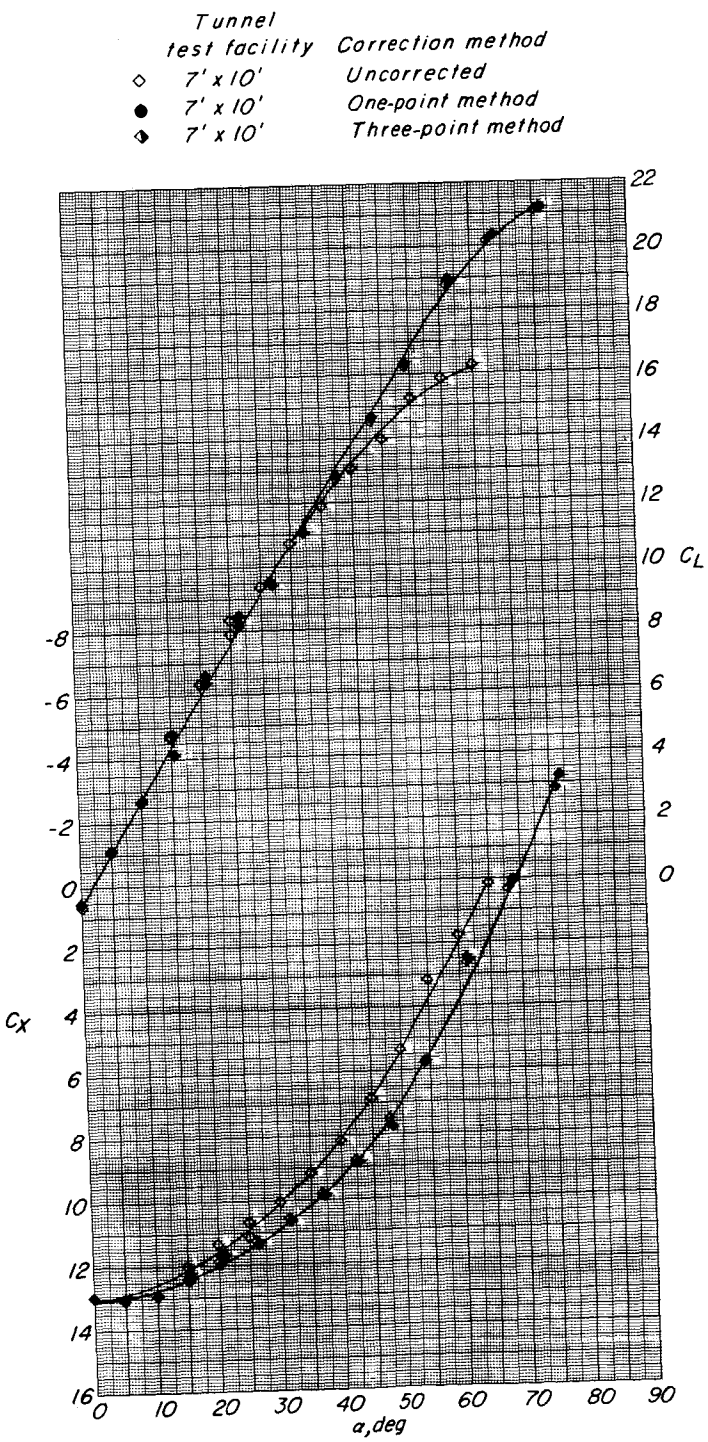

(b) Concluded.

Figure 13.- Concluded.

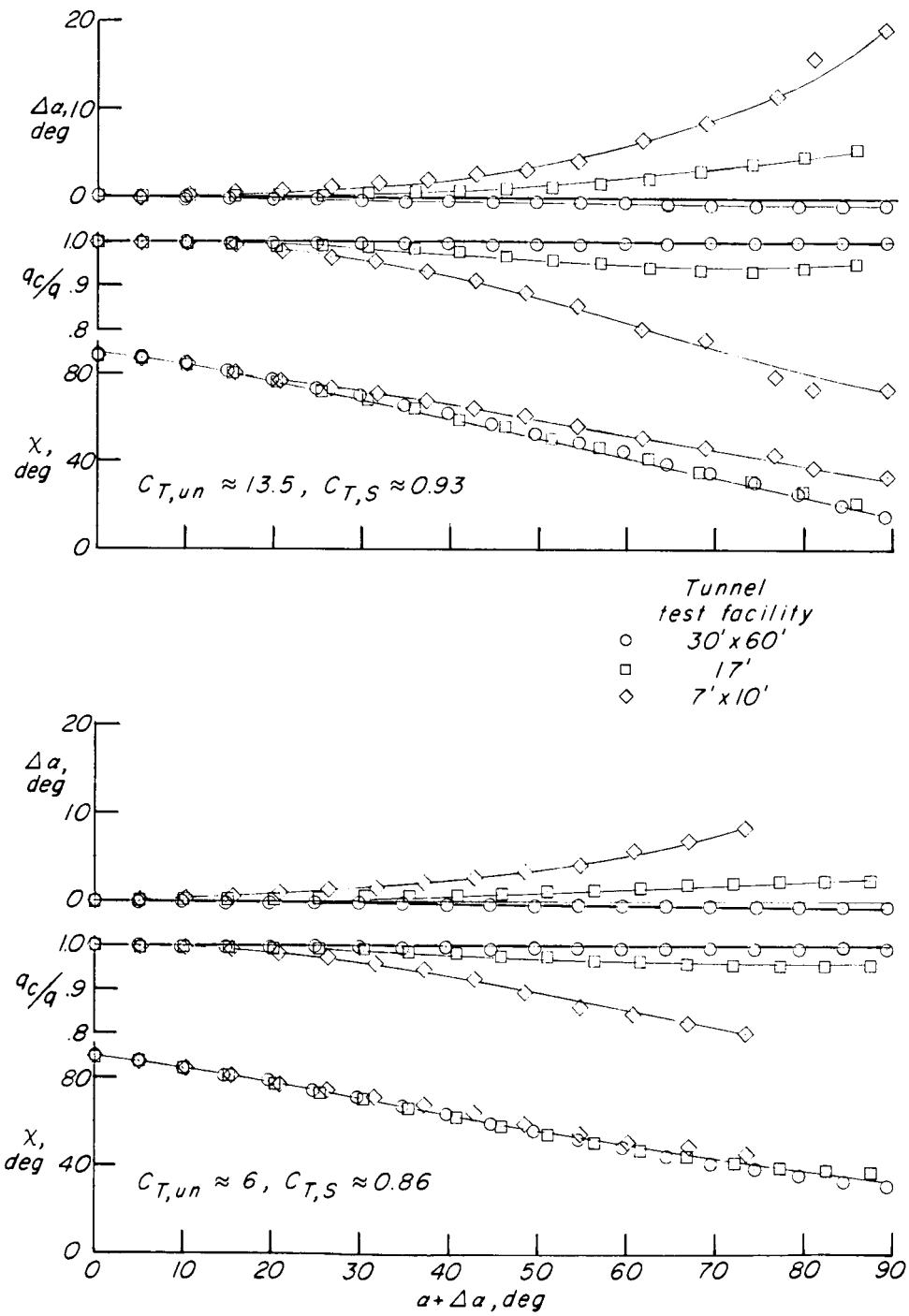

(a) Flaps off.

Figure 14.- Typical $\Delta\alpha$ and q_c/q corrections and values of χ, determined by using the method of reference 1.

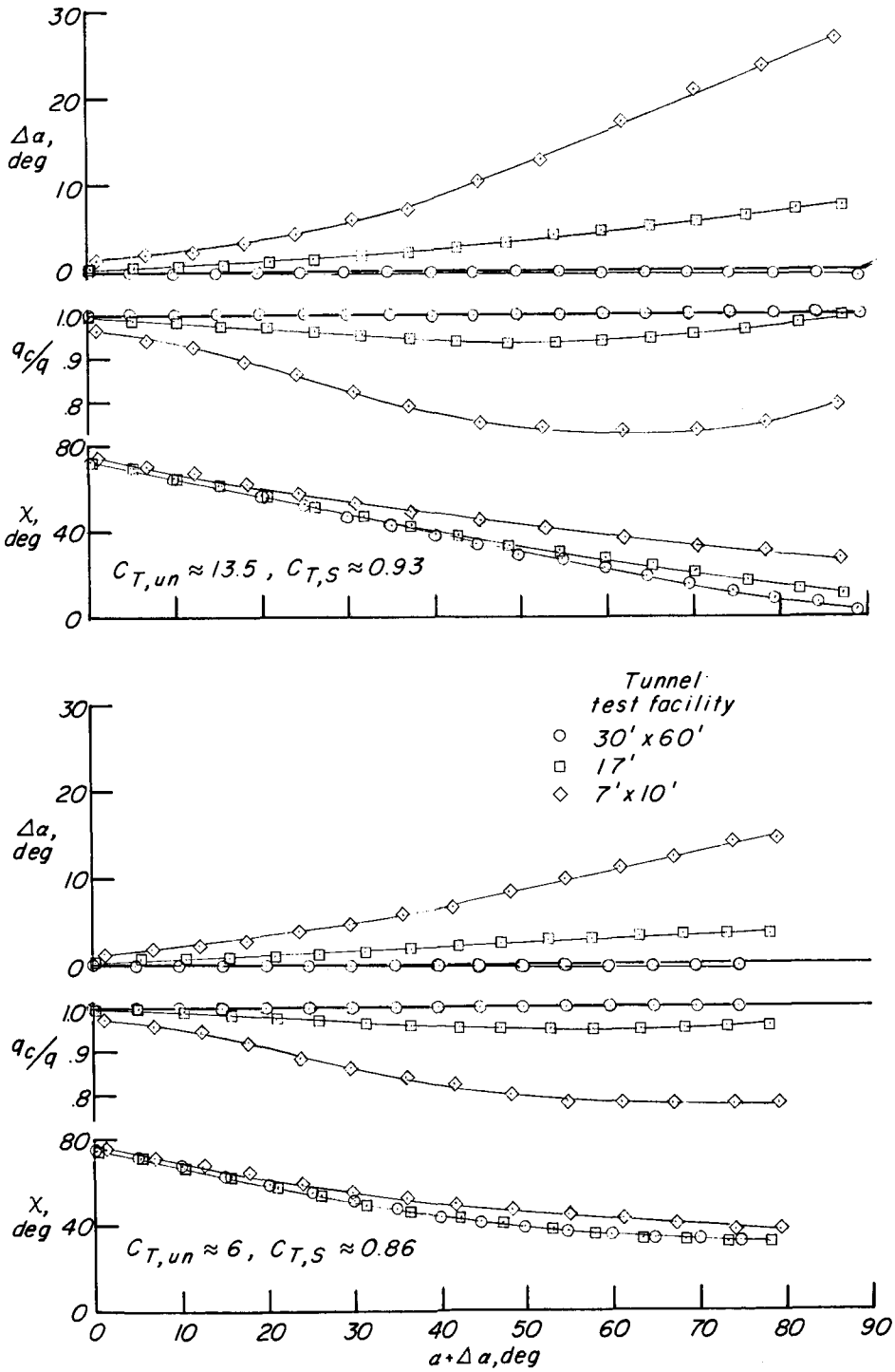

(b) Flaps on.

Figure 14.- Concluded.

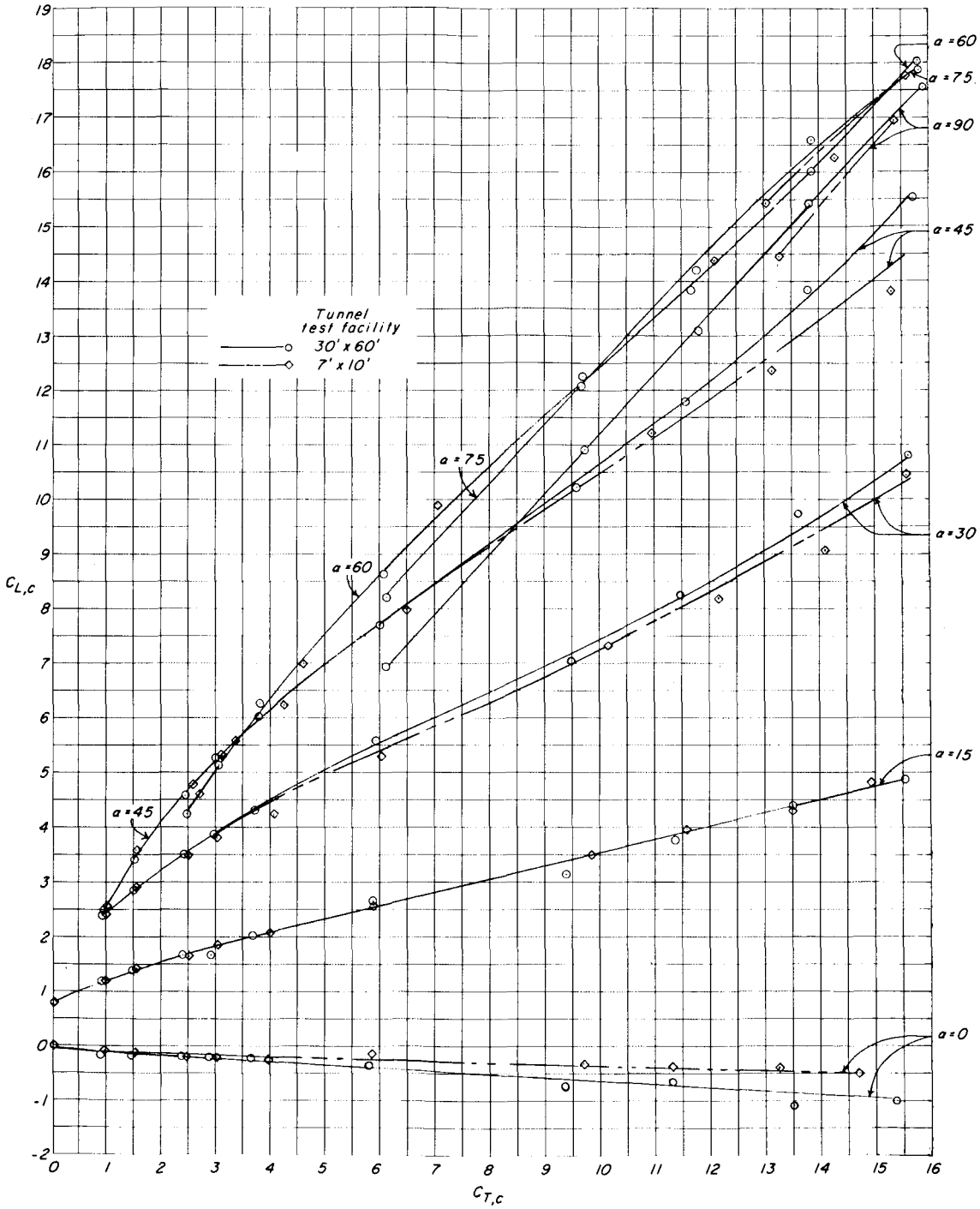

(a) Lift coefficient as a function of thrust coefficient.

Figure 15.- Comparison of data from 7- by 10-foot tunnel and 30- by 60-foot tunnel, corrected for wall effects by method of reference 1. Flaps off.

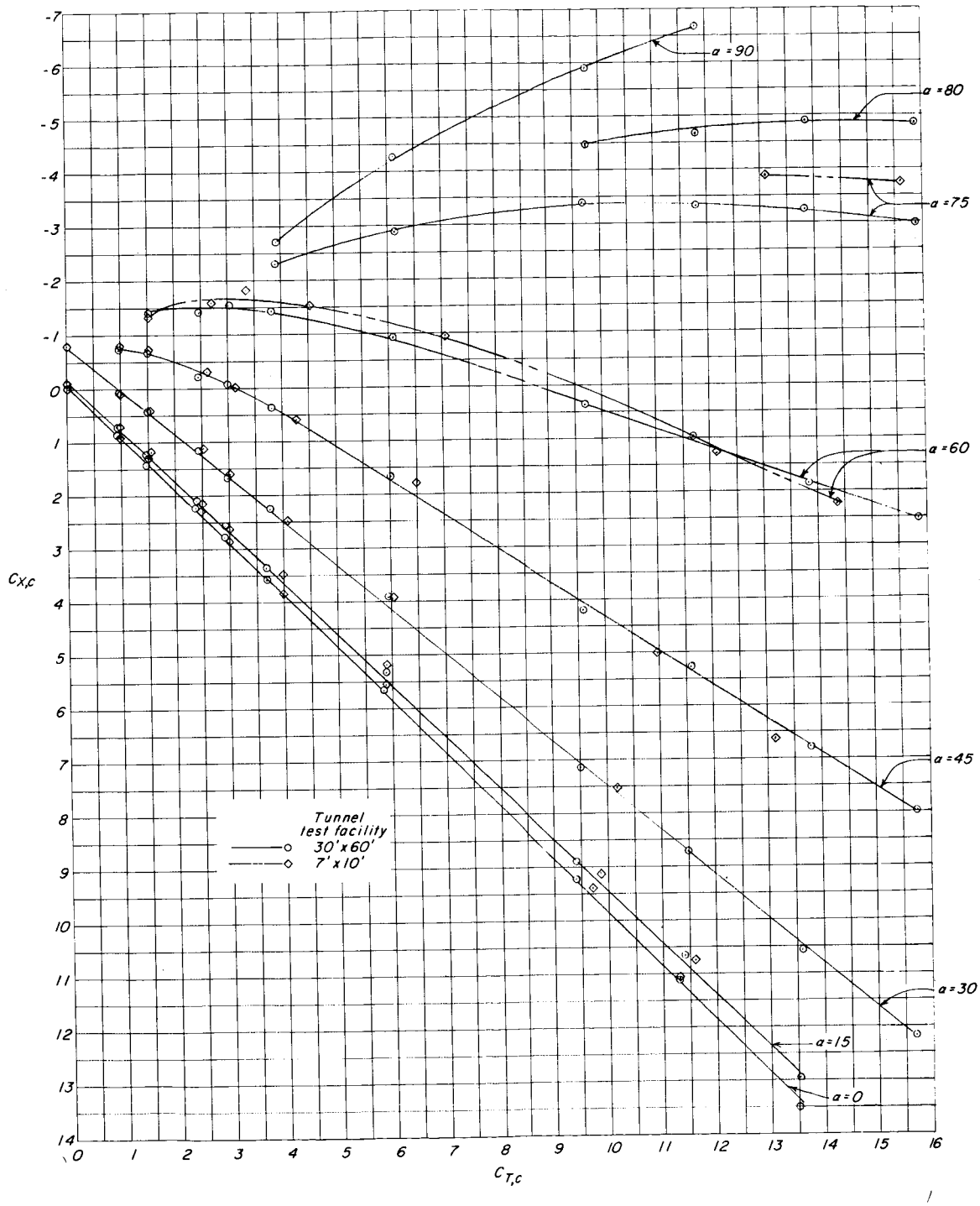

(b) Longitudinal-force coefficient as a function of thrust coefficient.

Figure 15.- Concluded.

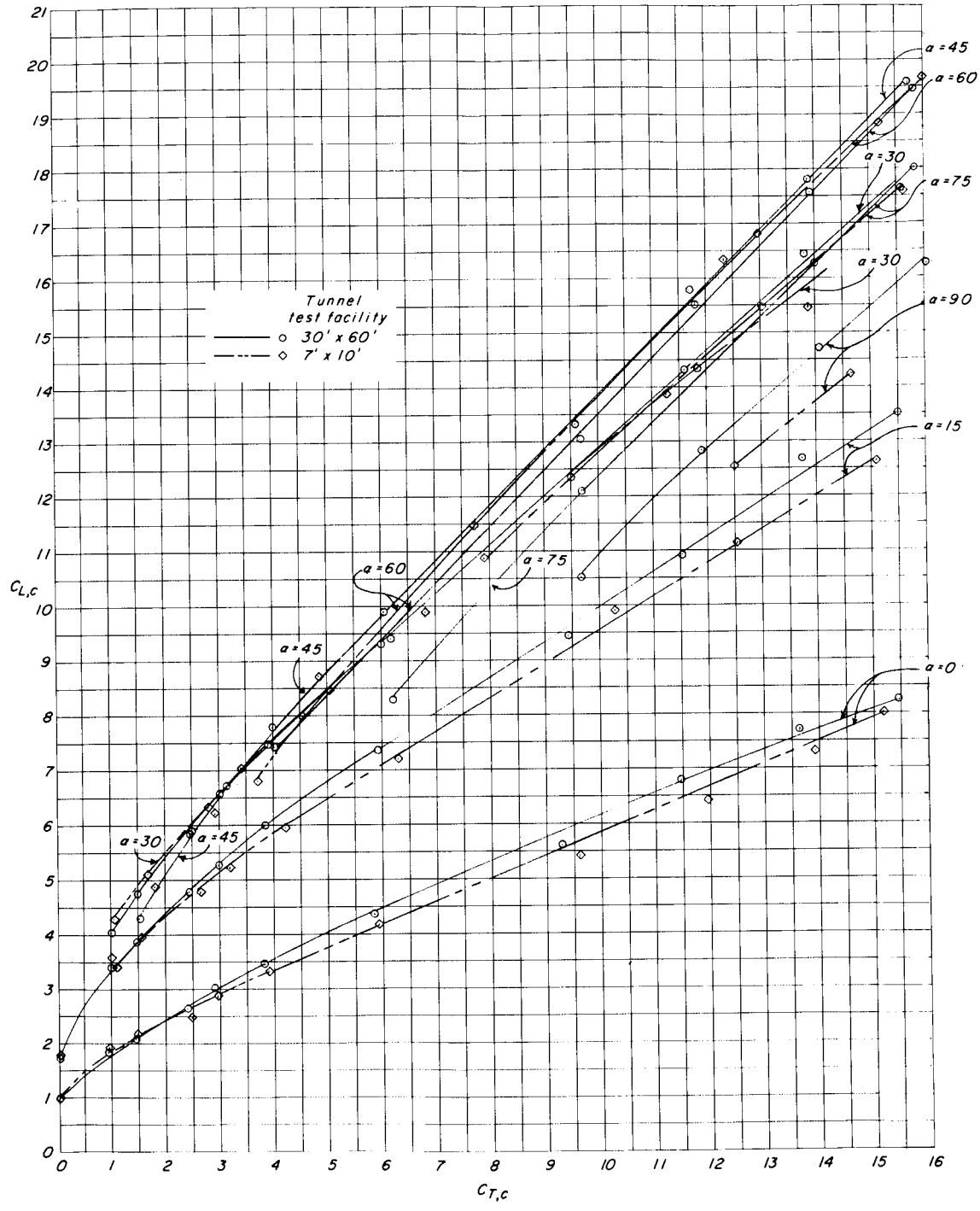

(a) Lift coefficient as a function of thrust coefficient.

Figure 16.- Comparison of data from 7- by 10-foot tunnel and 30- by 60-foot tunnel, corrected for wall effects by method of reference 1. Flaps on.

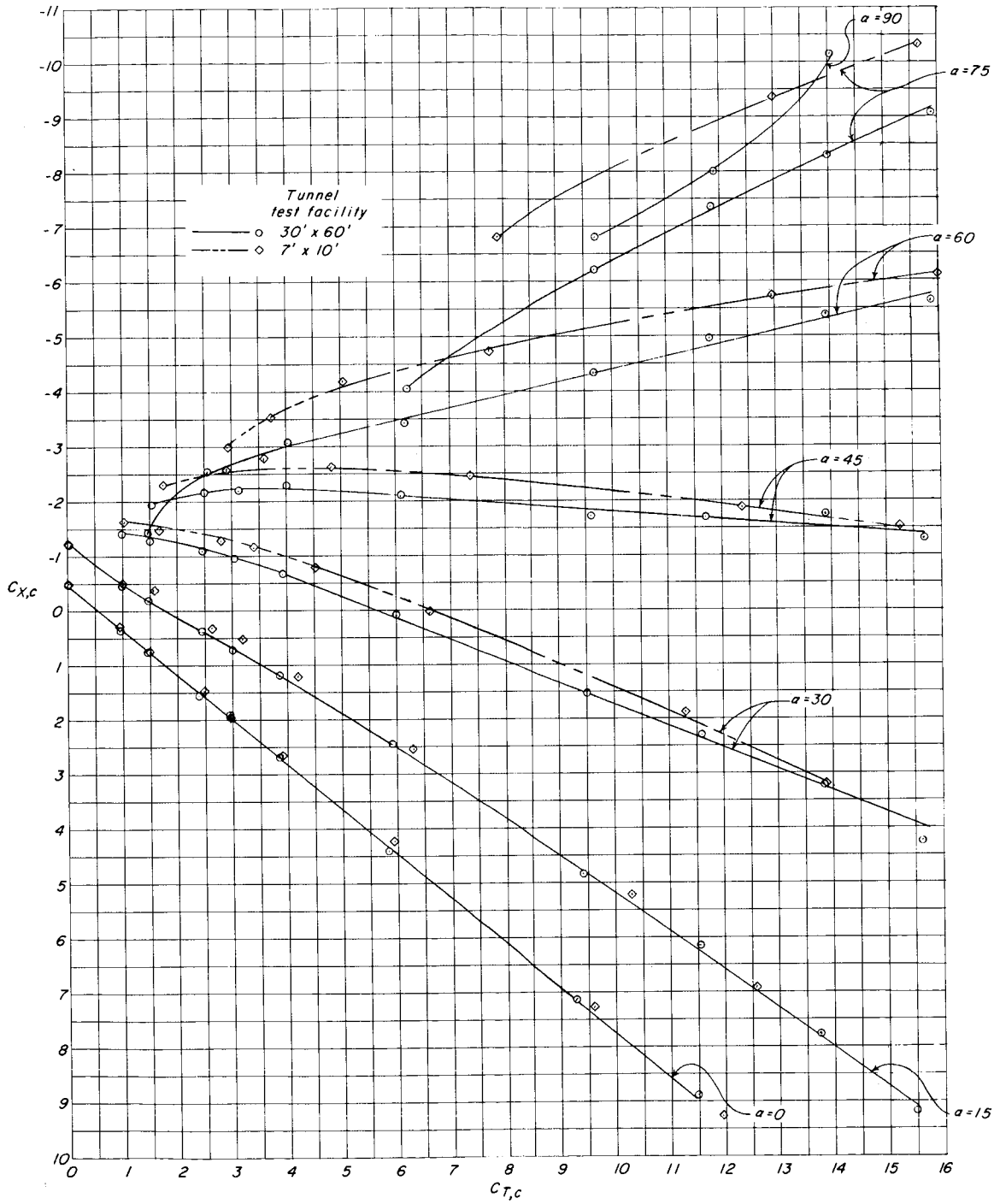

(b) Longitudinal-force coefficient as a function of thrust coefficient.

Figure 16.- Concluded.

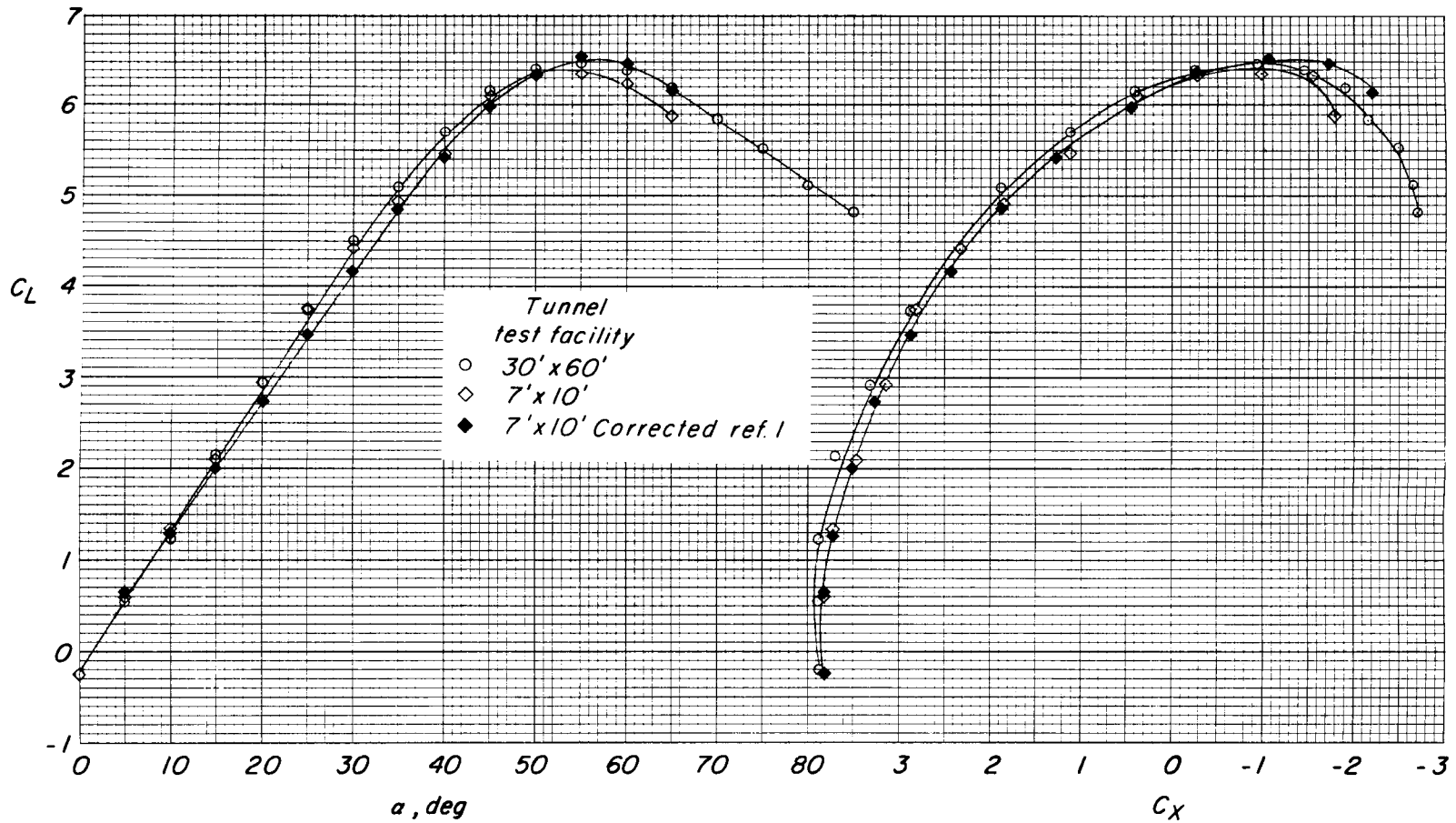

(a) $C_T = 4$; $C_{T,S} = 0.80$.

Figure 17.- Comparison of data from 7- by 10-foot tunnel (corrected and uncorrected) and data from 30- by 60-foot tunnel at constant thrust coefficients. Flaps off.

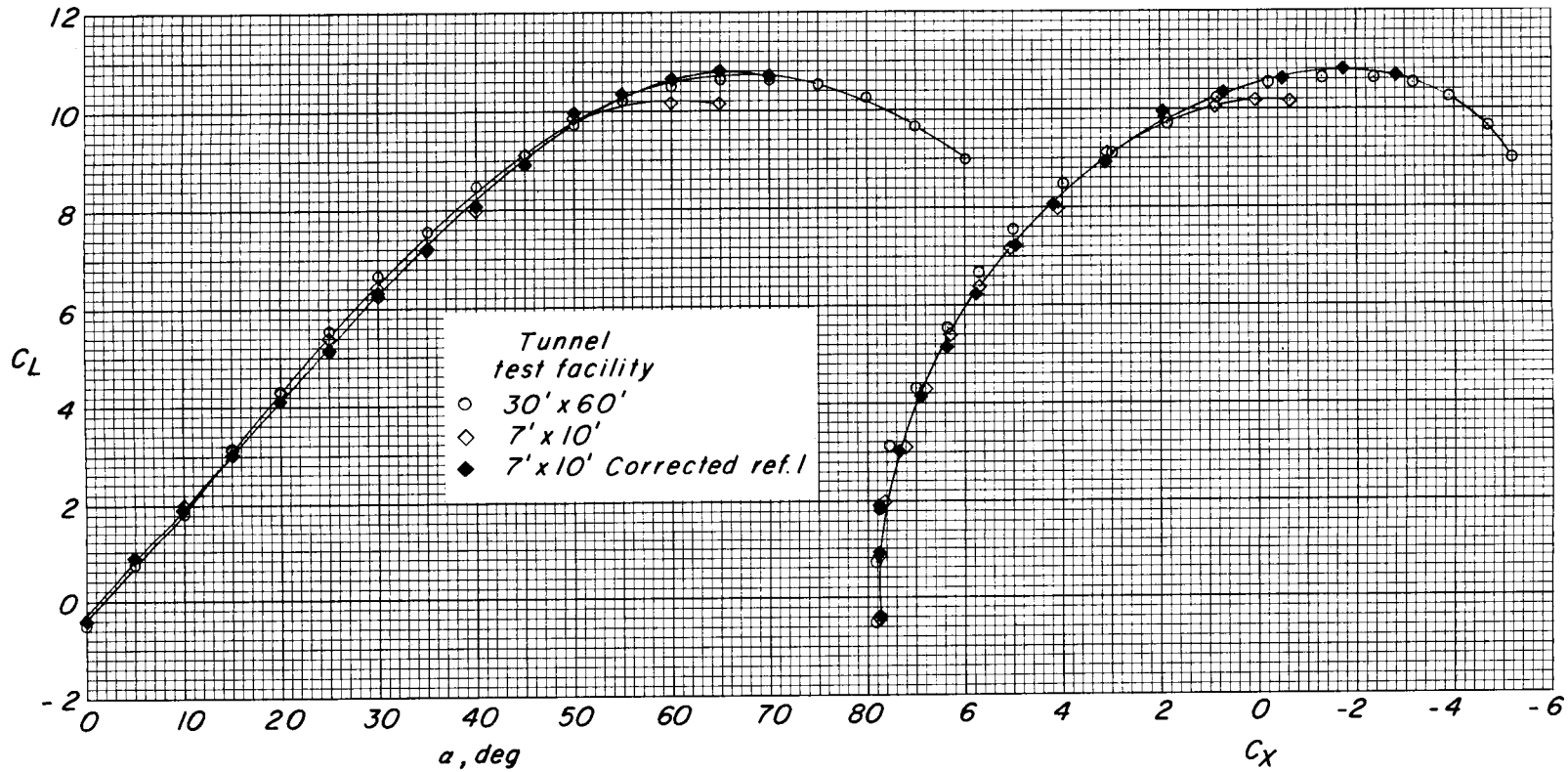

(b) $C_T = 8$; $C_{T,S} = 0.88$.

Figure 17.- Continued.

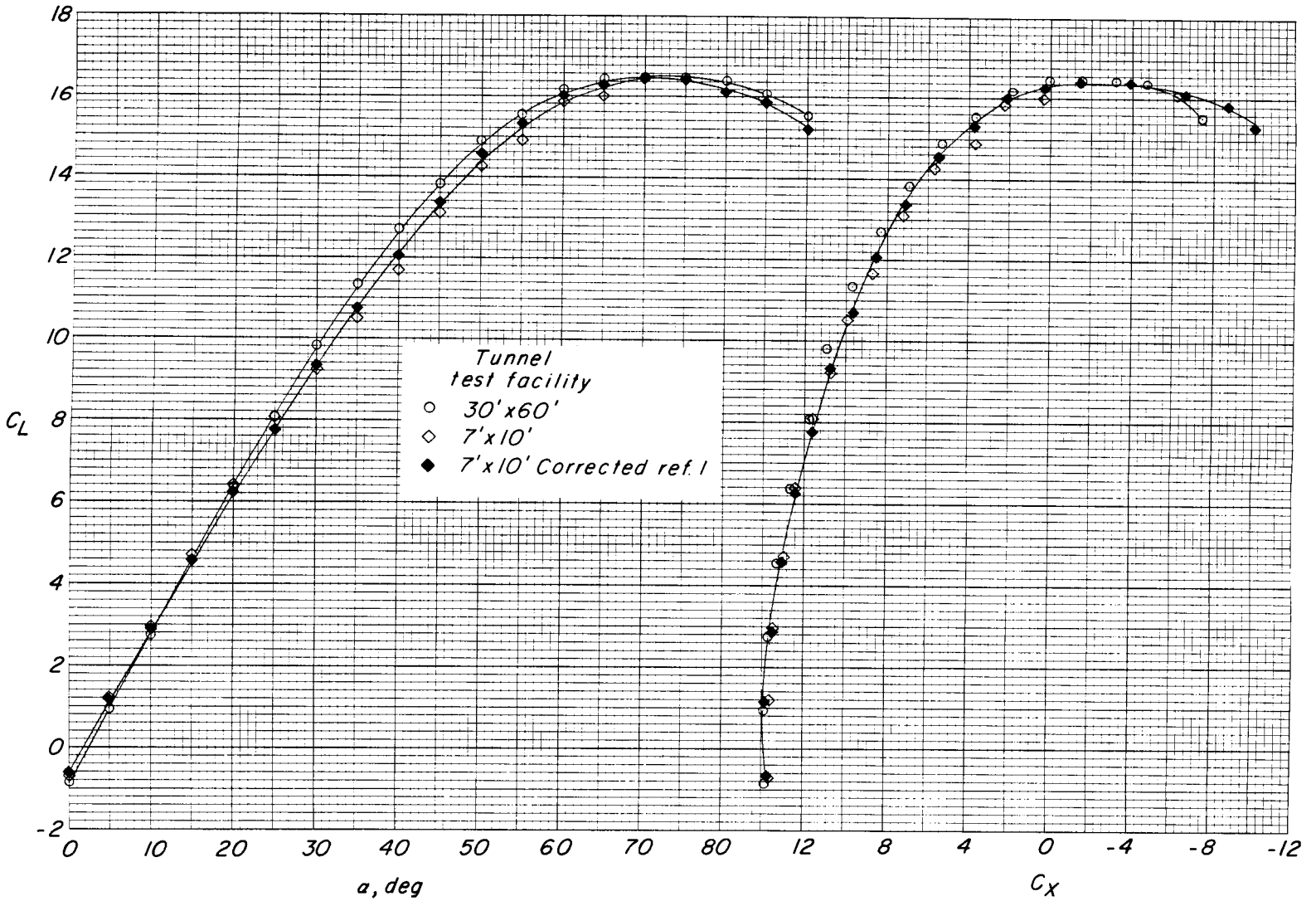

(c) $C_T = 14$; $C_{T,S} = 0.93$.

Figure 17.- Concluded.

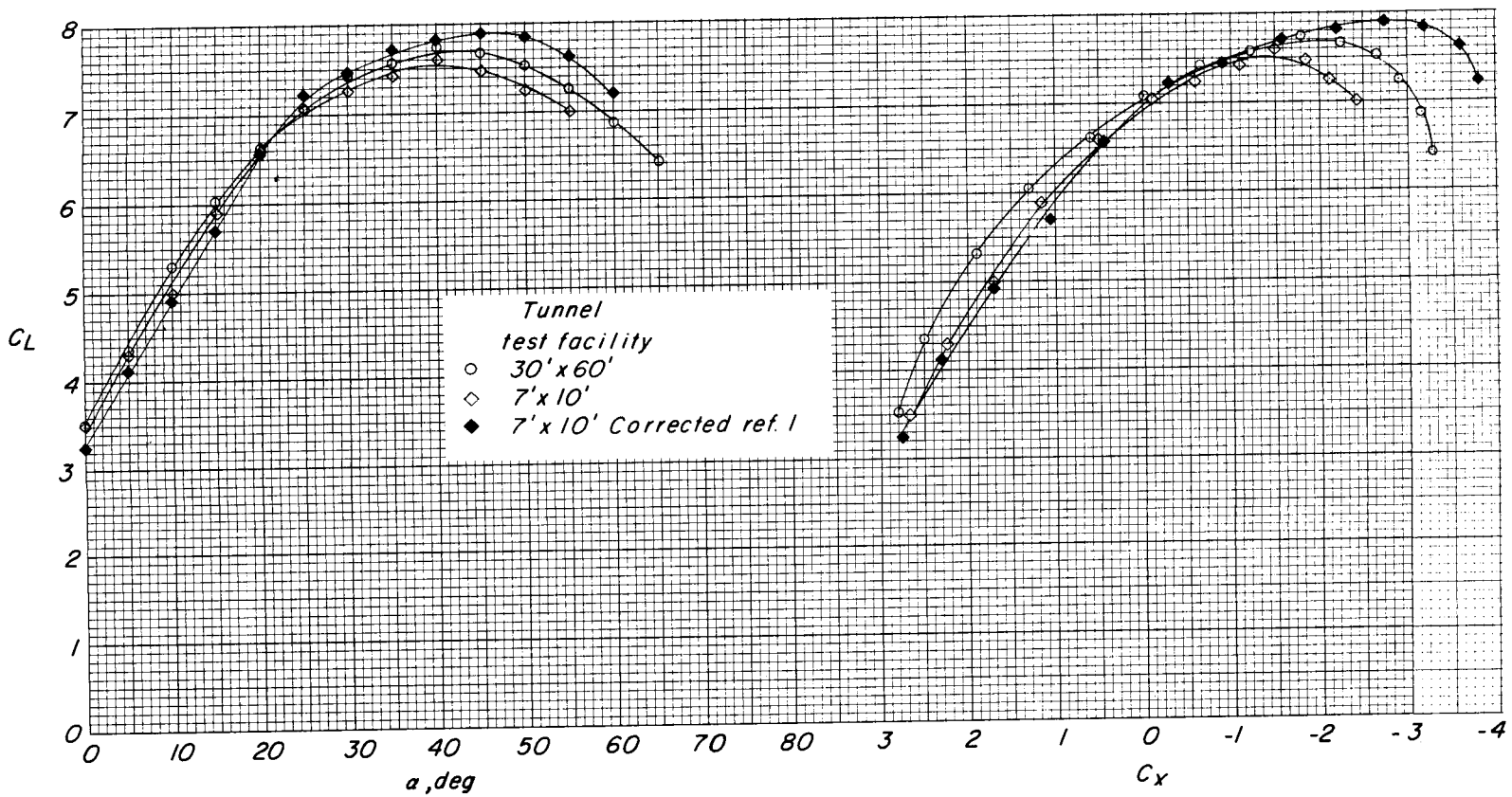

(a) $C_T = 4$; $C_{T,S} = 0.80$.

Figure 18.- Comparison of data from 7- by 10-foot tunnel (corrected and uncorrected) and data from 30- by 60-foot tunnel at constant thrust coefficients. Flaps on.

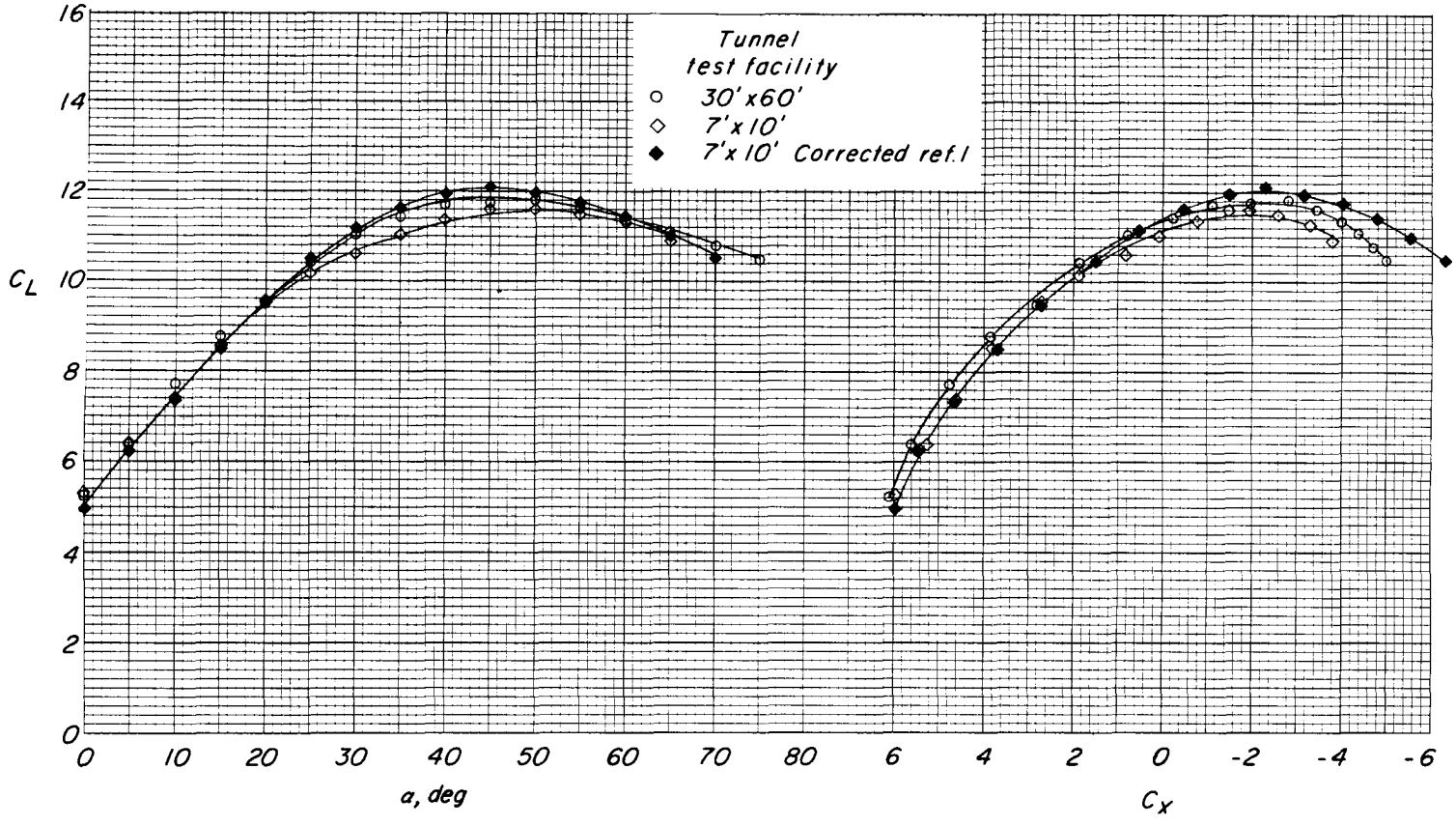

(b) $C_T = 8$; $C_{T,S} = 0.88$.

Figure 18.- Continued.

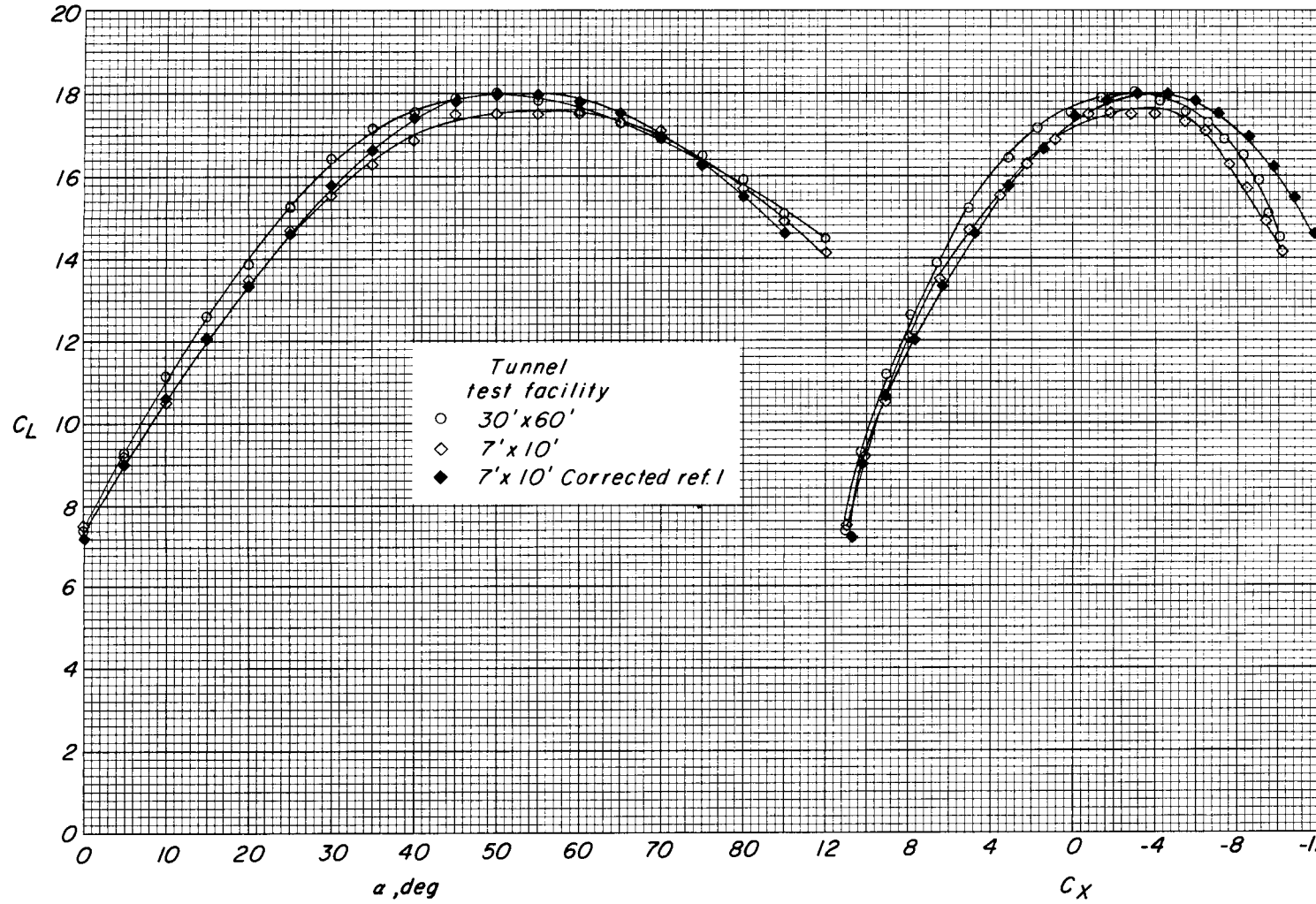

(c) $C_T = 14$; $C_{T,S} = 0.93$.

Figure 18.- Concluded.

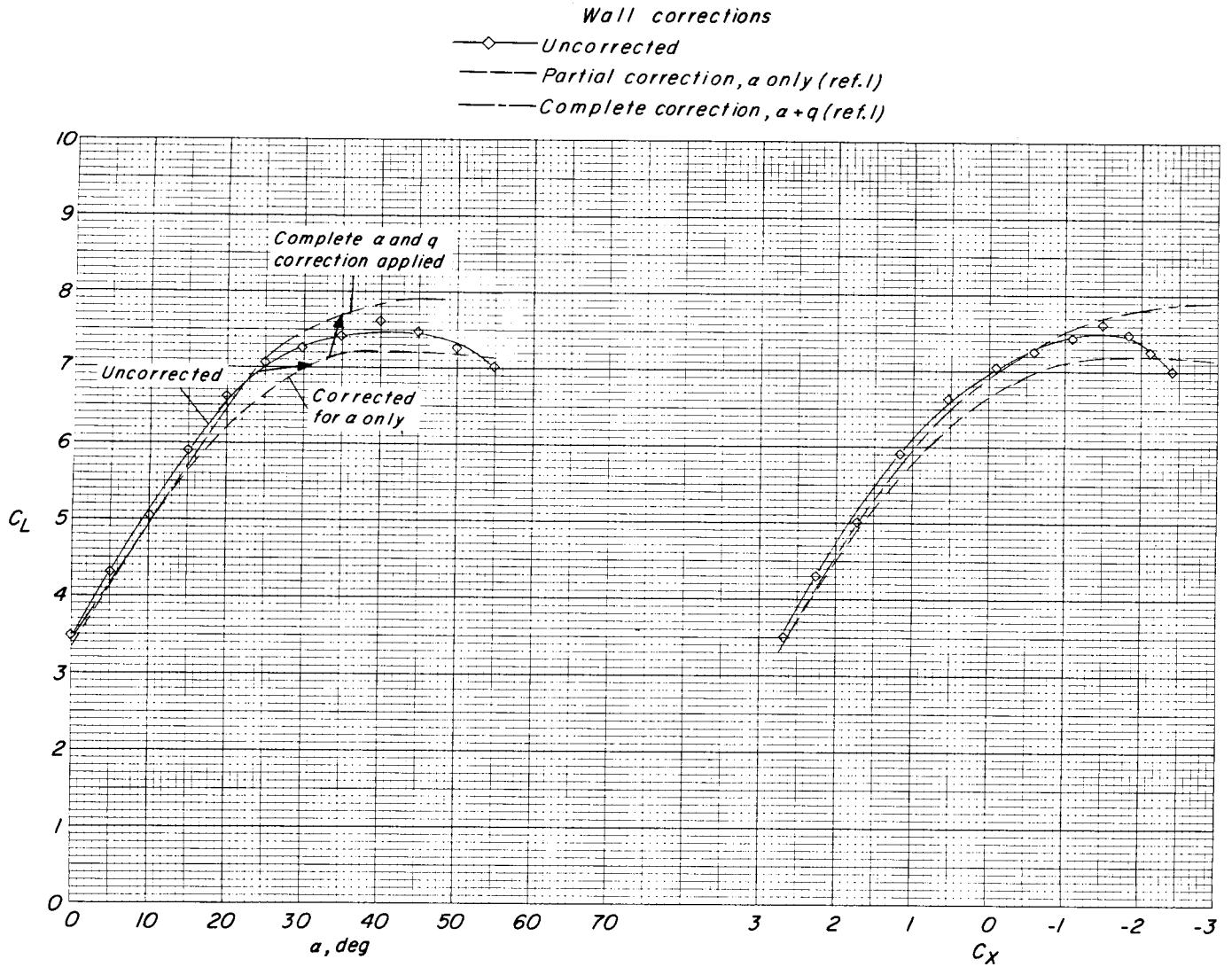

(a) $C_T = 4$; $C_{T,S} = 0.80$.

Figure 19.- Effects on data from 7- by 10-foot tunnel of wall corrections applied in steps, α correction first and then q correction. Flaps on.

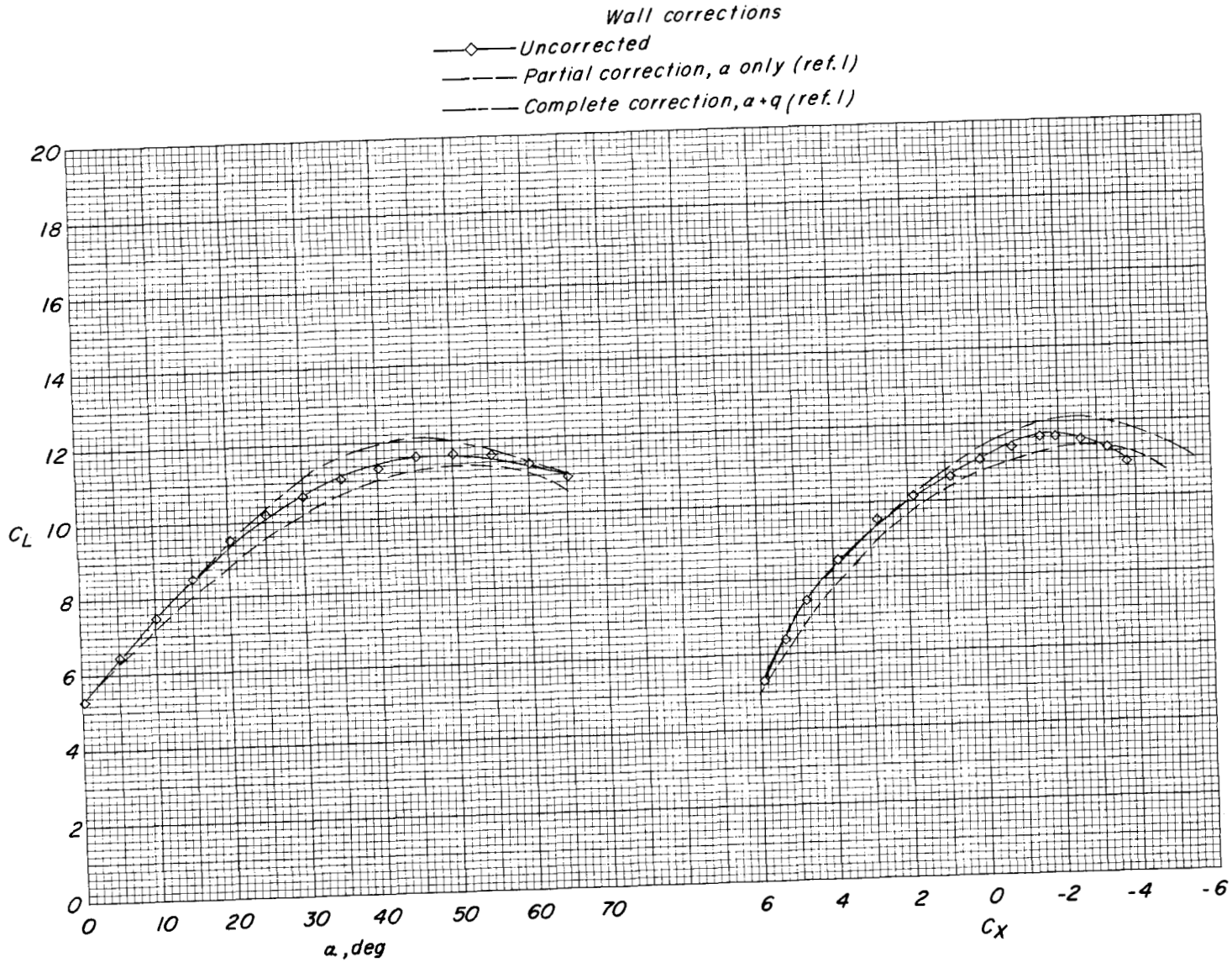

(b) $C_T = 8$; $C_{T,S} = 0.88$.

Figure 19.- Continued.

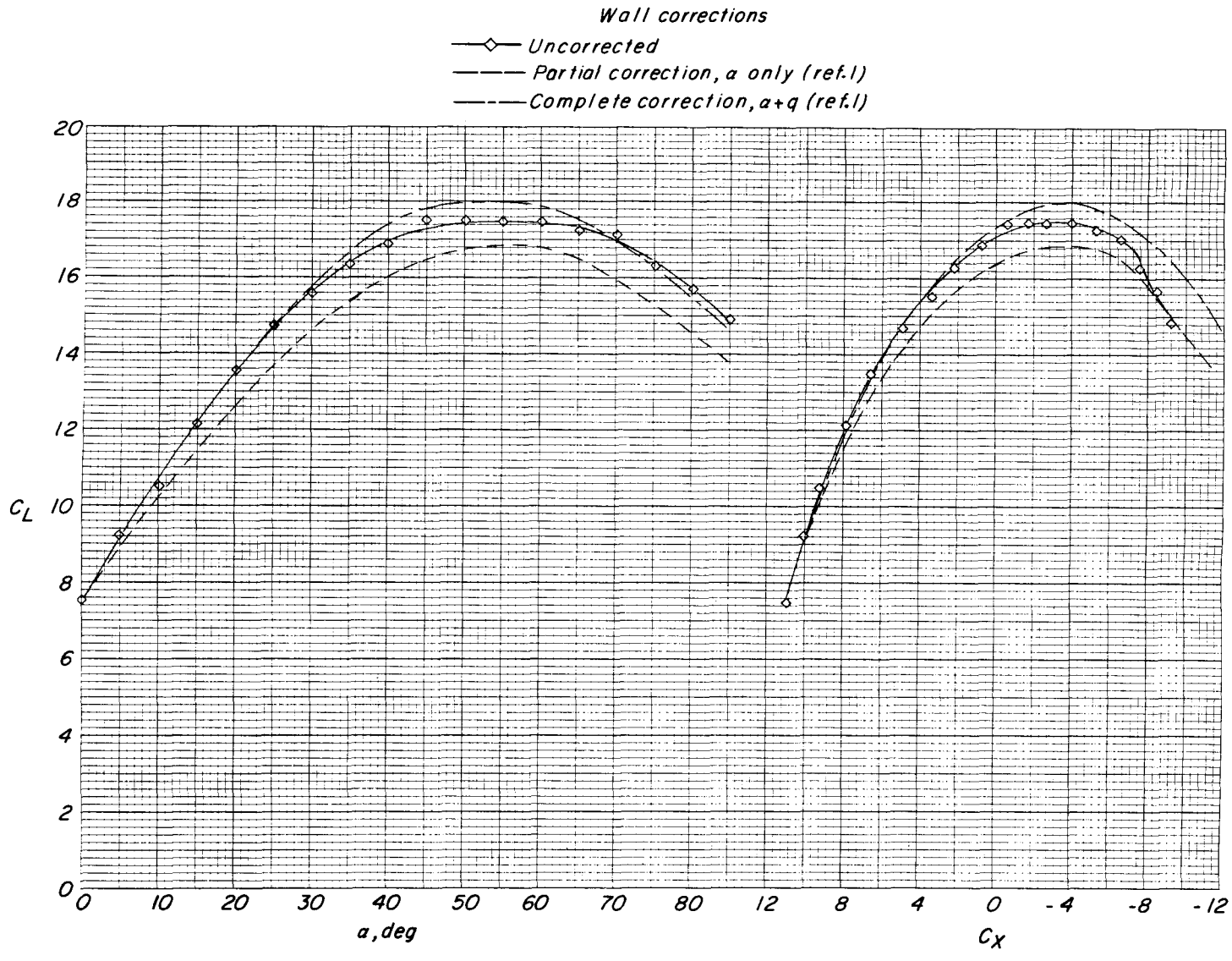

(c) $\epsilon_T = 14$; $C_{T,S} = 0.93$.

Figure 19.- Concluded.

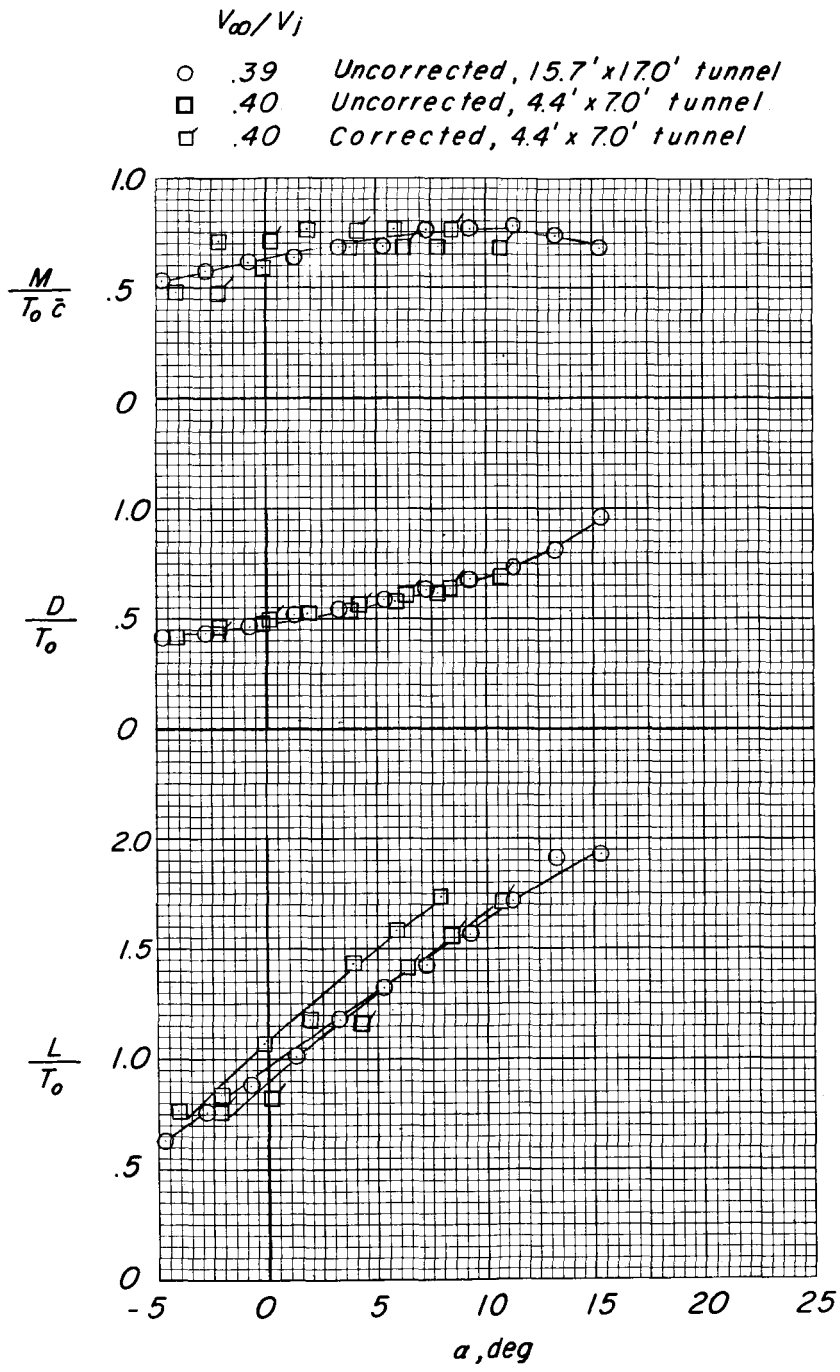

Figure 20.- Example of noncompensating wall effect on lift for buried-fan model (corrected and uncorrected data) taken from figure 18(c) of reference 4 for various values of ratio of free-stream velocity to jet-exit velocity V_∞/V_j. M, D, and L are pitching moment, drag, and lift for complete model, respectively; T_o is fan thrust in pounds; $\bar{c}$ is mean aerodynamic chord (0.814 foot).

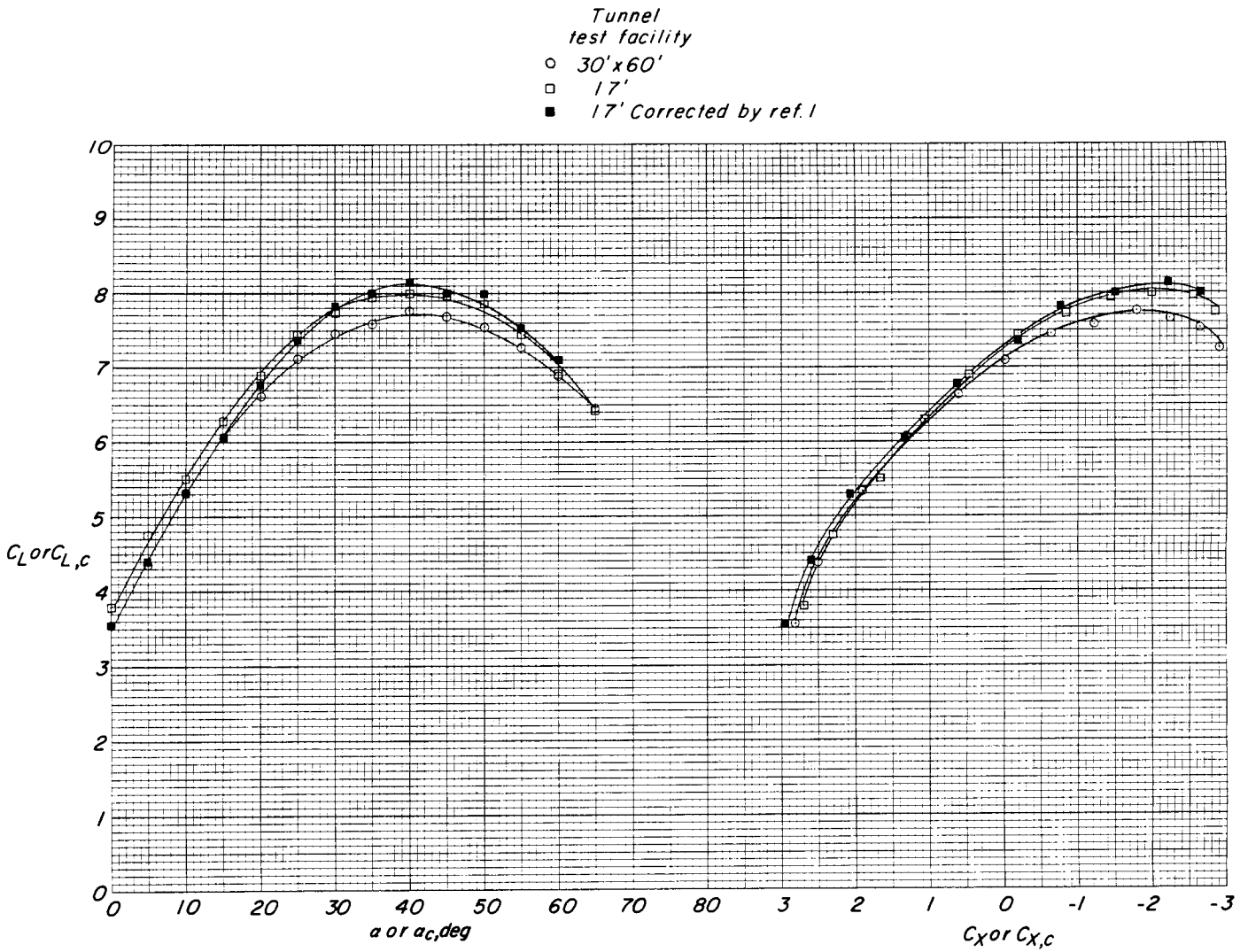

(a) $C_T = 4$; $C_{T,S} = 0.80$.

Figure 21.- Comparison of data from 17-foot test section (corrected and uncorrected) and data from 30- by 60-foot tunnel at constant thrust coefficients. Flaps on.

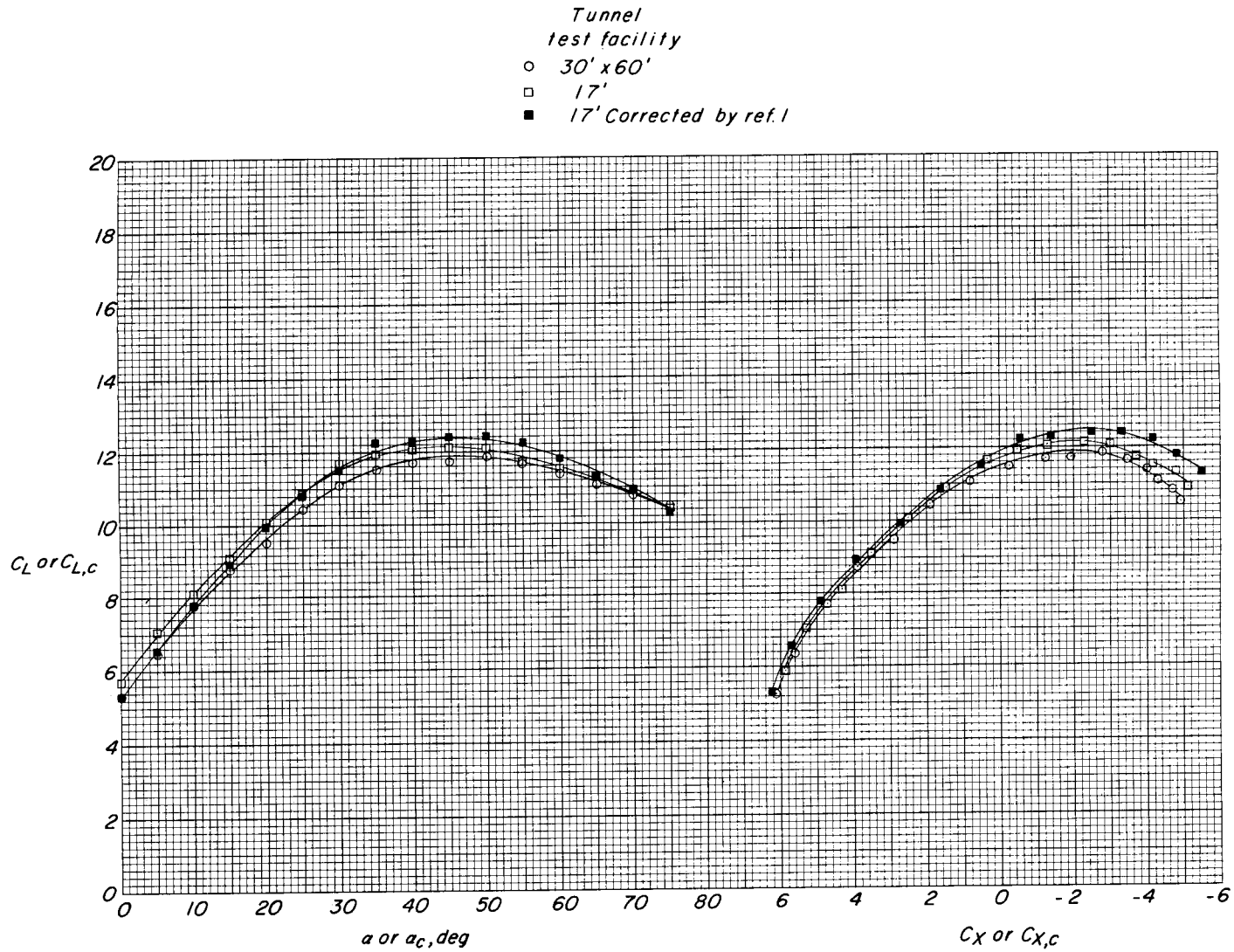

(b) $C_T = 8$; $C_{T,S} = 0.88$.

Figure 21.- Continued.

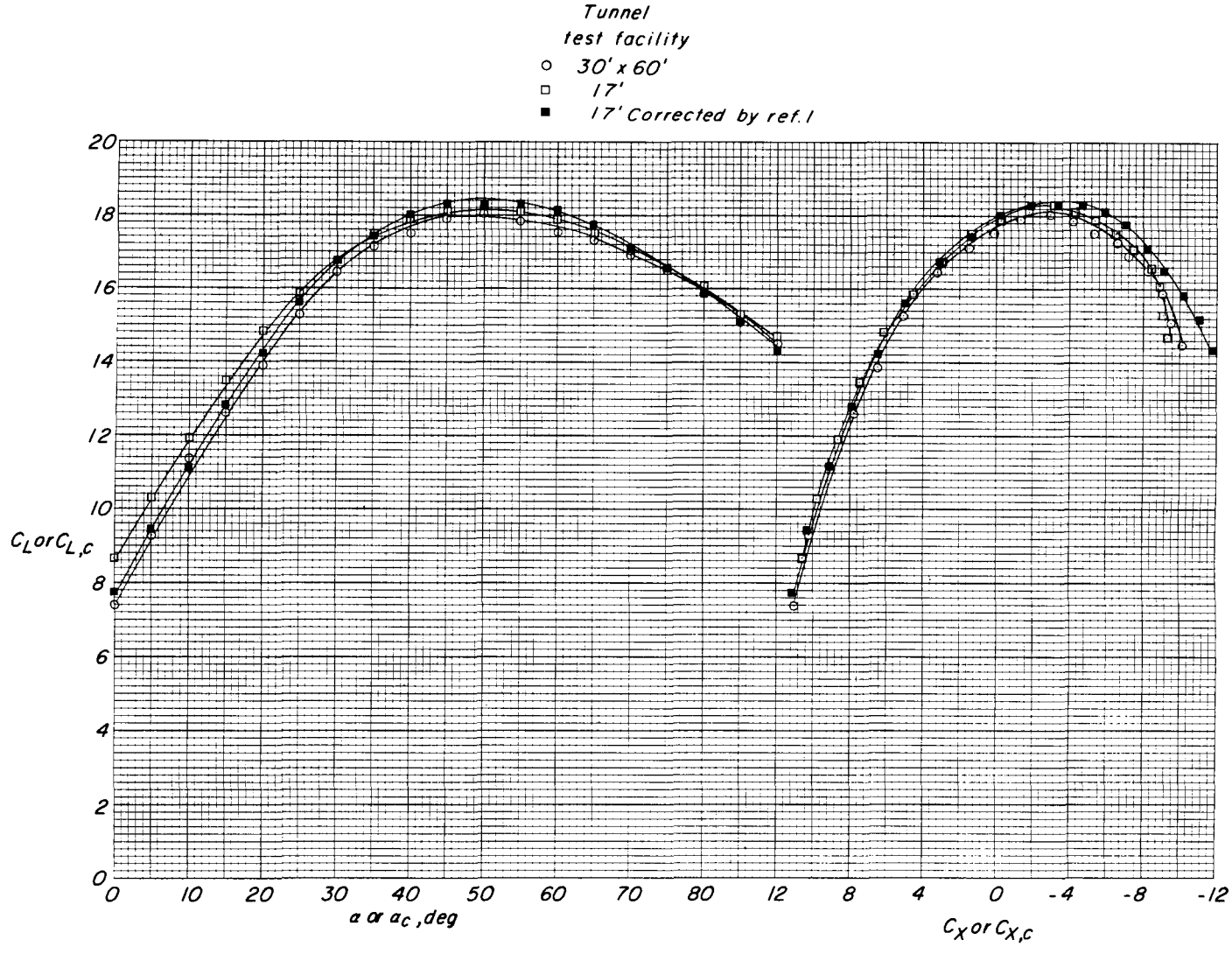

(c) $C_T = 14$; $C_{T,S} = 0.93$.

Figure 21.- Concluded.

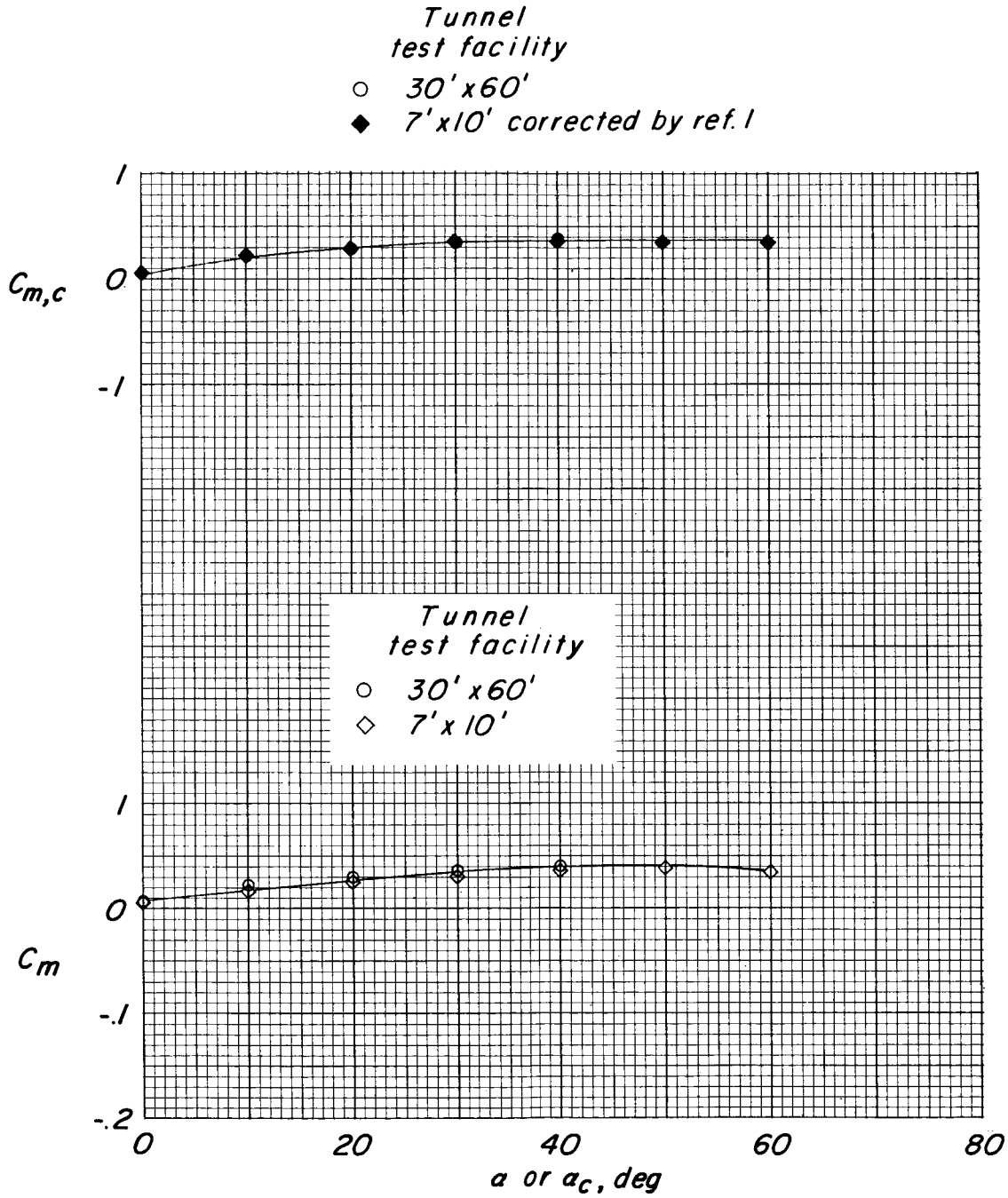

(a) $C_T = 4$; $C_{T,S} = 0.80$.

Figure 22.- Comparison of pitching-moment coefficients at constant thrust coefficients for basic data and data corrected for wall effects by method of reference 1 for 7- by 10-foot and 30- by 60-foot tunnels. Flaps off.

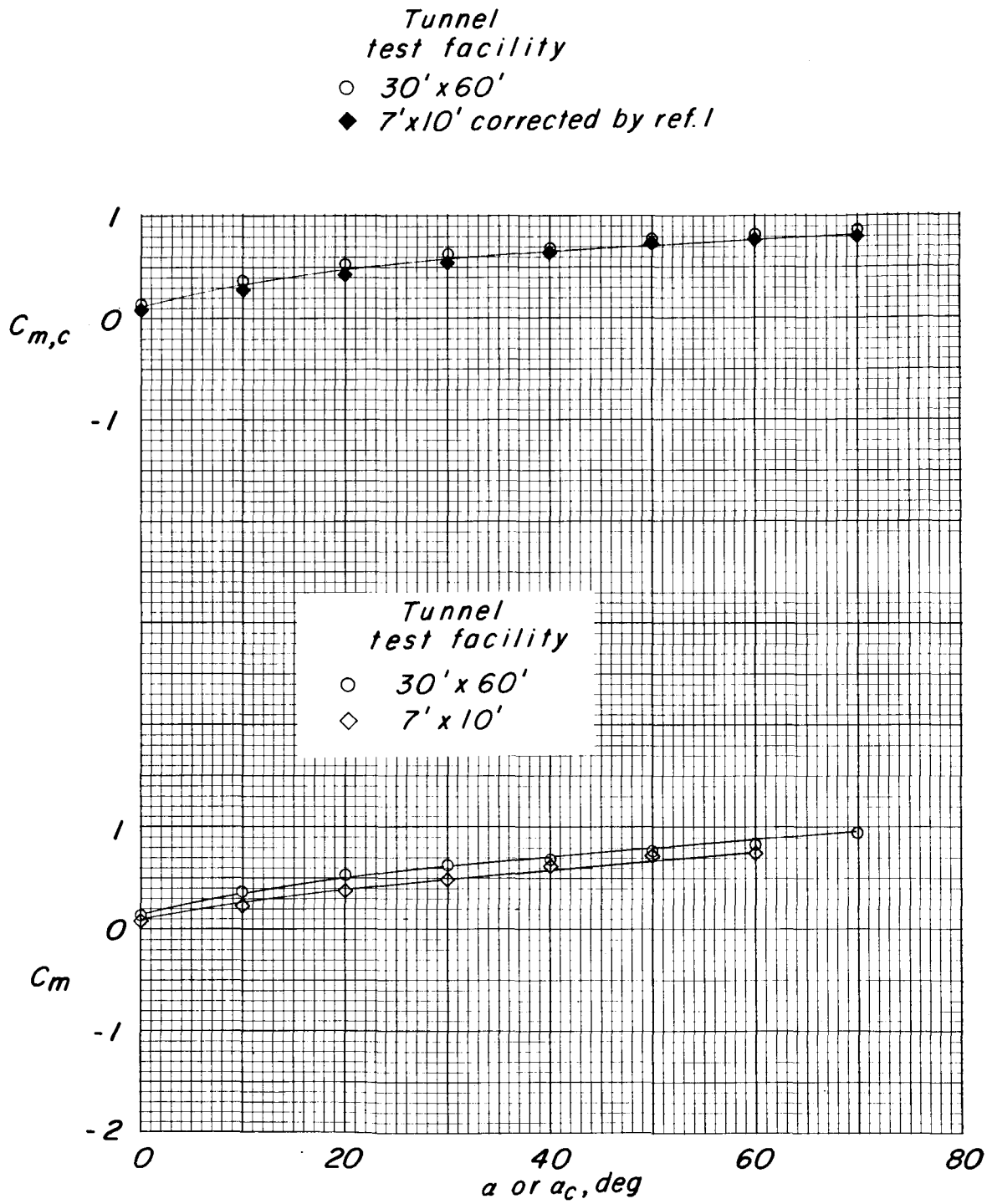

(b) $C_T = 8$; $C_{T,S} = 0.88$.

Figure 22.- Continued.

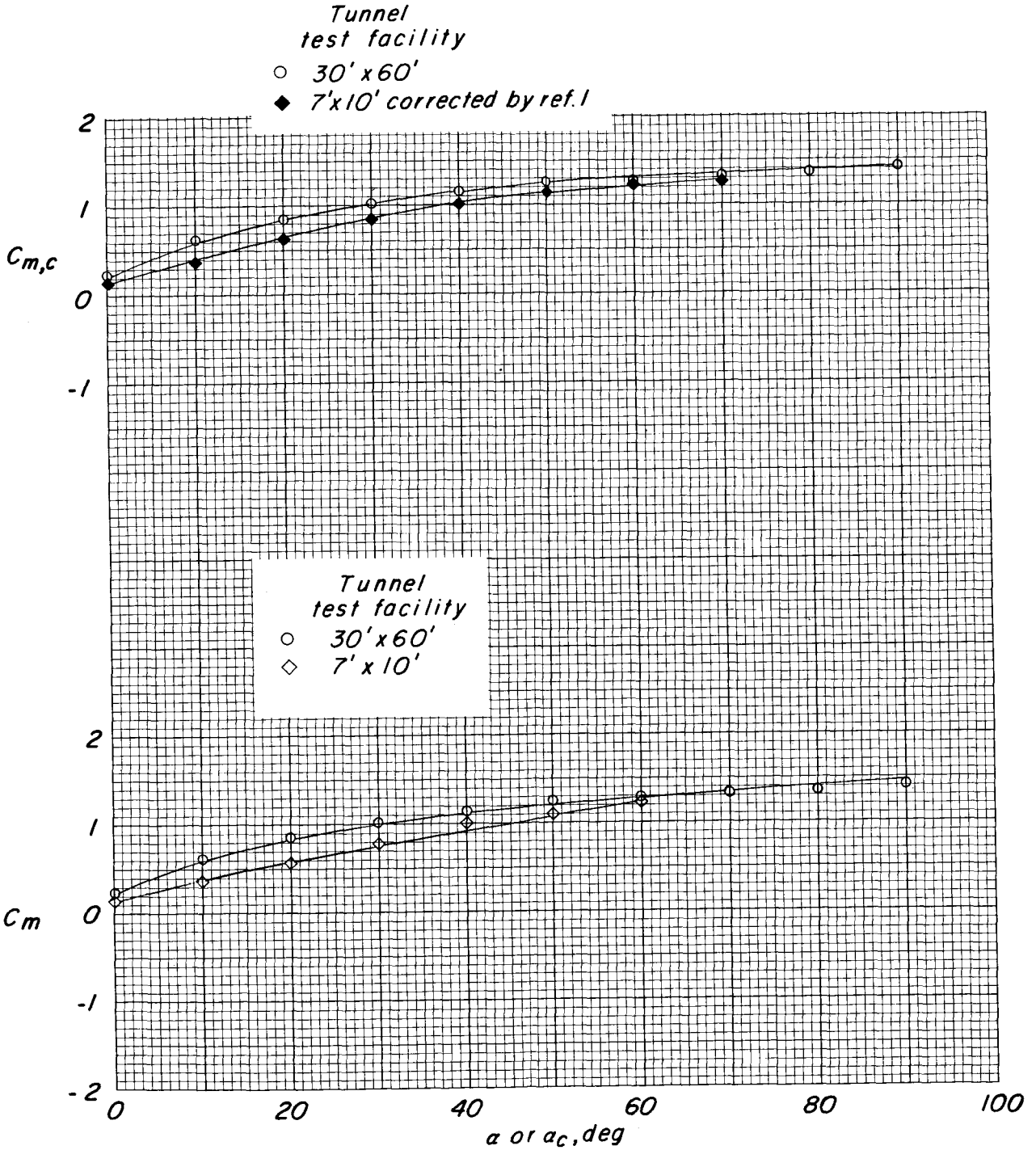

(c) $C_T = 14$; $C_{T,S} = 0.93$.

Figure 22.- Concluded.

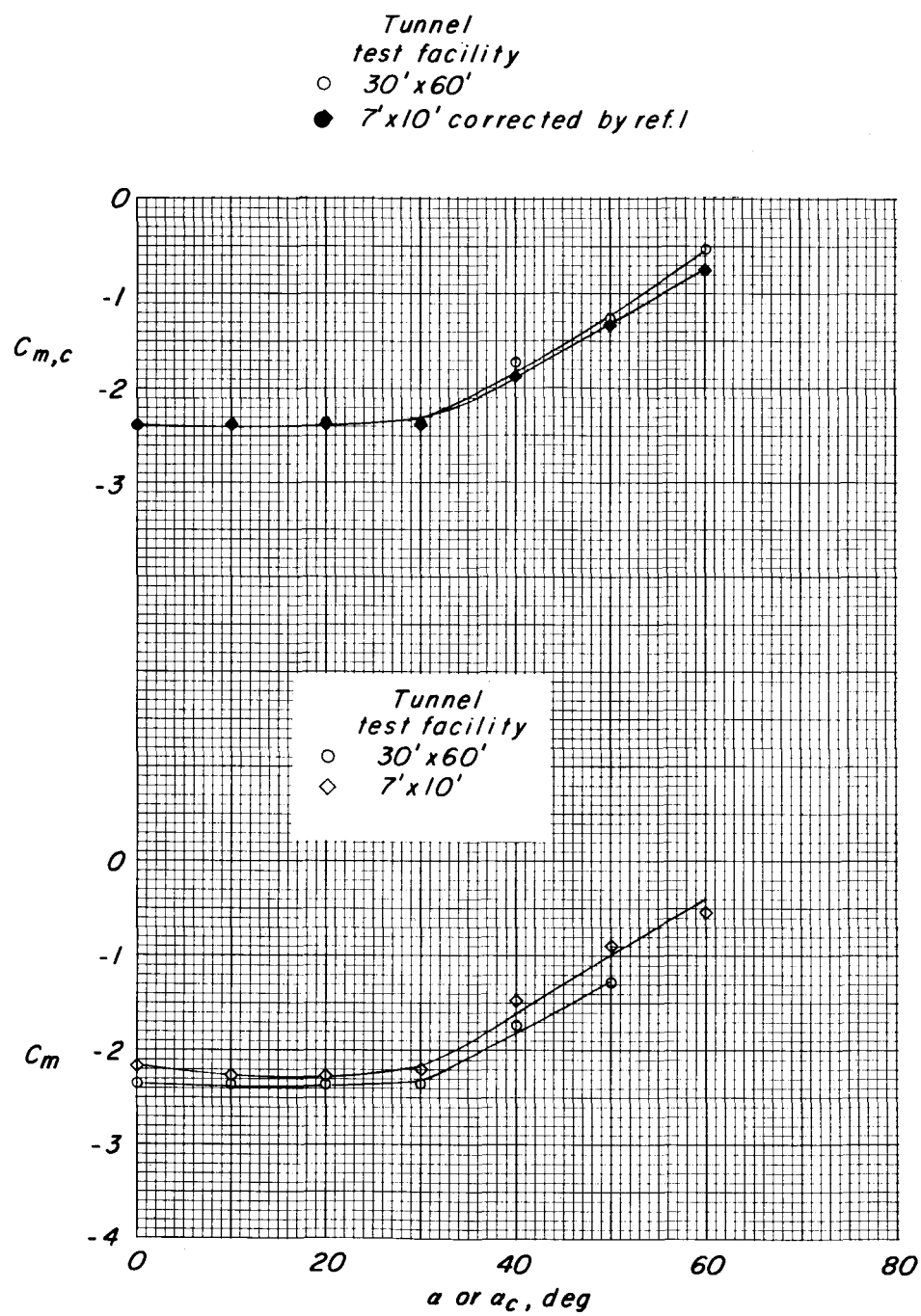

(a) $C_T = 4$; $C_{T,S} = 0.80$.

Figure 23.- Comparison of pitching-moment coefficients at constant thrust coefficients for basic data and data corrected for wall effects by method of reference 1 for 7- by 10-foot and 30- by 60-foot tunnels. Flaps on.

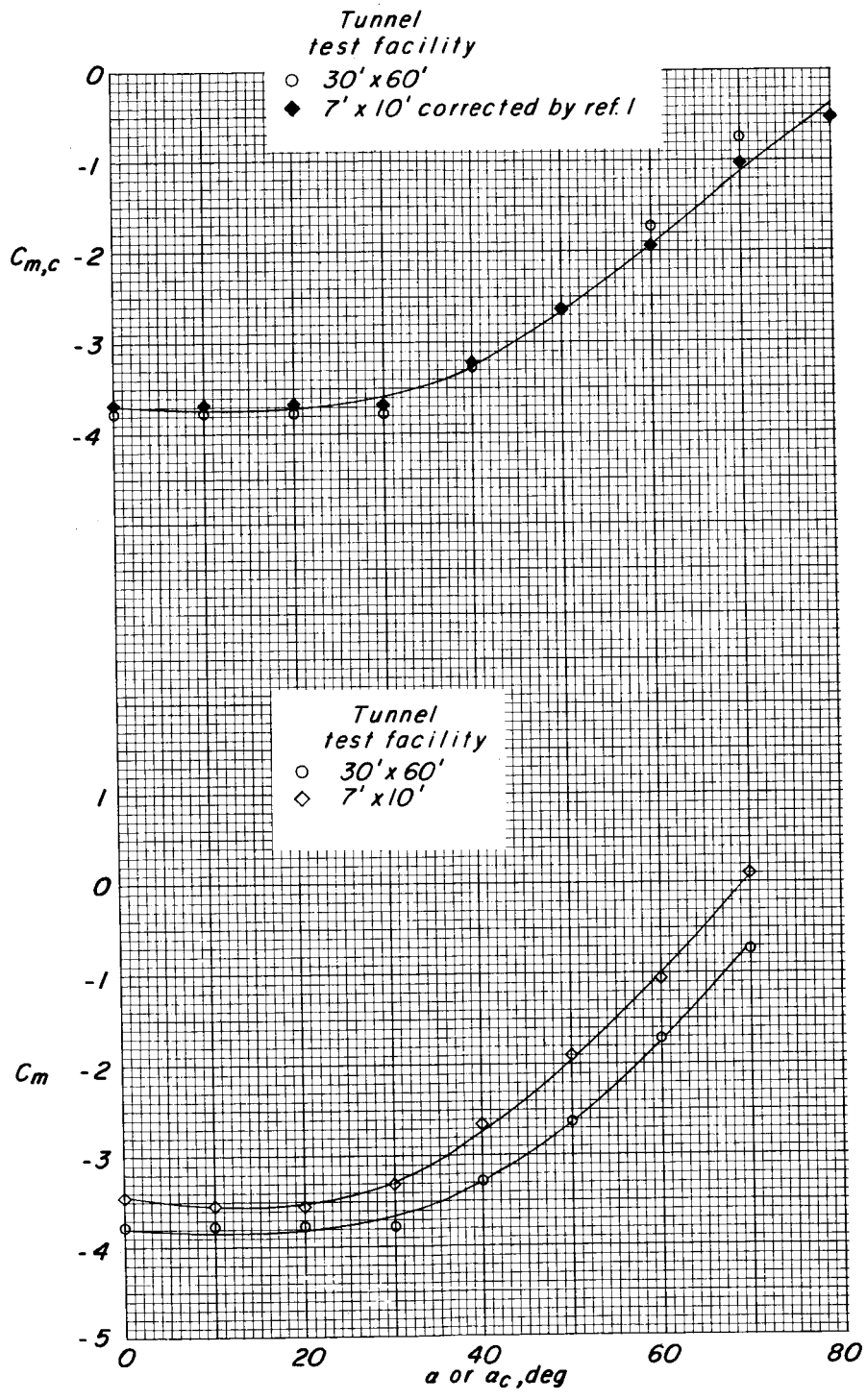

(b) $C_T = 8$; $C_{T,S} = 0.88$.

Figure 23.- Continued.

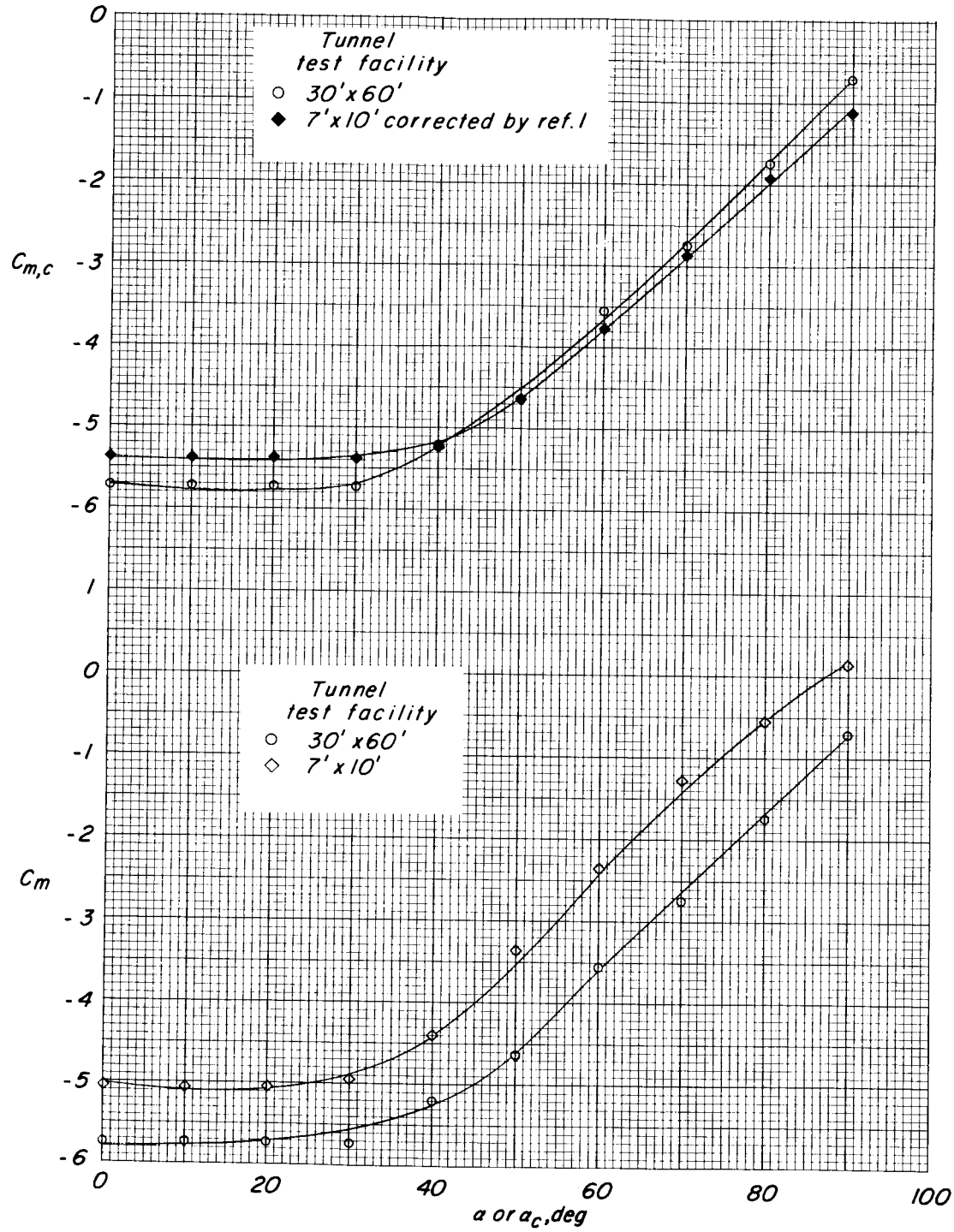

(c) $C_T = 14$; $C_{T,S} = 0.93$.

Figure 23.- Concluded.

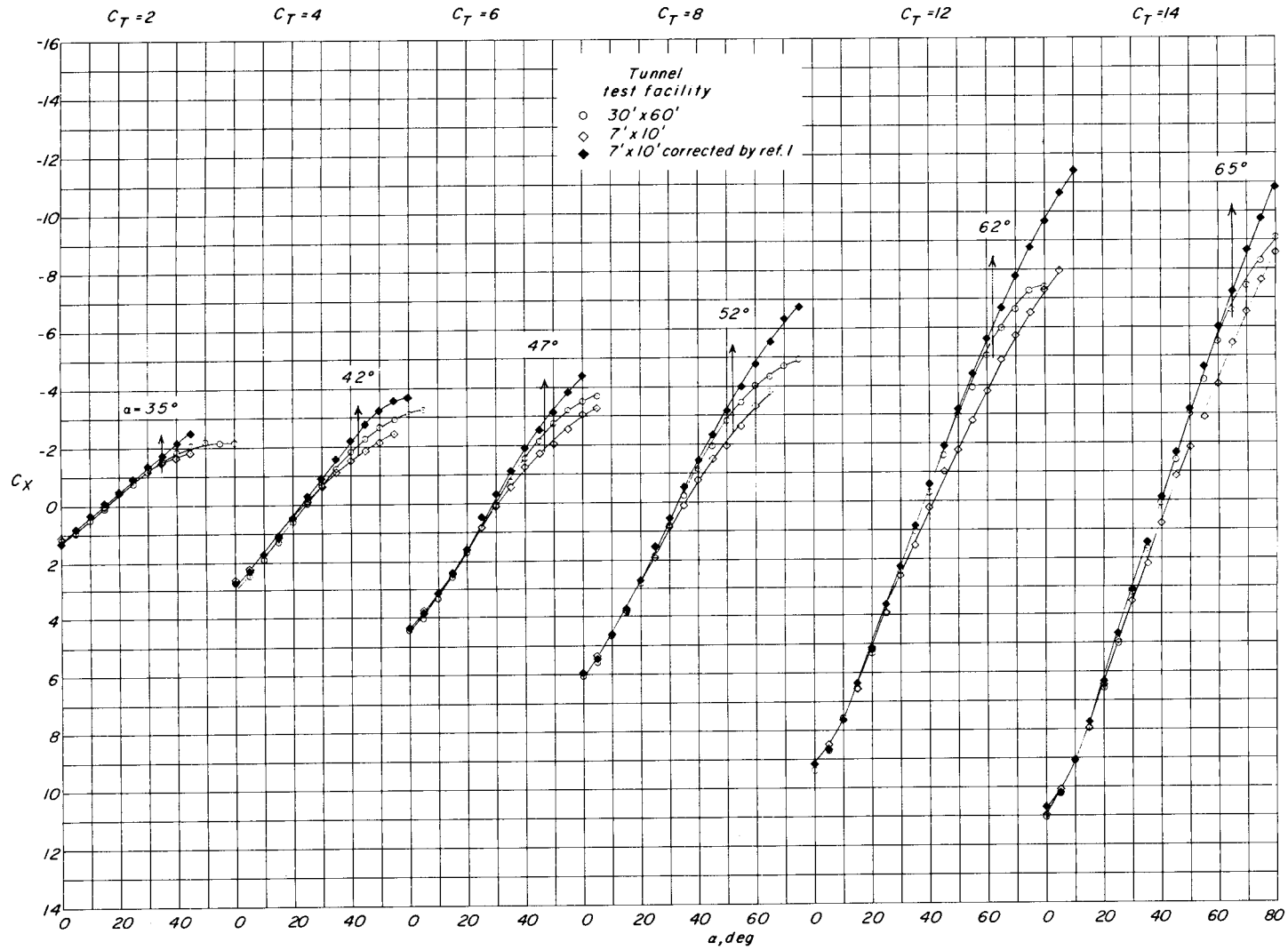

(a) Flaps on.

Figure 24.- Longitudinal-force-coefficient polars indicating overcorrection of data from 7- by 10-foot tunnel. Data presented for constant thrust coefficients.

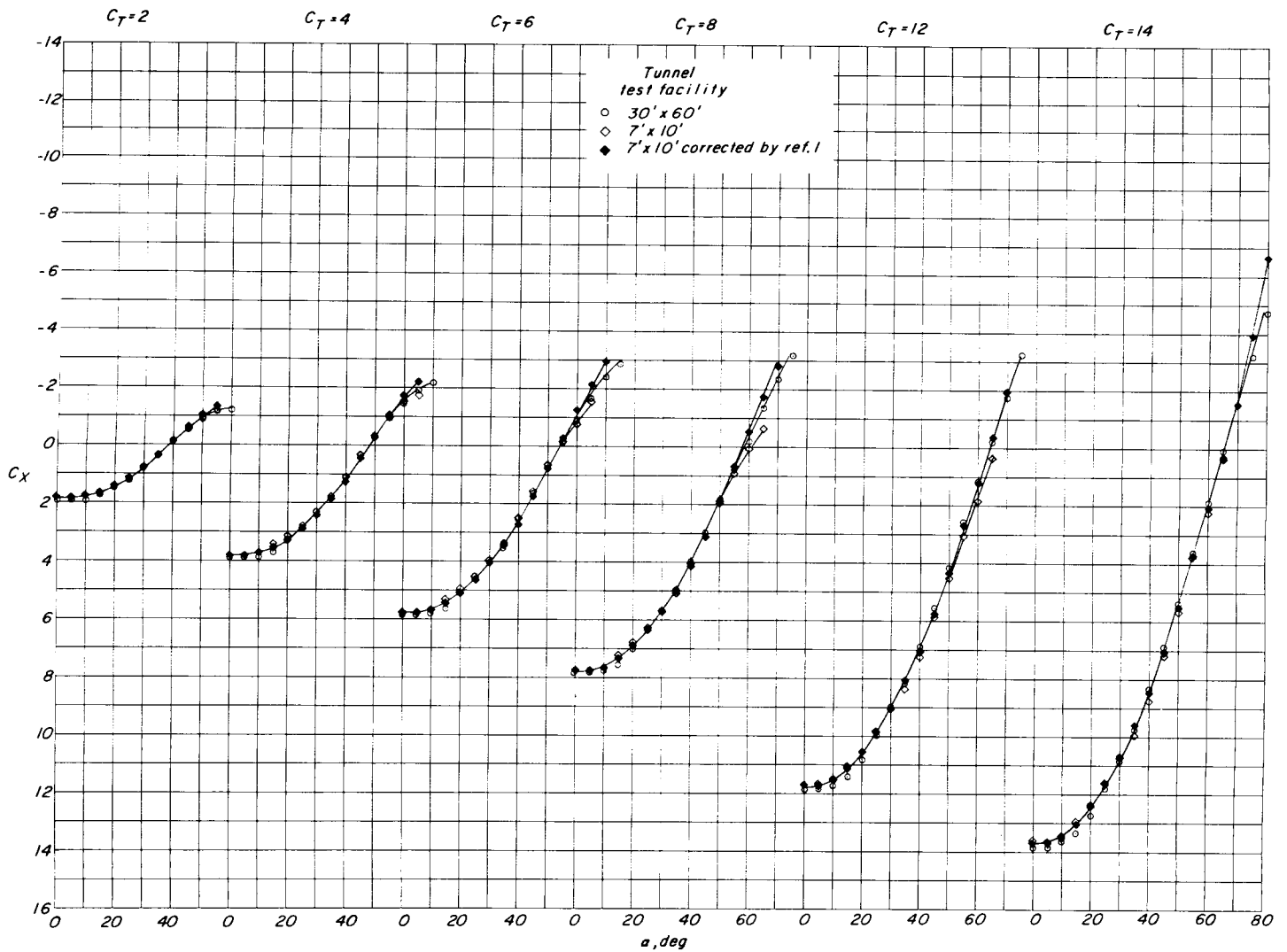

(b) Flaps off.

Figure 24.- Concluded.

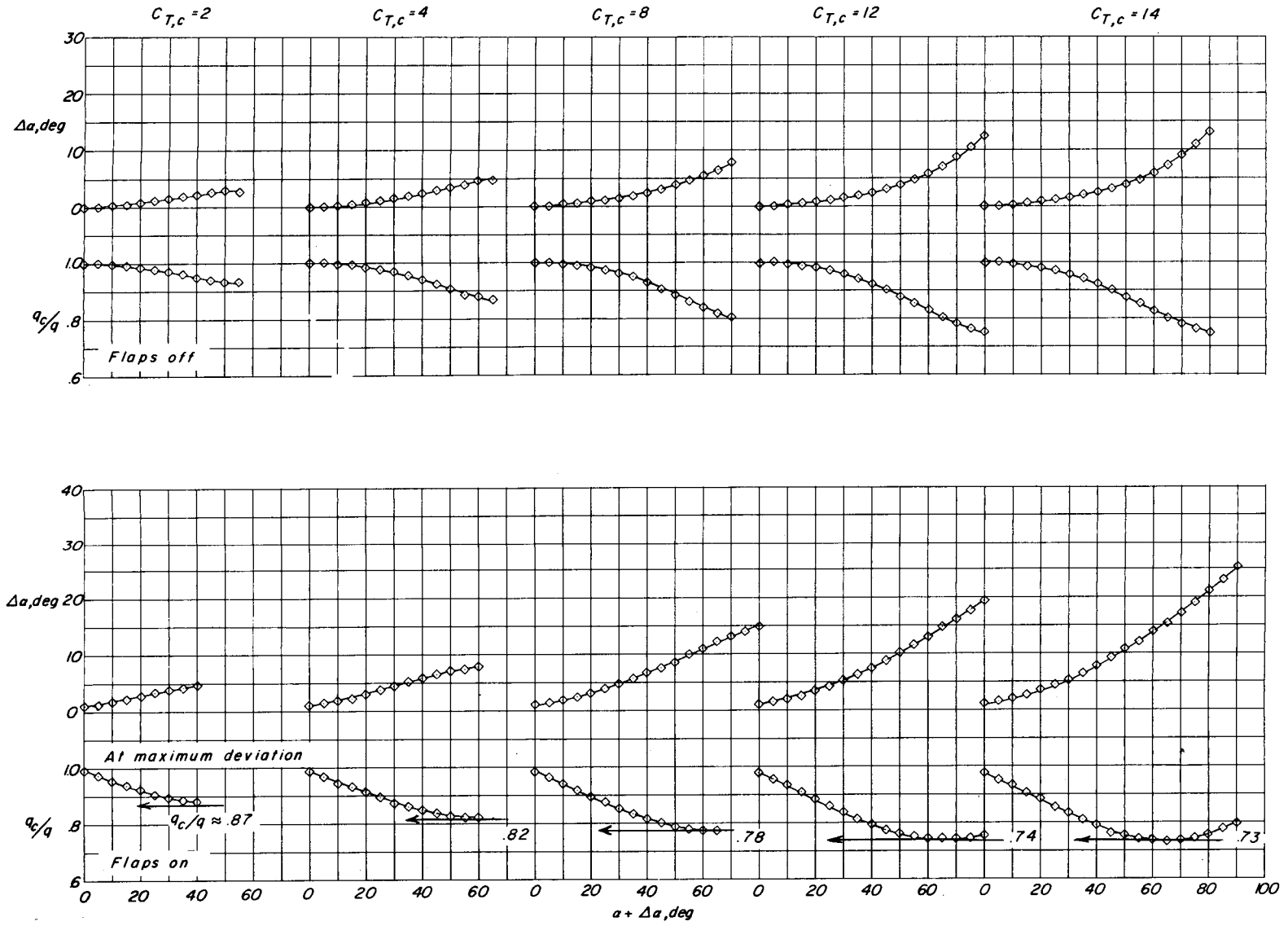

Figure 25.- Wall corrections of q_c/q and $\Delta\alpha$ for data from 7- by 10-foot tunnel at selected thrust coefficients.

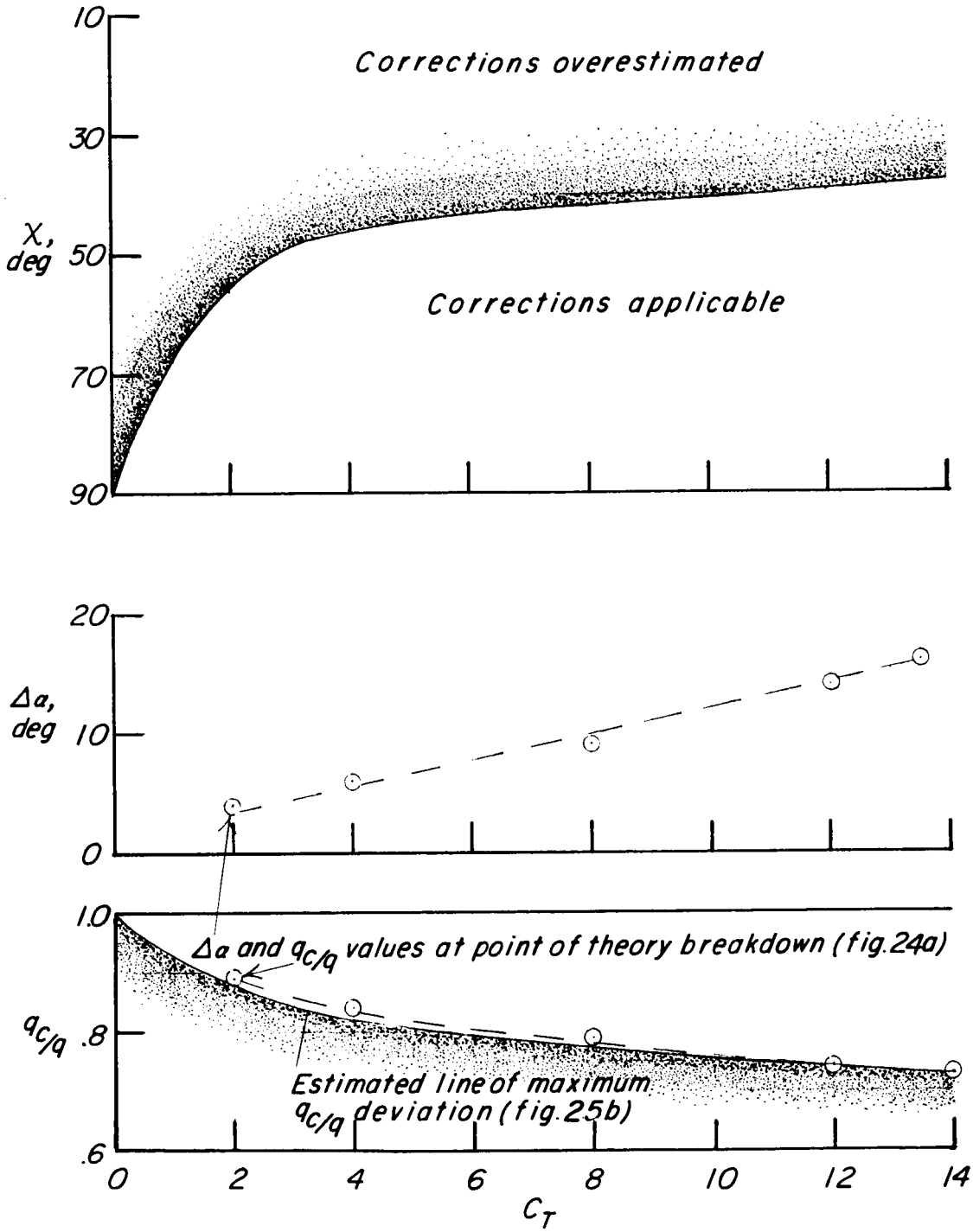

Figure 26.- Boundaries for X, $\Delta\alpha$, and q_c/q at which the theory overestimation of longitudinal-force coefficient C_X occurred, taken from flaps-on data from 7- by 10-foot tunnel.

APPENDIX A

METHOD USED IN APPLYING CORRECTIONS

The general method of applying corrections is presented in appendix C of reference 1. However, no discussion is included for minimizing electronic machine time.

A method of applying corrections to test data with attention to certain time-saving features for machine calculation is presented in this appendix.

Equations (A1), (A2), and (A3) are basic equations (35), (37), and (36), respectively, from reference 1 and are written as follows:

$$W_h = -\sqrt{\frac{L}{n\rho A_m}} \qquad n = 2 \text{(for wing-propeller configuration)} \tag{A1}$$

Then compute

$$\frac{V}{W_h} = \frac{V}{W_o}\frac{W_o}{W_h} \tag{A2}$$

and

$$\left(\frac{W_o}{W_h}\right)^4 = \frac{1}{1 + \left(\frac{V}{W_o} + \frac{D_i}{L}\right)^2} \tag{A3}$$

Assume $D = D_i$ for purposes of simplicity. This assumption is approximately correct at very low speeds and, therefore

$$\frac{D}{L} = \frac{D_i}{L} \tag{A4}$$

Given $\frac{D}{L}$ and $\frac{V}{W_h}$ the nomograph in reference 1 can be used to solve for $\frac{W_o}{W_h}$ and X. However, this is a slow hand process for computing corrections. For machine use, the quartic in equation (A3) must be solved. Since only one root, the root between zero and one, is needed to determine $\frac{W_o}{W_h}$ and then the skew angle, the solution of the entire quartic wastes time.

APPENDIX A

A method for solving a quartic with a root between zero and one is the Newton-Raphson method (ref. 12). This method is outlined as follows:

Putting equation (A3) in the form

$$f(x) = \left[1 + \left(\frac{D_i}{L}\right)^2\right]\left(\frac{W_o}{W_h}\right)^4 + 2\,\frac{V}{W_h}\,\frac{D_i}{L}\left(\frac{W_o}{W_h}\right)^3 + \left(\frac{V}{W_h}\right)^2\left(\frac{W_o}{W_h}\right)^2 - 1 = 0 \qquad (A5)$$

Assume $D = D_i$ and set

$$A = 1 + \left(\frac{D}{L}\right)^2 \qquad B = 2\,\frac{V}{W_h}\,\frac{D}{L} \qquad C = \left(\frac{V}{W_h}\right)^2 \qquad D = 0 \qquad E = -1$$

Equation (A5) can be written

$$f(x) = A\left(\frac{W_o}{W_h}\right)^4 + B\left(\frac{W_o}{W_h}\right)^3 + C\left(\frac{W_o}{W_h}\right)^2 + D\left(\frac{W_o}{W_h}\right) + E = 0 \qquad (A6)$$

$$f'(x) = 4A\left(\frac{W_o}{W_h}\right)^3 + 3B\left(\frac{W_o}{W_h}\right)^2 + 2C\left(\frac{W_o}{W_h}\right) + D = 0 \qquad (A7)$$

Assume that $\frac{W_o}{(W_h)_1} = 0.5$ and substitute this value in equations (A6) and (A7) for $\frac{W_o}{W_h}$; then

$$\frac{W_o}{(W_h)_2} = \frac{W_o}{(W_h)_1} - \frac{f(x)}{f'(x)} \qquad (A8)$$

Substitute $\frac{W_o}{(W_h)_2}$ in equations (A6) and (A7) and iterate until $\frac{f(x)}{f'(x)} < 0.001$. This now gives the solution for $\frac{W_o}{W_h}$ to three decimal places. This procedure takes an average of 10 seconds on a computer. The general solution for all 4 roots of a quartic on this machine takes 130 seconds. Obviously considerable time can be saved in the computing by using the Newton-Raphson method.

APPENDIX A

Solve for $\frac{V}{W_o}$ as follows:

$$\frac{V}{W_o} = \frac{V/W_h}{W_o/W_h} \tag{A9}$$

The wake skew angle can be determined from

$$|\chi| = \cos^{-1}\left(\frac{W_o}{W_h}\right)^2 \tag{A10}$$

and the test for the sign of χ is as follows:

$$\text{If } \frac{V}{-W_o} > \frac{D}{L}, \quad \chi \text{ is positive; if } \frac{V}{-W_o} < \frac{D}{L}, \quad \chi \text{ is negative.}$$

At this point the four interference factors δ must be determined. These δ values can be taken from references 7, 8, 9, and 10. If the model (lifting element) remains in the same location in the tunnel for all tests these δ values will hold for all the data. Each time the model location is changed the δ values must be changed to correspond to the new location.

The δ values can be programed into a lookup table by using slope intercept method or the values can be programed into a curve fit. Both methods present δ factor as a function of χ. The slope intercept method is the faster of the two for this type of curve. After the values of δ have been determined the data reduction is straightforward.

Compute as follows:

$$\frac{\Delta w_L}{V} = \delta_{w,L} \frac{M_w}{M_T}$$

where

$$\frac{M_w}{M_T} = \frac{A_m/A_T}{V/W_o}$$

$$\frac{\Delta u_L}{V} = \delta_{u,L} \frac{M_w}{M_T}$$

$$\frac{\Delta w_D}{V} = \delta_{w,D} \frac{M_u}{M_T}$$

where

$$\frac{M_u}{M_T} = \frac{M_w}{M_T}\frac{D_i}{L}$$

$$\frac{\Delta u_D}{V} = \delta_{u,D}\frac{M_u}{M_T} \tag{A11}$$

$$\frac{\Delta w}{V} = \frac{\Delta w_L}{V} + \frac{\Delta w_D}{V}$$

$$\frac{\Delta u}{V} = \frac{\Delta u_L}{V} + \frac{\Delta u_D}{V} \tag{A12}$$

$$\Delta\alpha = \arctan\left(\frac{\frac{\Delta w}{V}}{1 + \frac{\Delta u}{V}}\right) \tag{A13}$$

$$\frac{q_c}{q} = \left(1 + \frac{\Delta u}{V}\right)^2 + \left(\frac{\Delta w}{V}\right)^2 \tag{A14}$$

$$L_c = L\cos\Delta\alpha - D\sin\Delta\alpha \tag{A15}$$

$$D_c = L\sin\Delta\alpha + D\cos\Delta\alpha \tag{A16}$$

$$q_c = \frac{q_c}{q}\,q \tag{A17}$$

$$C_{L,c} = \frac{L_c}{q_c S} \tag{A18}$$

$$C_{D,c} = \frac{D_c}{q_c S} \tag{A19}$$

$$C_{m,c} = \frac{M_Y}{q_c S\bar{c}} \tag{A20}$$

APPENDIX B

BASIC UNCORRECTED POWER-ON LIFT, LONGITUDINAL-FORCE, AND PITCHING-MOMENT DATA

The basic uncorrected power-on lift, longitudinal-force, and pitching-moment data from the tests in the three tunnels are presented for a number of nearly constant thrust-coefficient conditions in figure B1 (flaps off) and figure B2 (flaps on).

The stall shown in the lift- and longitudinal-force data from the 17-foot test section (for flaps off, at low thrust coefficients, figs. B1(a) to (d)) is not believed to be a wall effect. Repeat tests showed that, although transition was fixed by a roughness strip (fig. 3), in this range of thrust coefficients the stall was not repeatable and the data would agree sometimes with that shown in the figures and sometimes with the data from the other two test sections.

Some of the differences in the lift- and longitudinal-force data for the three test facilities are due to the fact that it was not possible to hold thrust coefficient exactly constant in each of the facilities. It was necessary, therefore, to cross-plot the data to obtain comparisons at constant thrust coefficient.

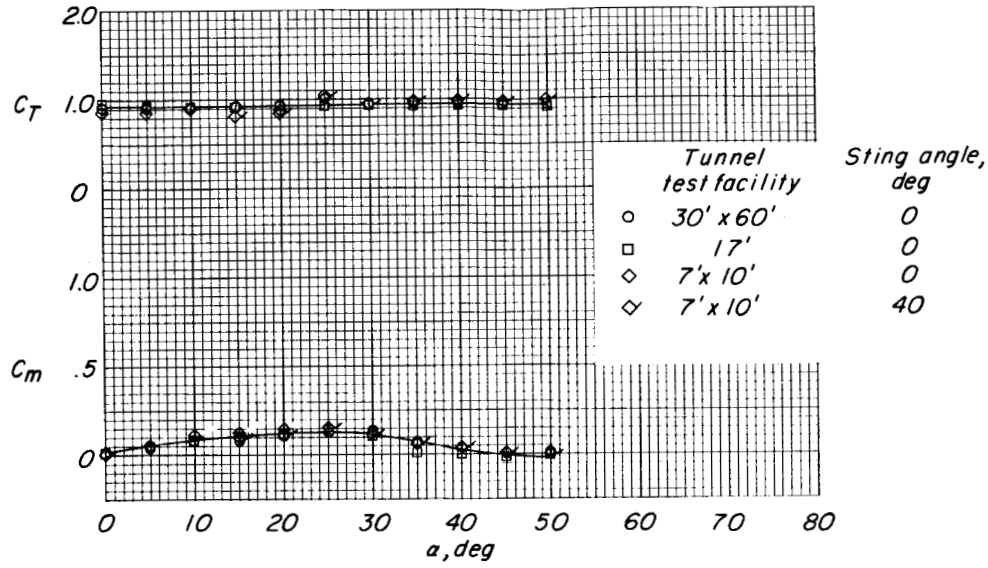

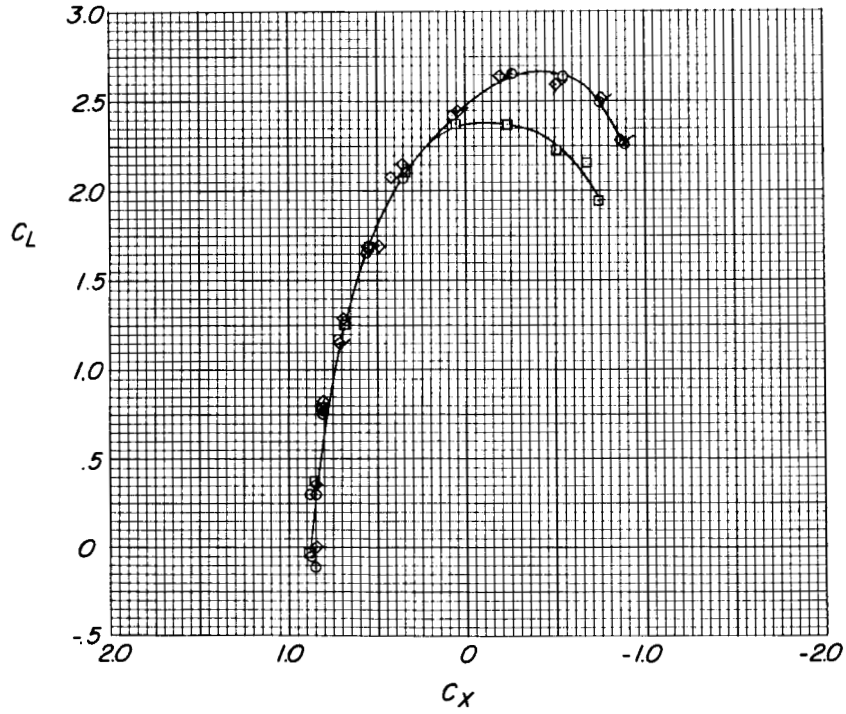

(a) $C_T \approx 1.0$; $C_{T,S} \approx 0.50$.

Figure B1.- Comparison of uncorrected data for tests in three facilities for a range of thrust coefficients. Flaps off.

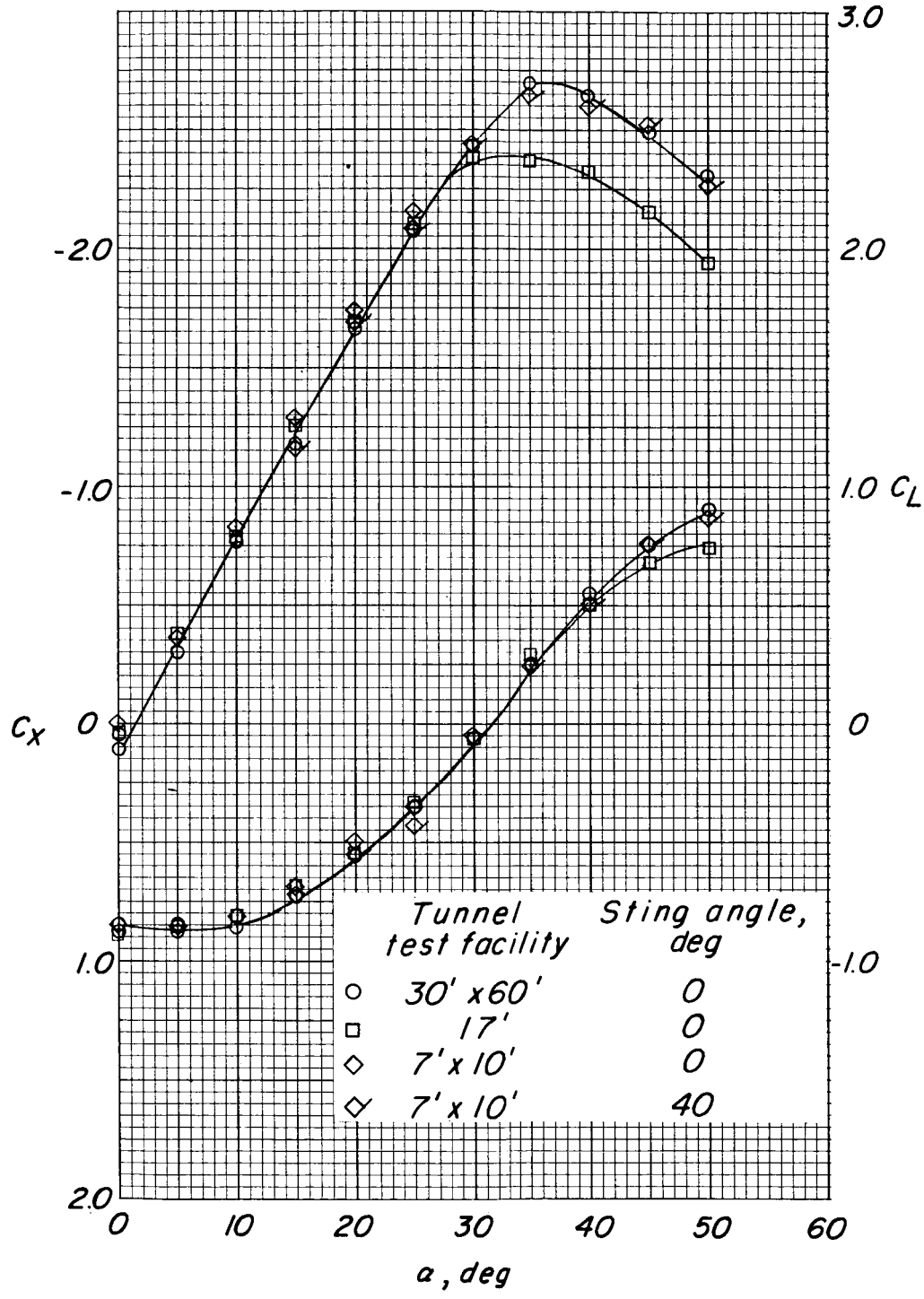

(a) Concluded.

Figure B1.- Continued.

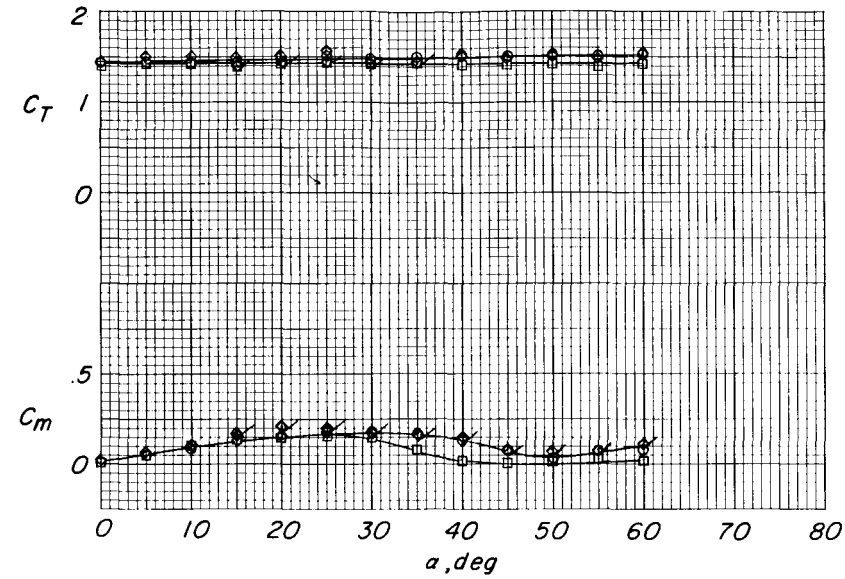

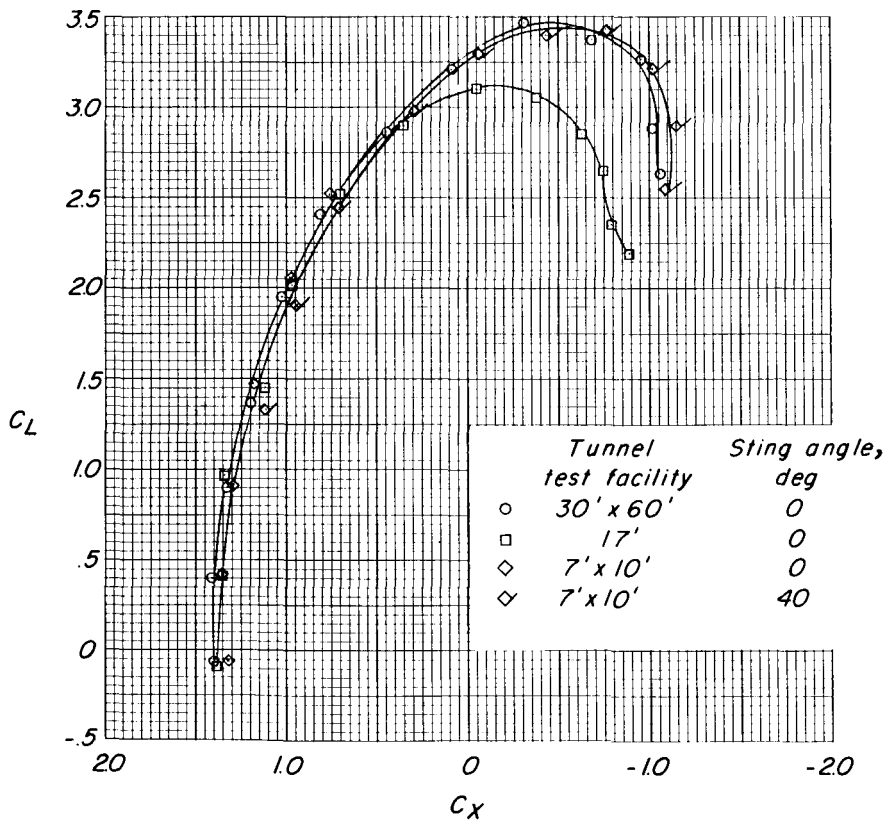

(b) $C_T \approx 1.5$; $C_{T,S} \approx 0.60$.

Figure B1.- Continued.

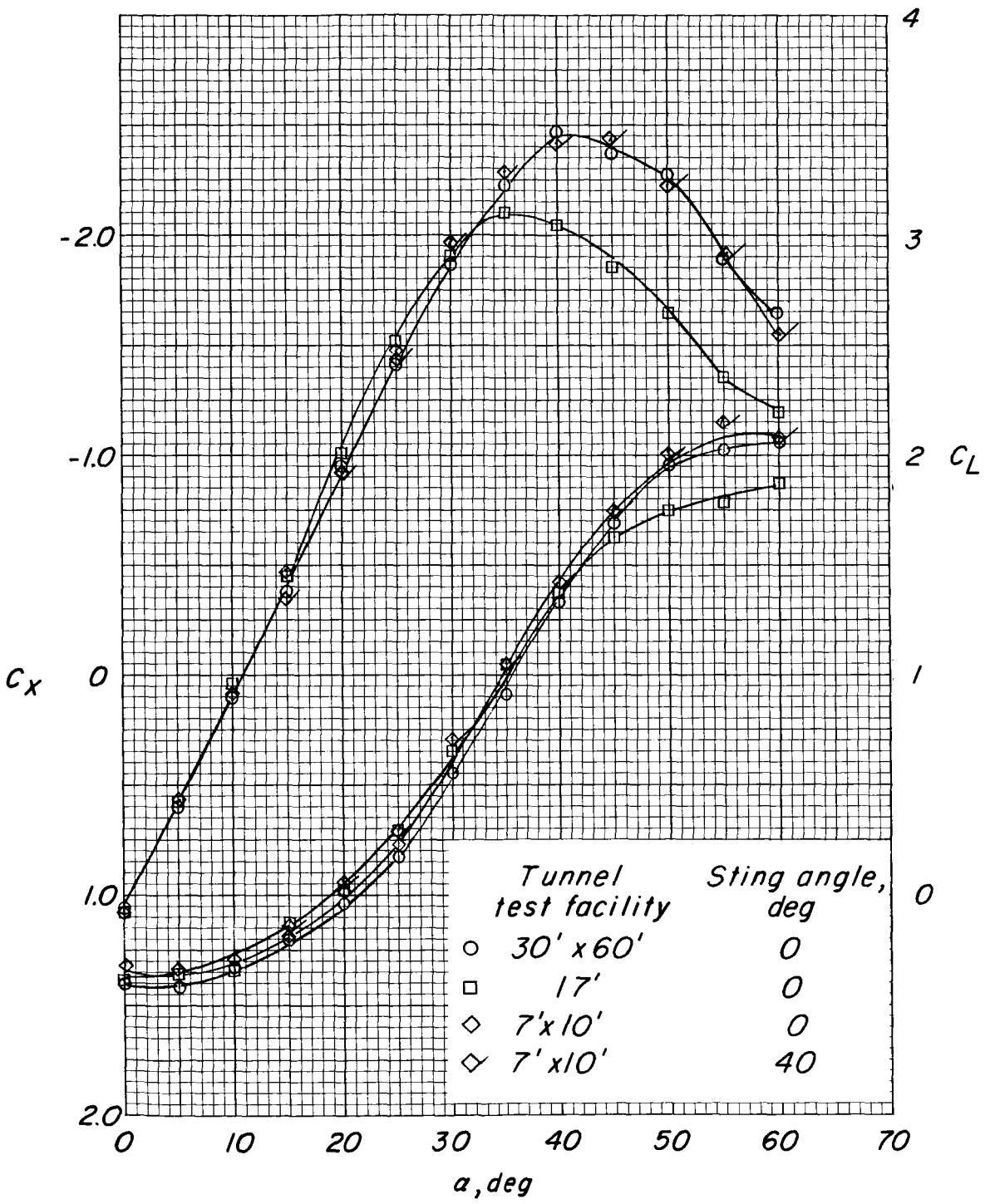

(b) Concluded.

Figure B1.- Continued.

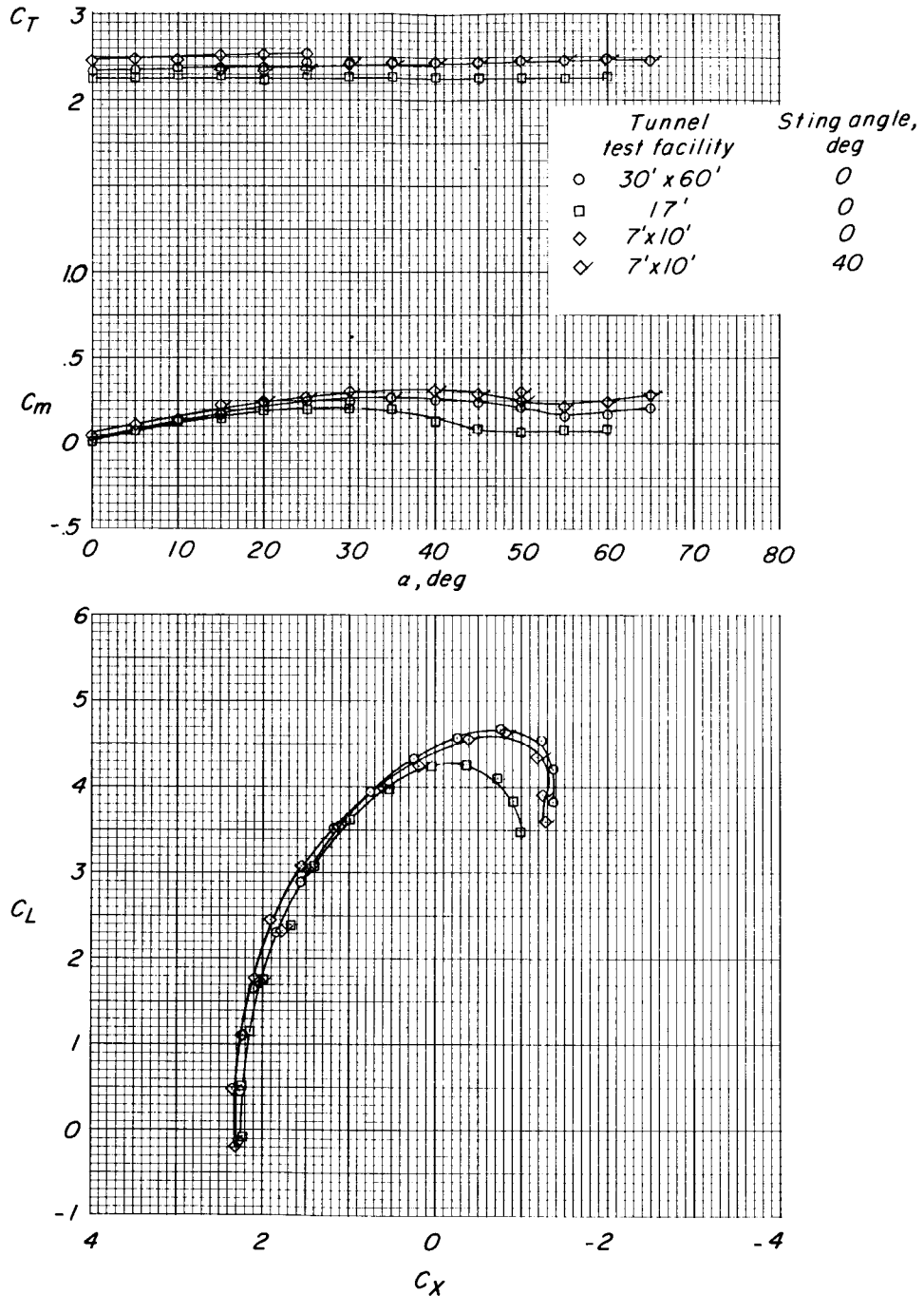

(c) $C_T \approx 2.5$; $C_{T,S} \approx 0.72$.

Figure B1.- Continued.

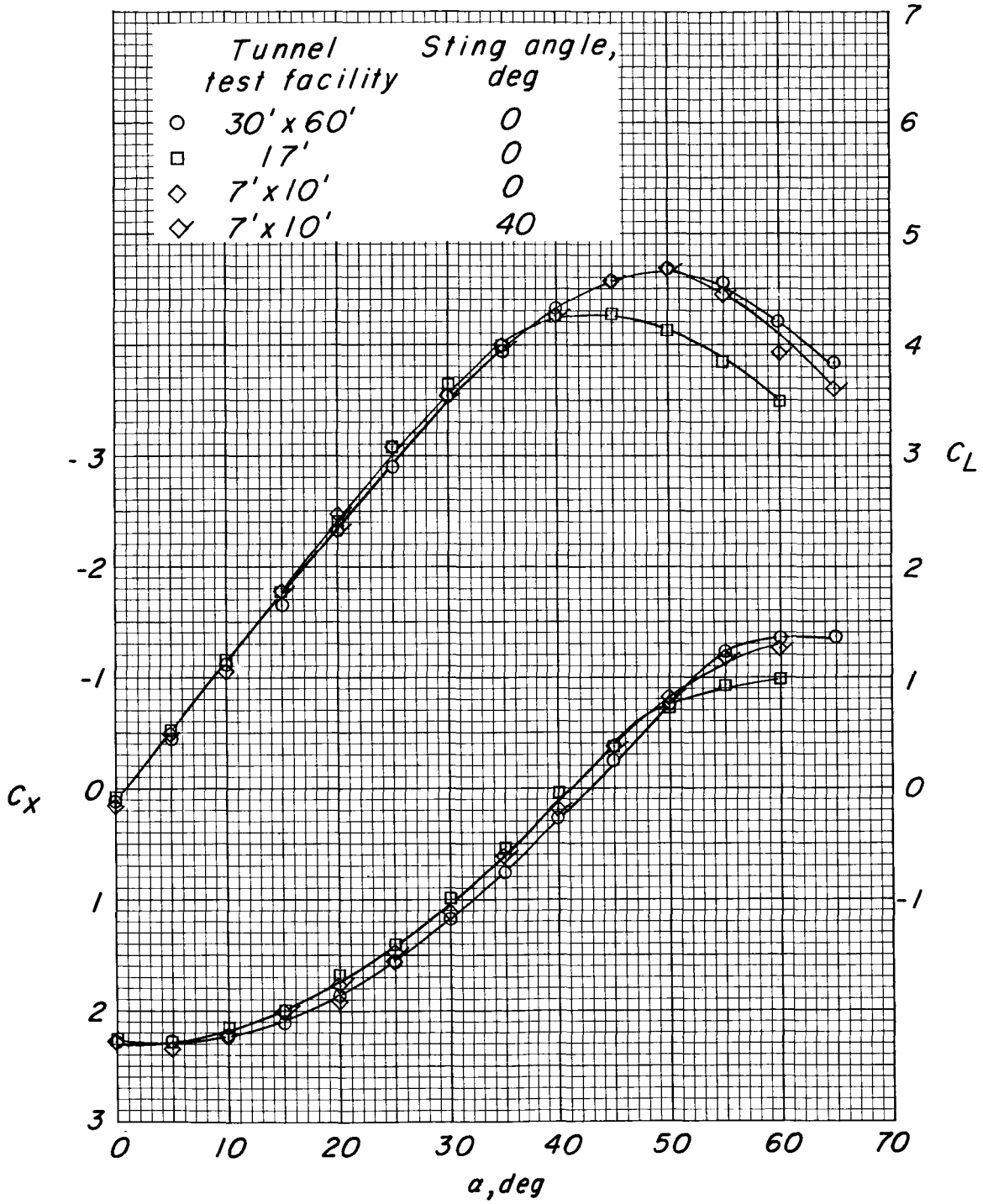

(c) Concluded.

Figure B1.- Continued.

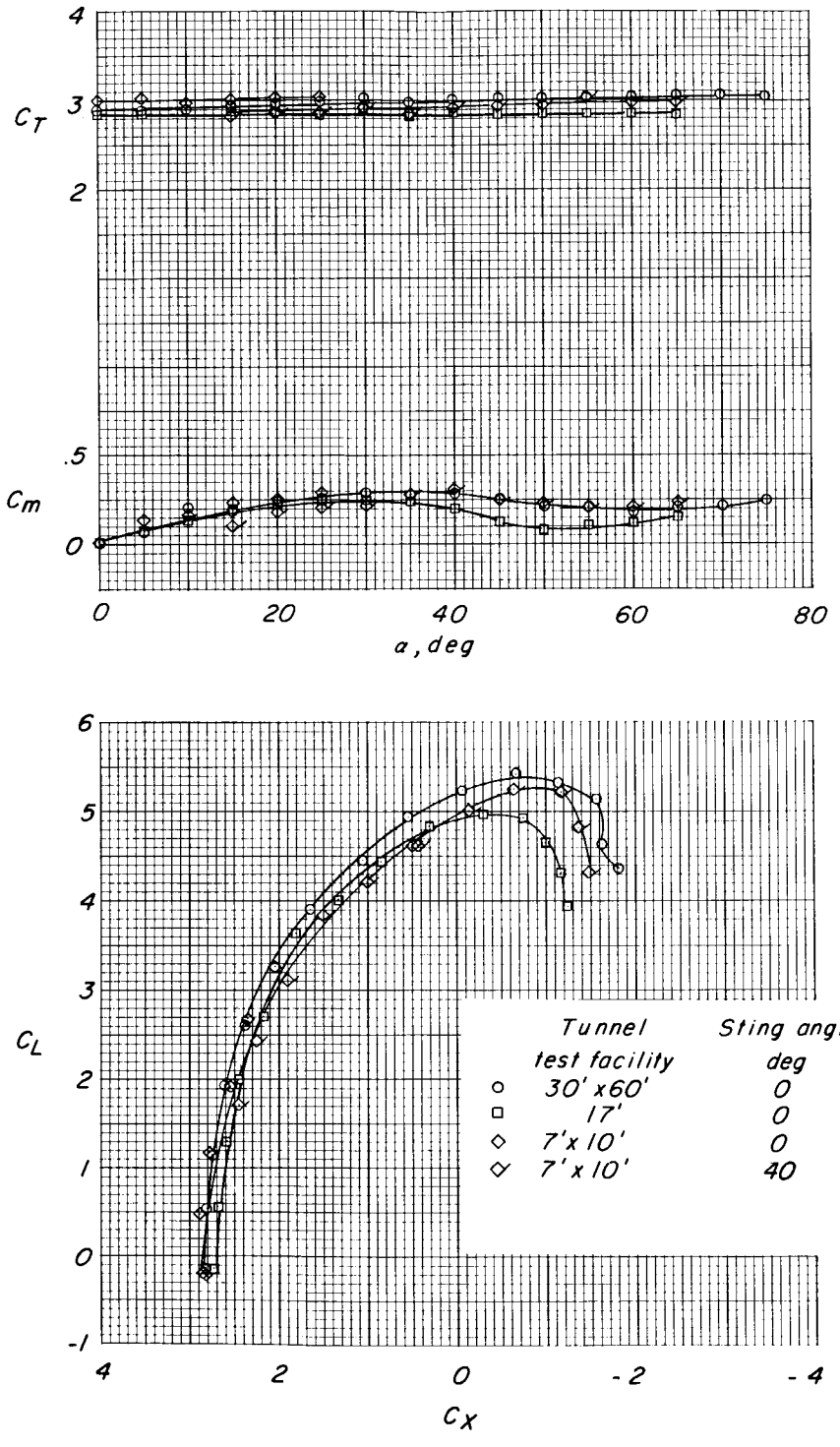

(d) $C_T \approx 3.0$; $C_{T,S} \approx 0.75$.

Figure B1.- Continued.

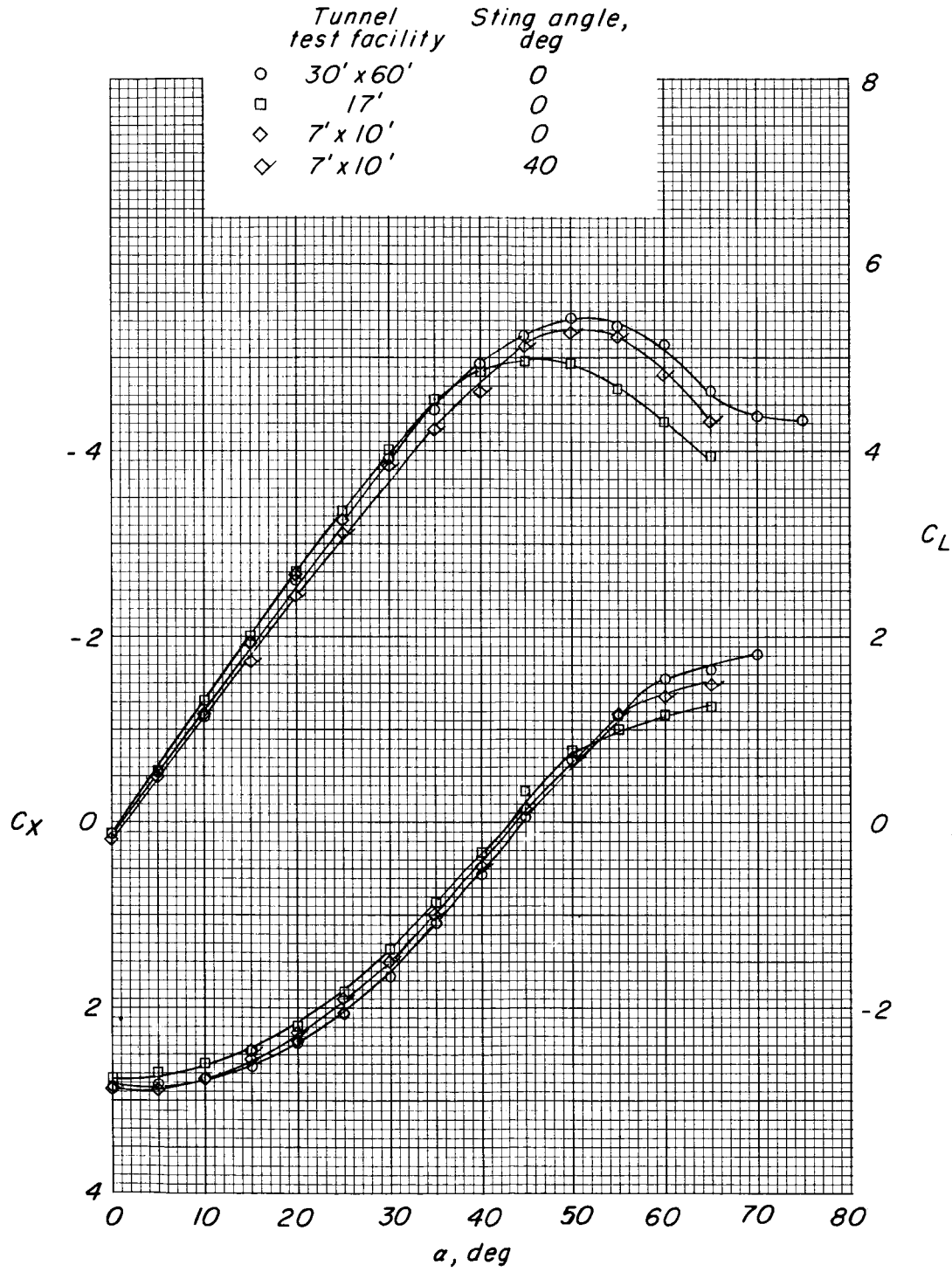

(d) Concluded.

Figure B1.- Continued.

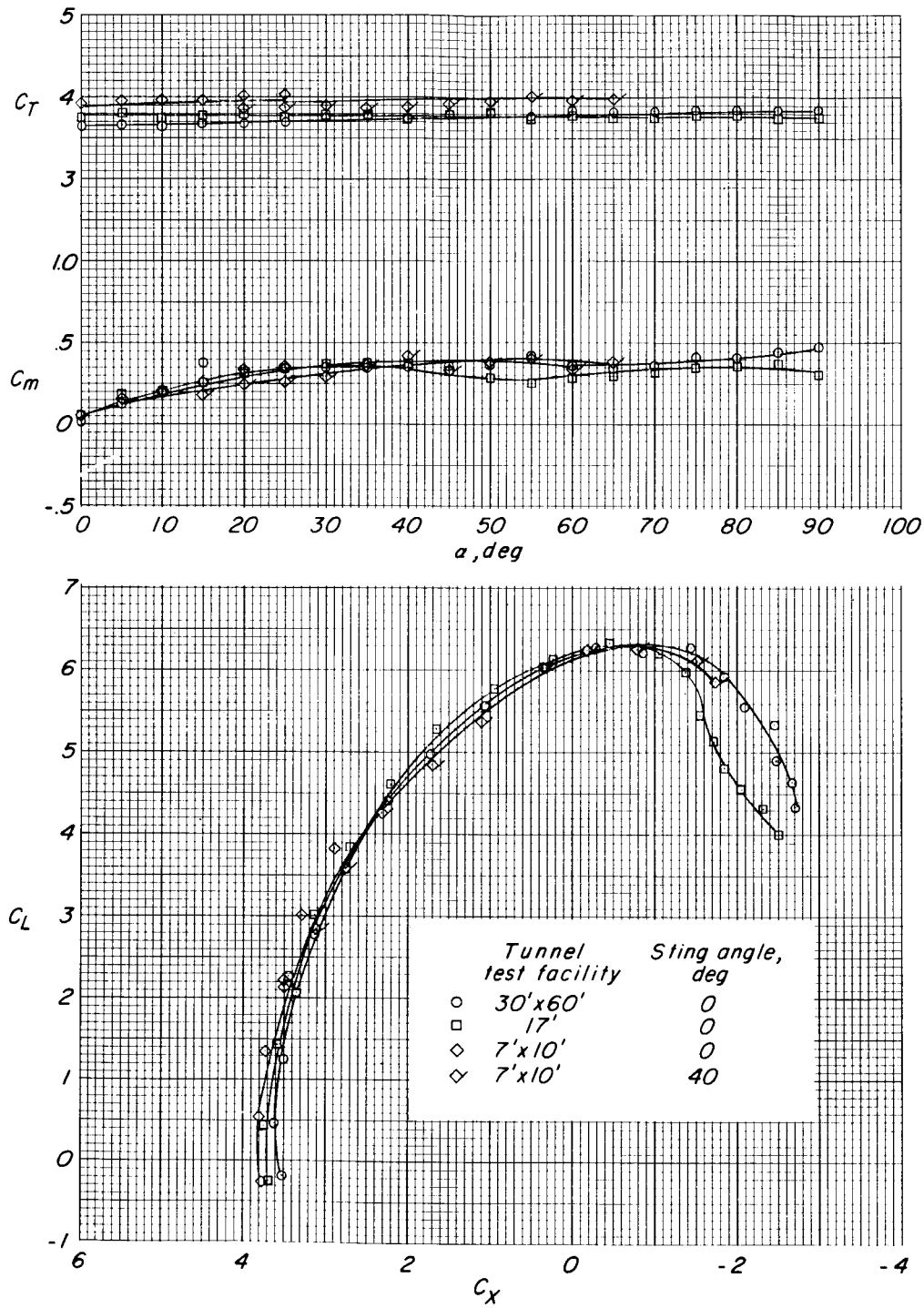

(e) $C_T \approx 4.0$; $C_{T,S} \approx 0.80$.

Figure B1.- Continued.

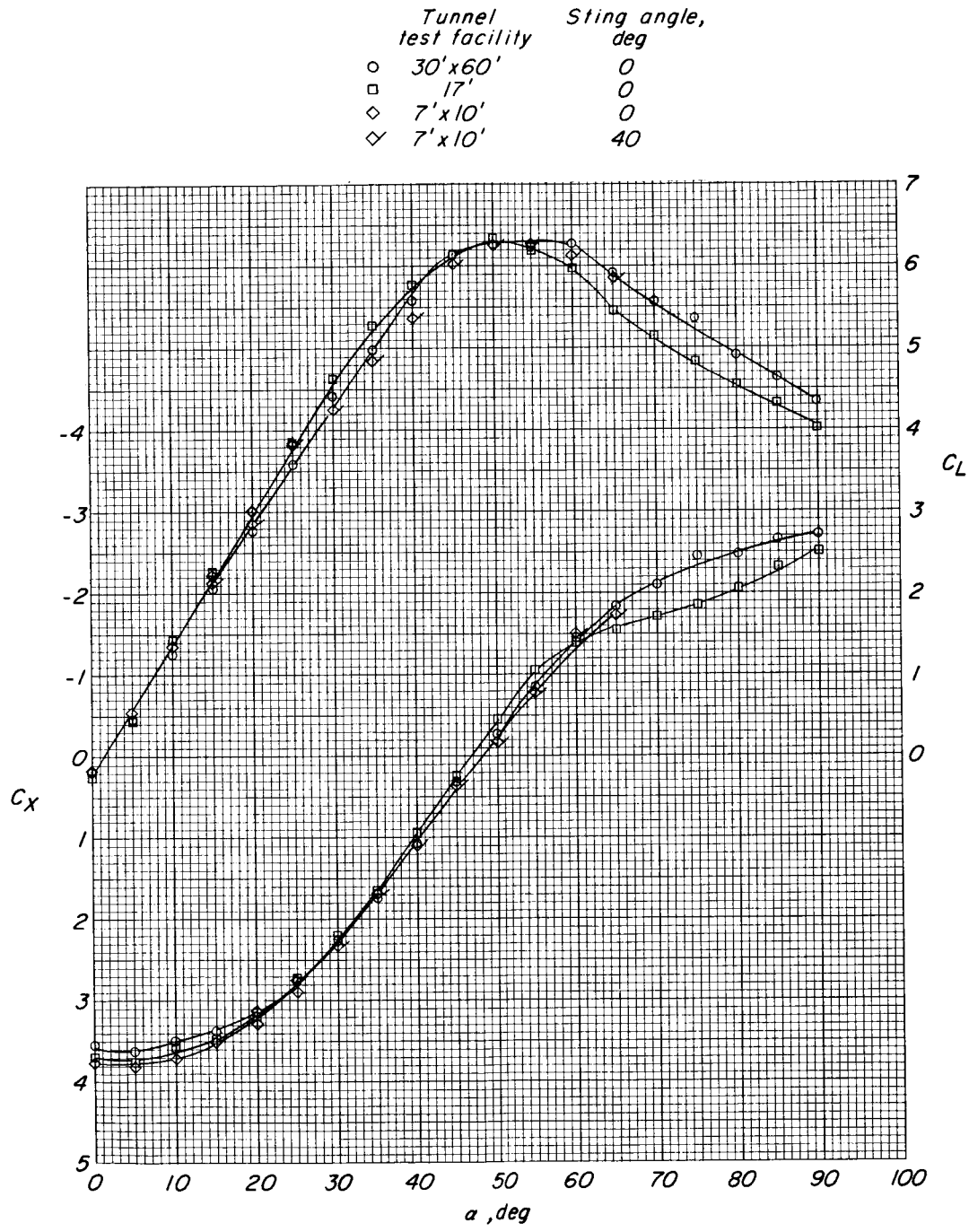

(e) Concluded.

Figure B1.- Continued.

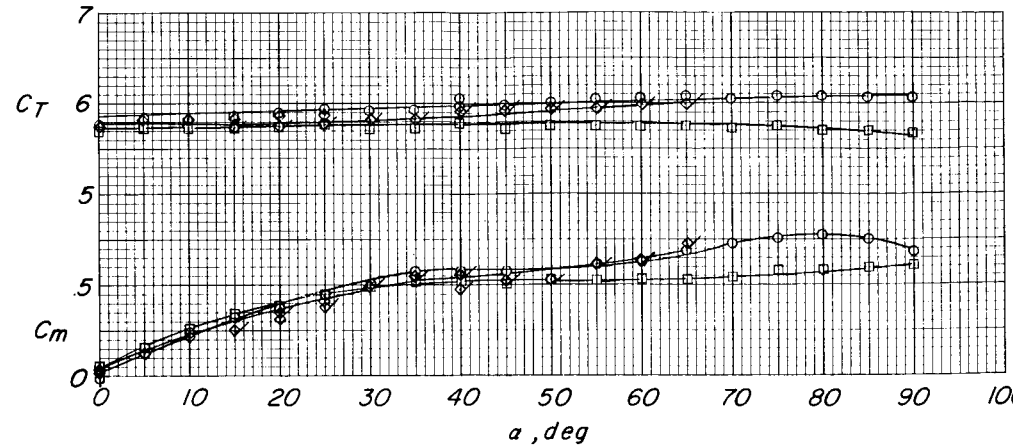

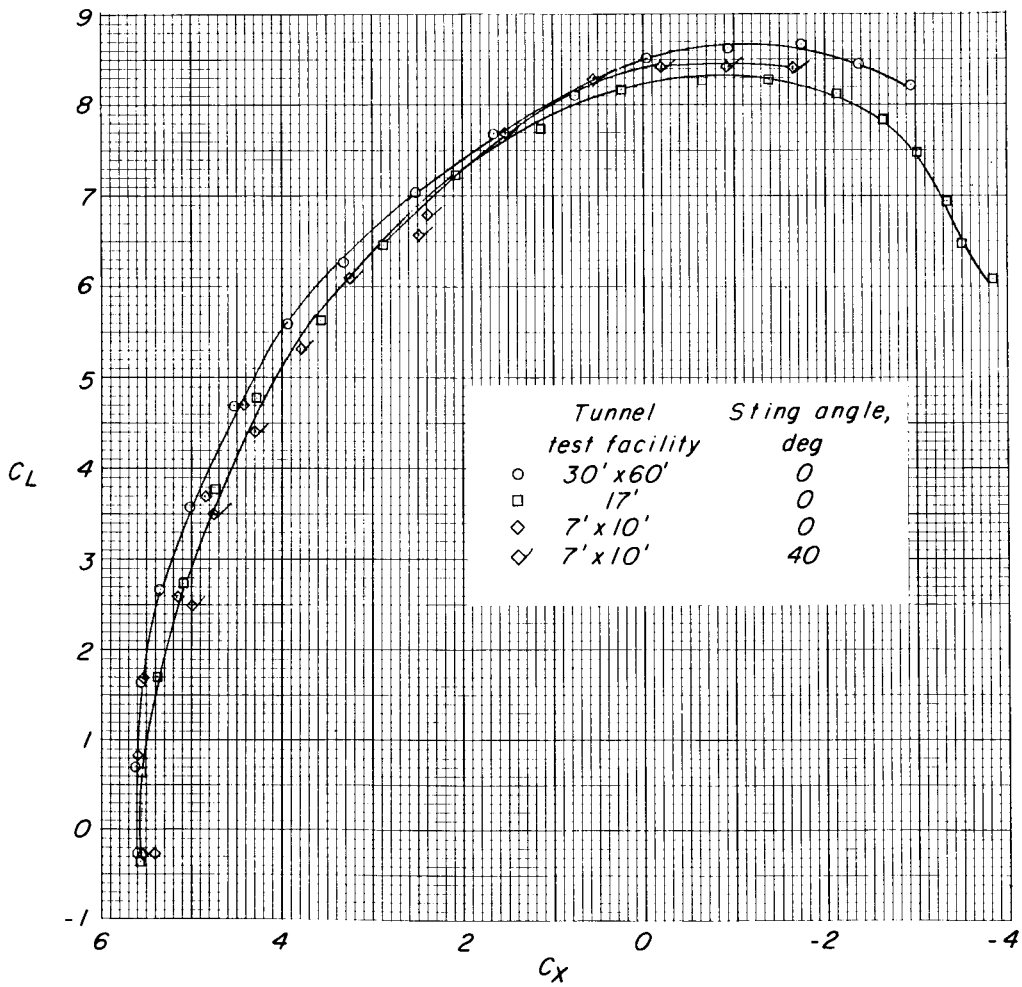

(f) $C_T \approx 6.0$; $C_{T,S} \approx 0.86$.

Figure B1.- Continued.

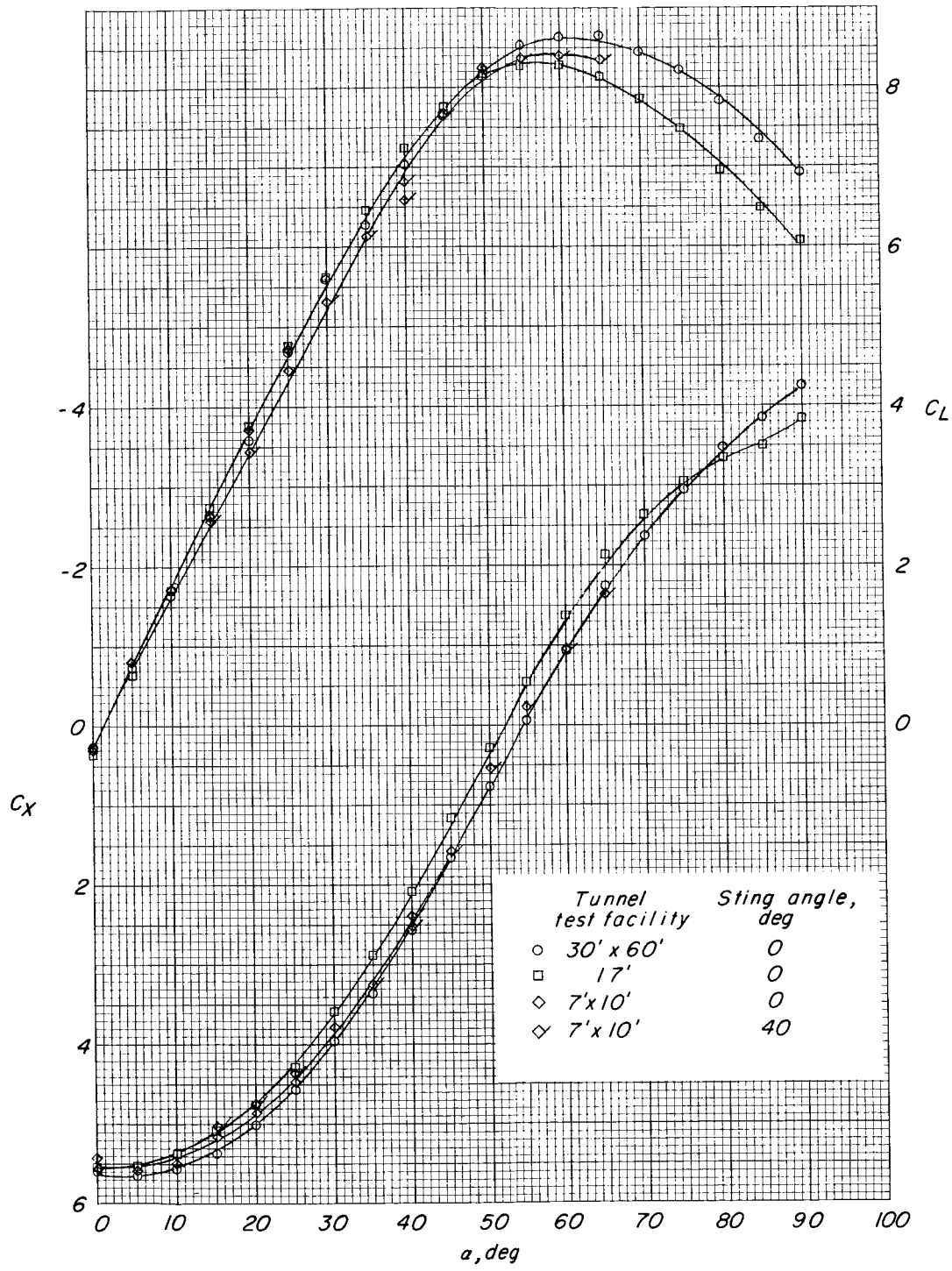

(f) Concluded.

Figure B1.- Continued.

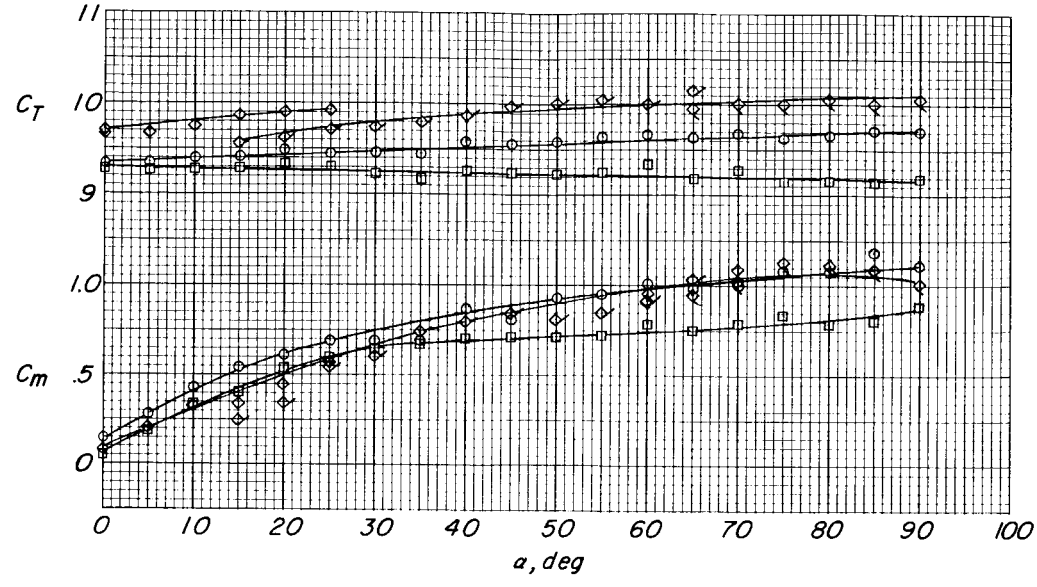

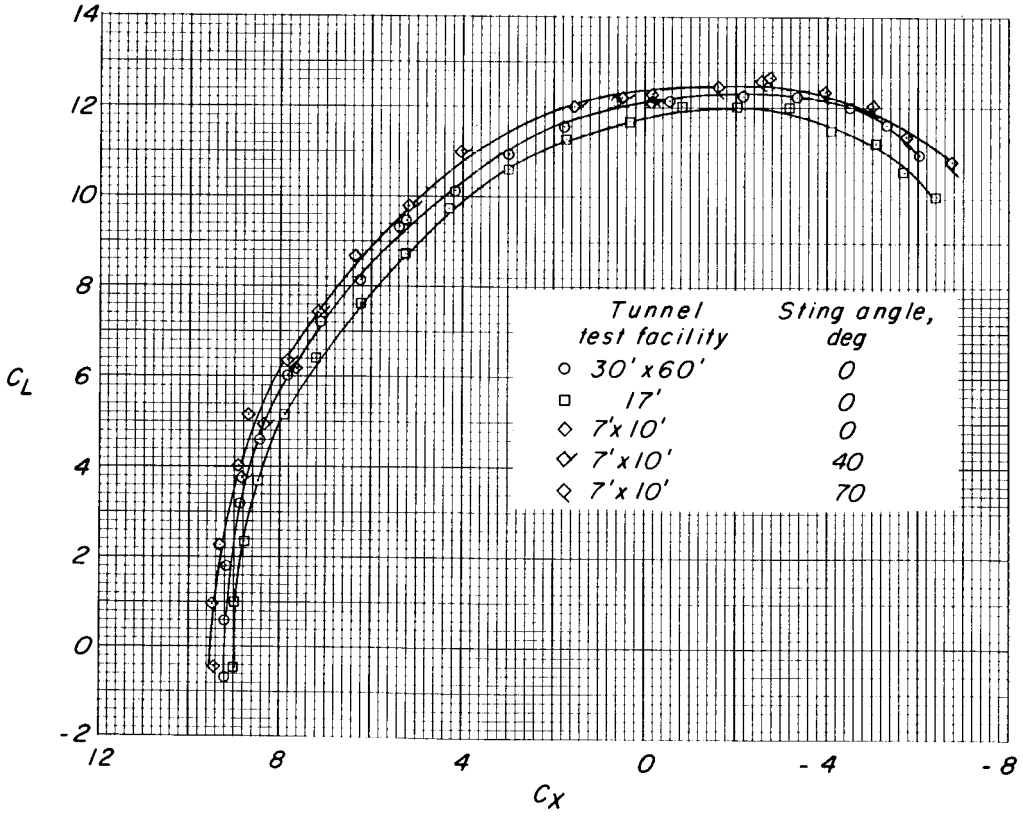

(g) $C_T \approx 9.5$; $C_{T,S} \approx 0.90$.

Figure B1.- Continued.

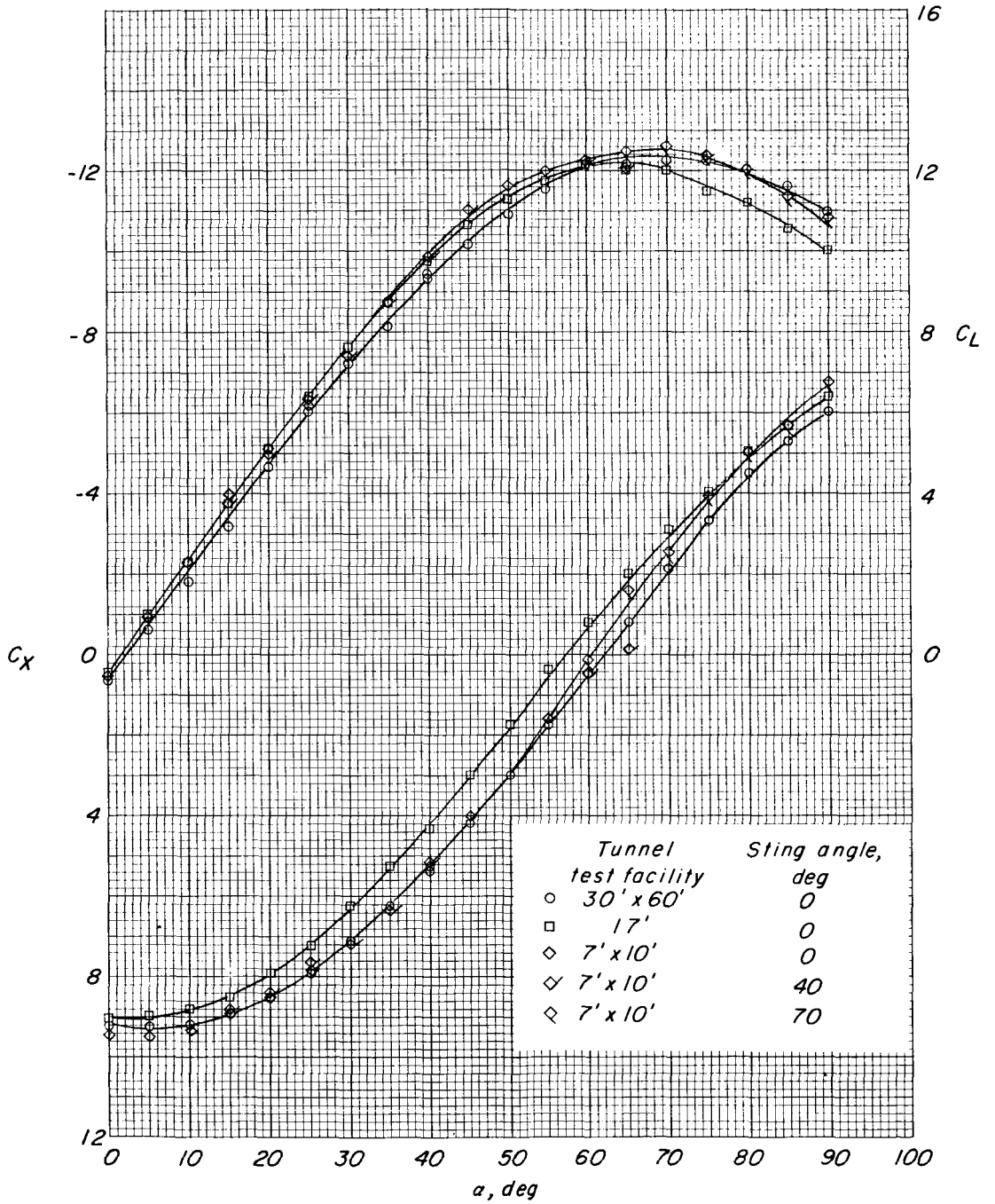

(g) Concluded.

Figure B1.- Continued.

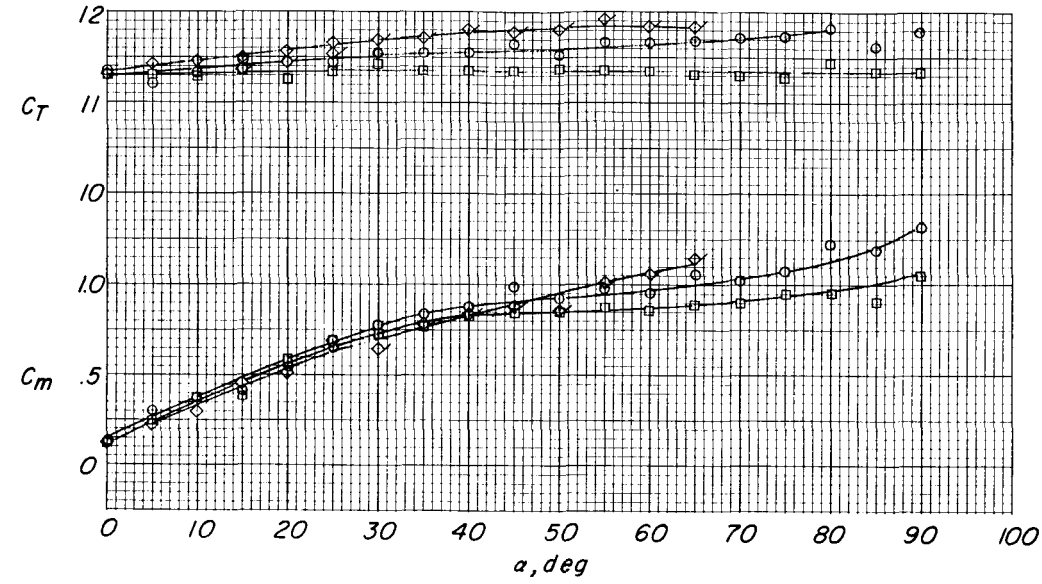

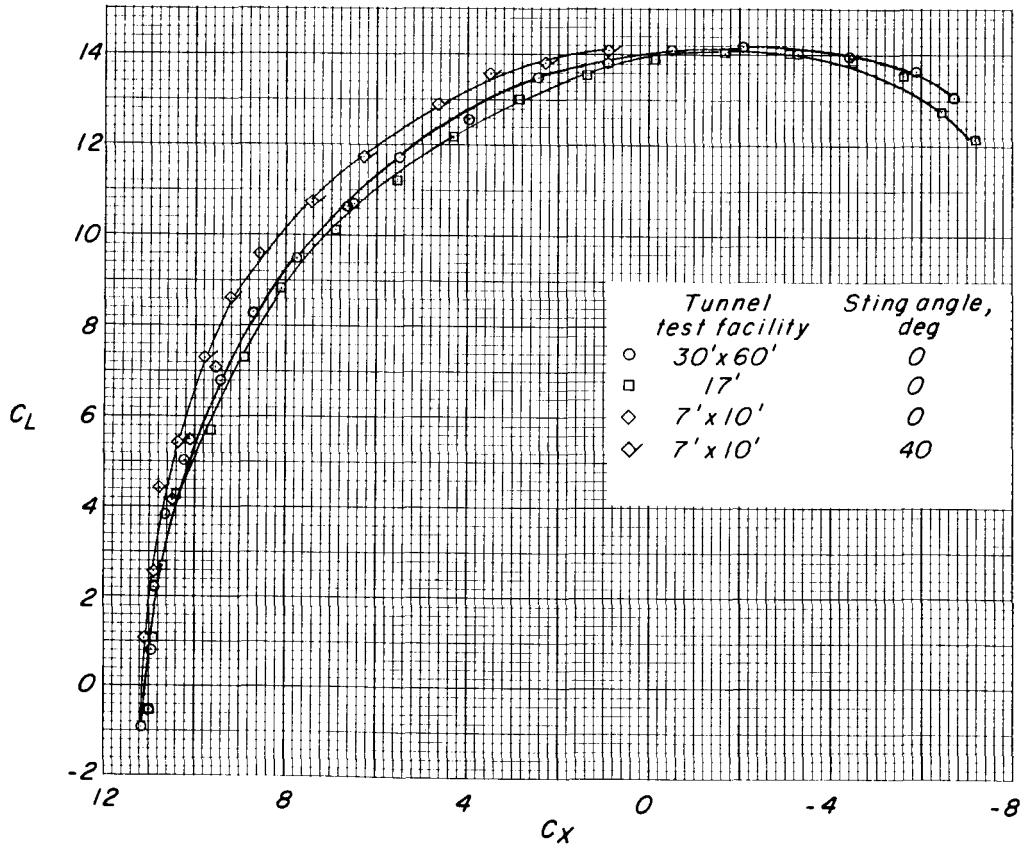

(h) $C_T \approx 11.5$; $C_{T,S} \approx 0.92$.

Figure B1.- Continued.

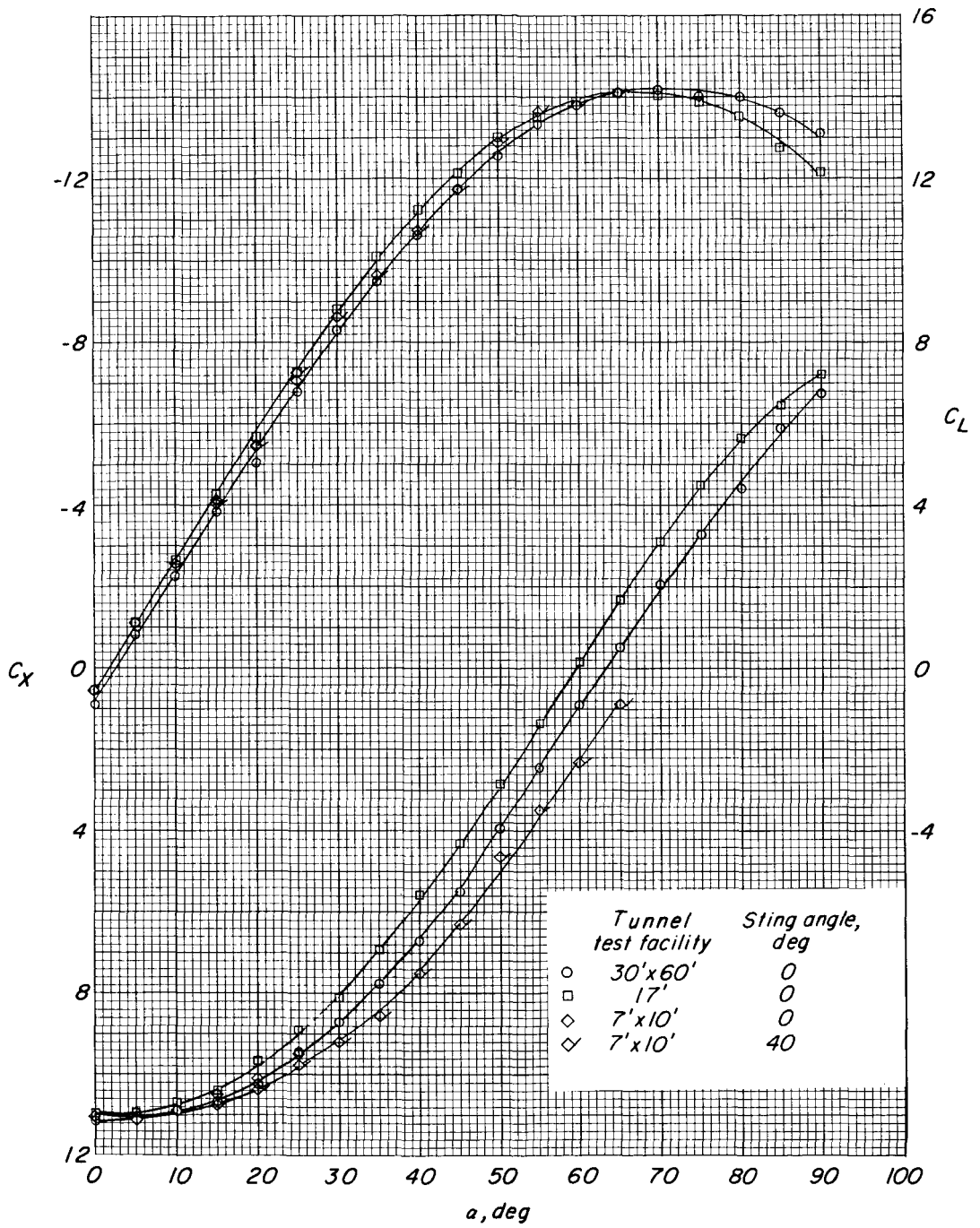

(h) Concluded.

Figure B1.- Continued.

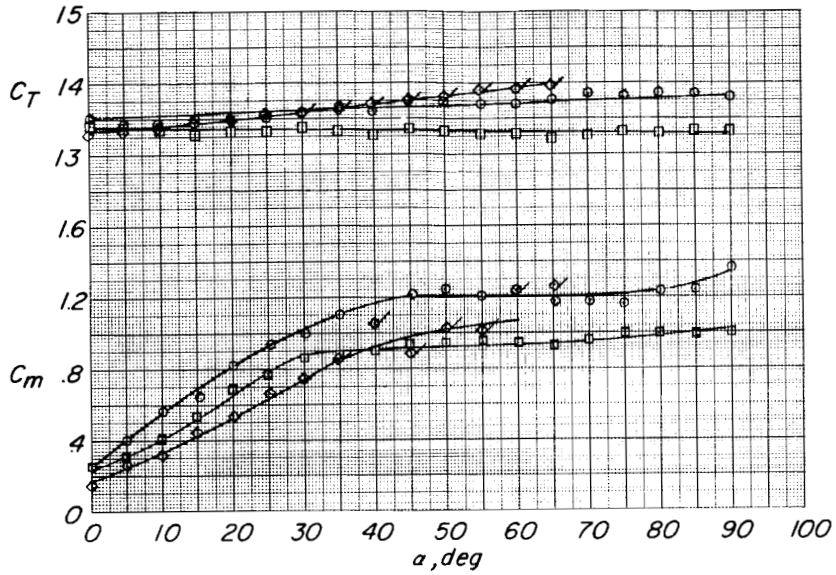

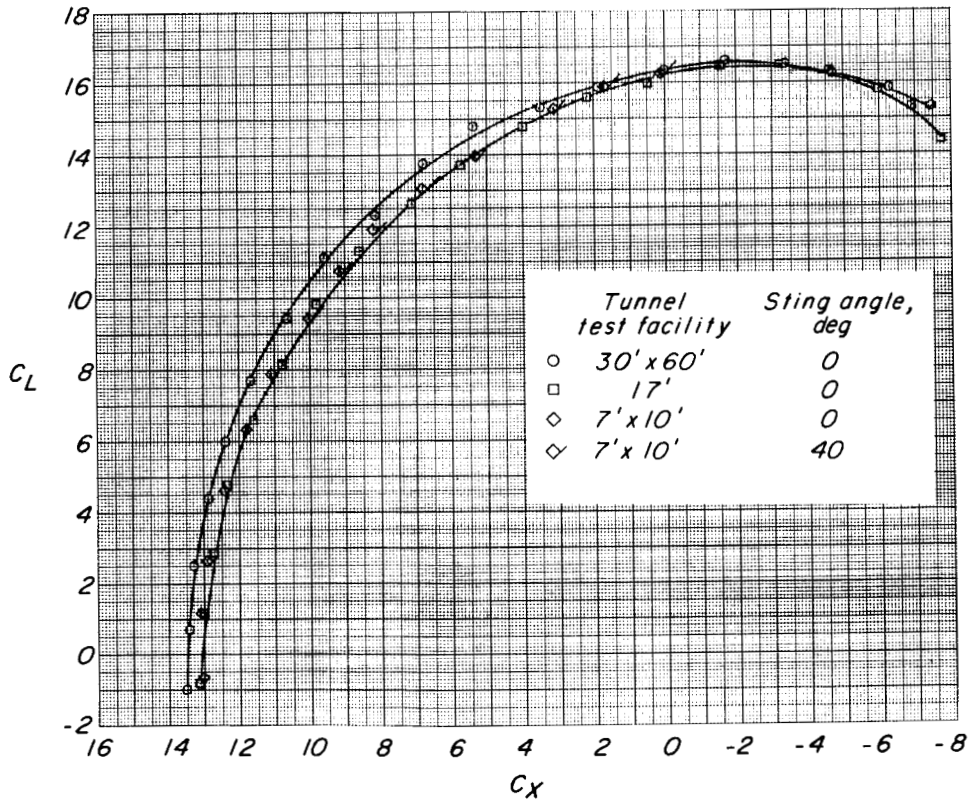

(i) $C_T \approx 13.5$; $C_{T,S} \approx 0.93$.

Figure B1.- Continued.

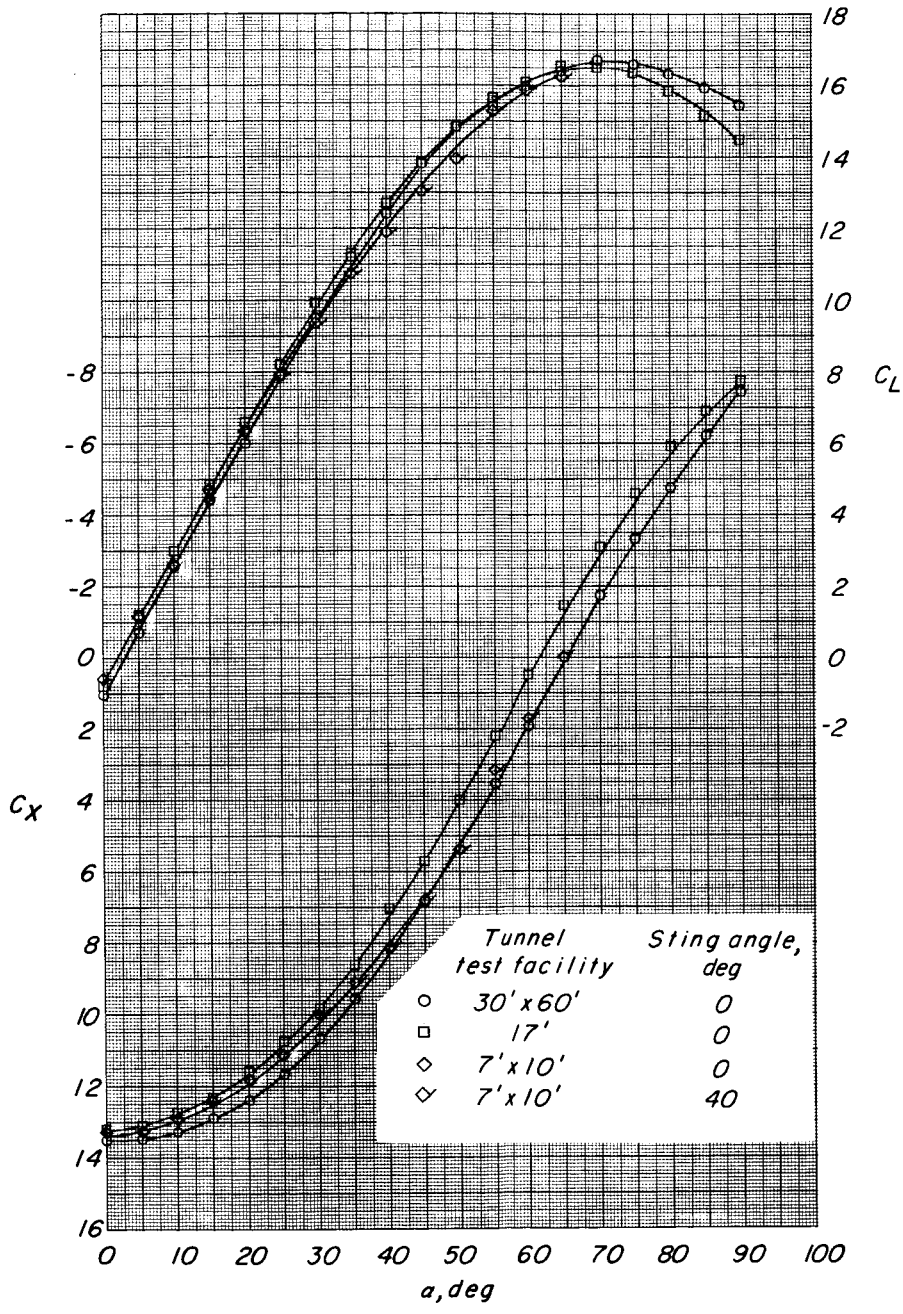

(i) Concluded.

Figure B1.- Continued.

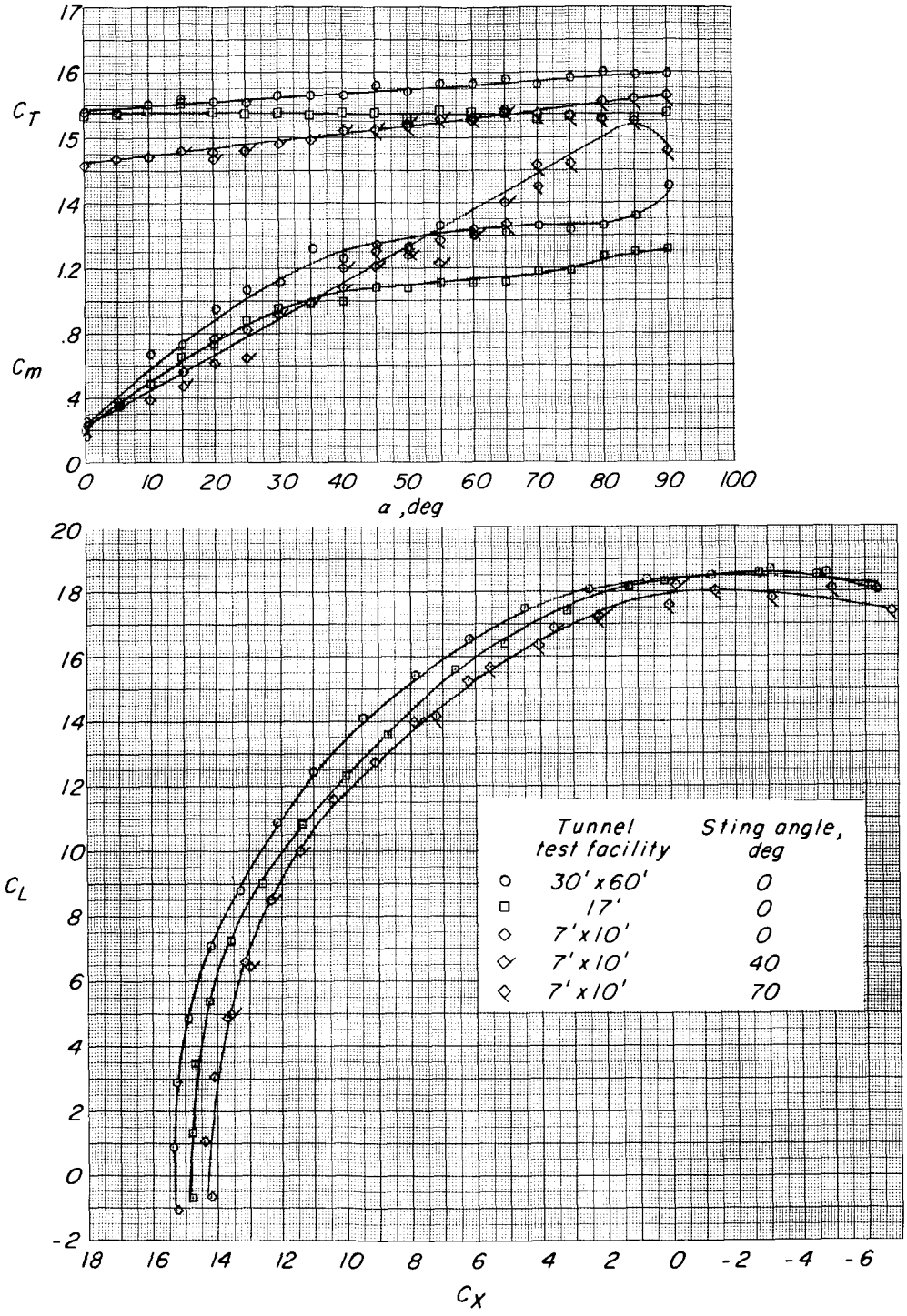

(j) $C_T \approx 15.5$; $C_{T,S} \approx 0.94$.

Figure B1.- Continued.

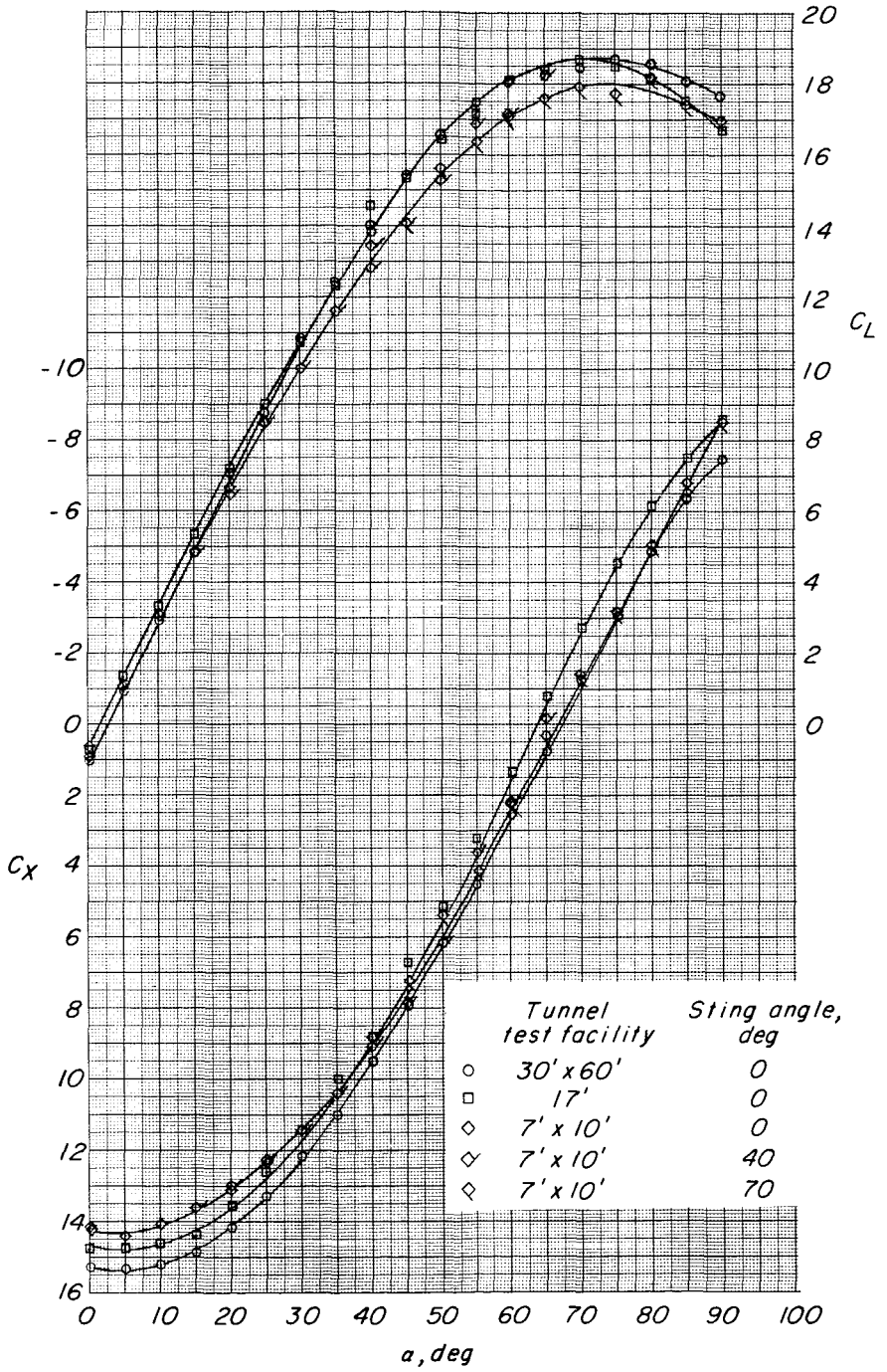

(j) Concluded.

Figure B1.- Continued.

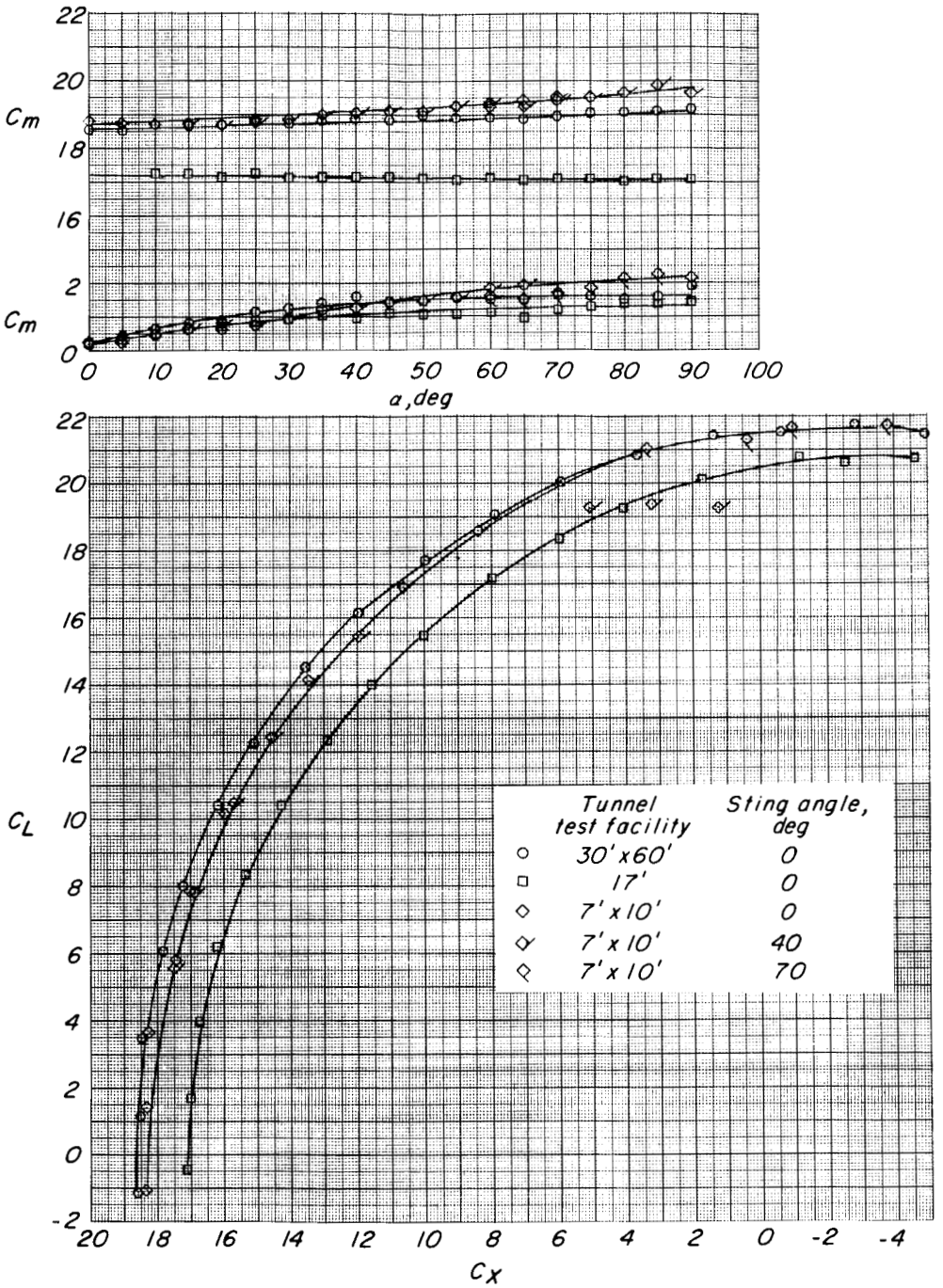

(k) $C_T \approx 18$; $C_{T,S} \approx 0.95$.

Figure B1.- Continued.

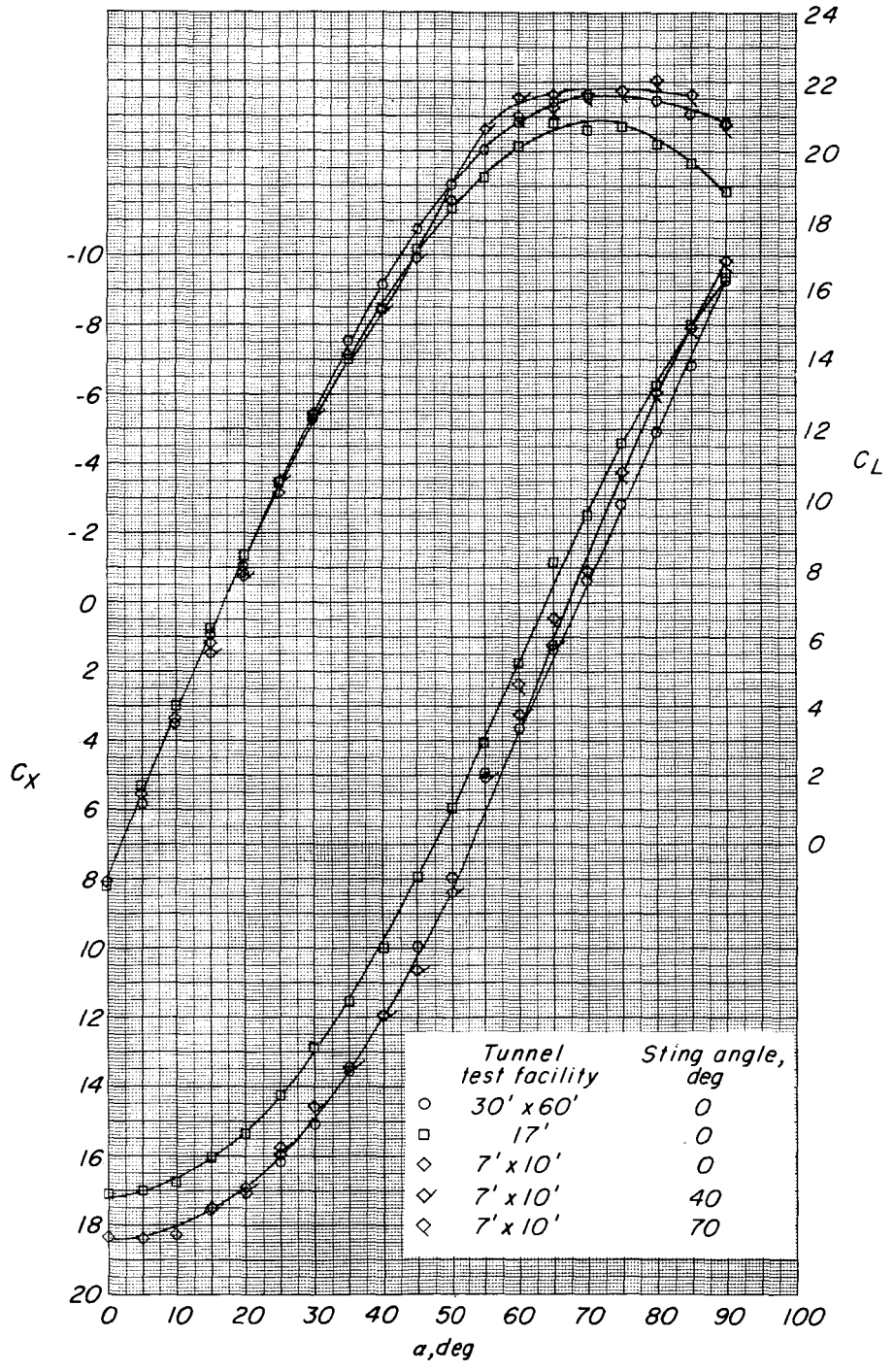

(k) Concluded.

Figure B1.- Concluded.

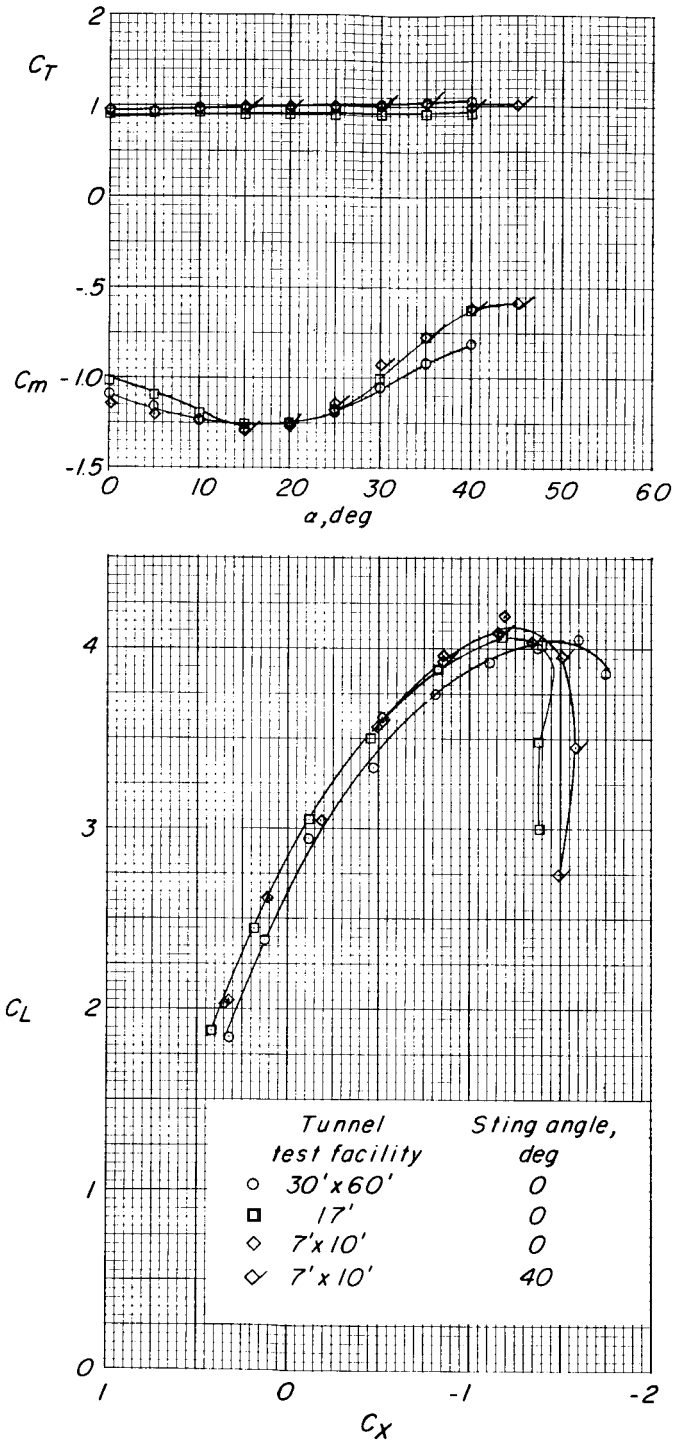

(a) $C_T \approx 1.0$; $C_{T,S} \approx 0.50$.

Figure B2.- Comparison of uncorrected data for tests in three facilities for a range of thrust coefficients. Flaps on (deflected 40°).

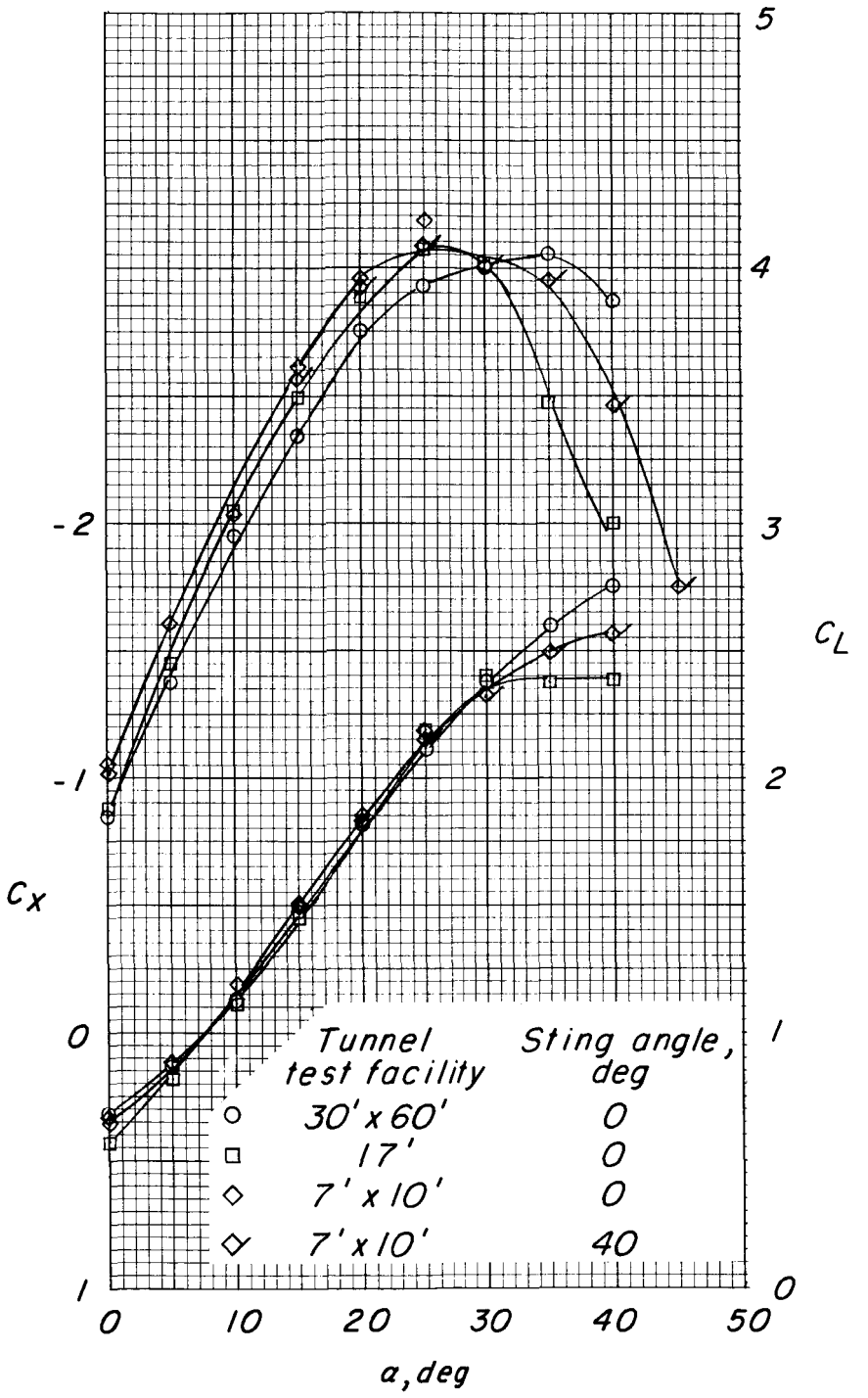

(a) Concluded.

Figure B2.- Continued.

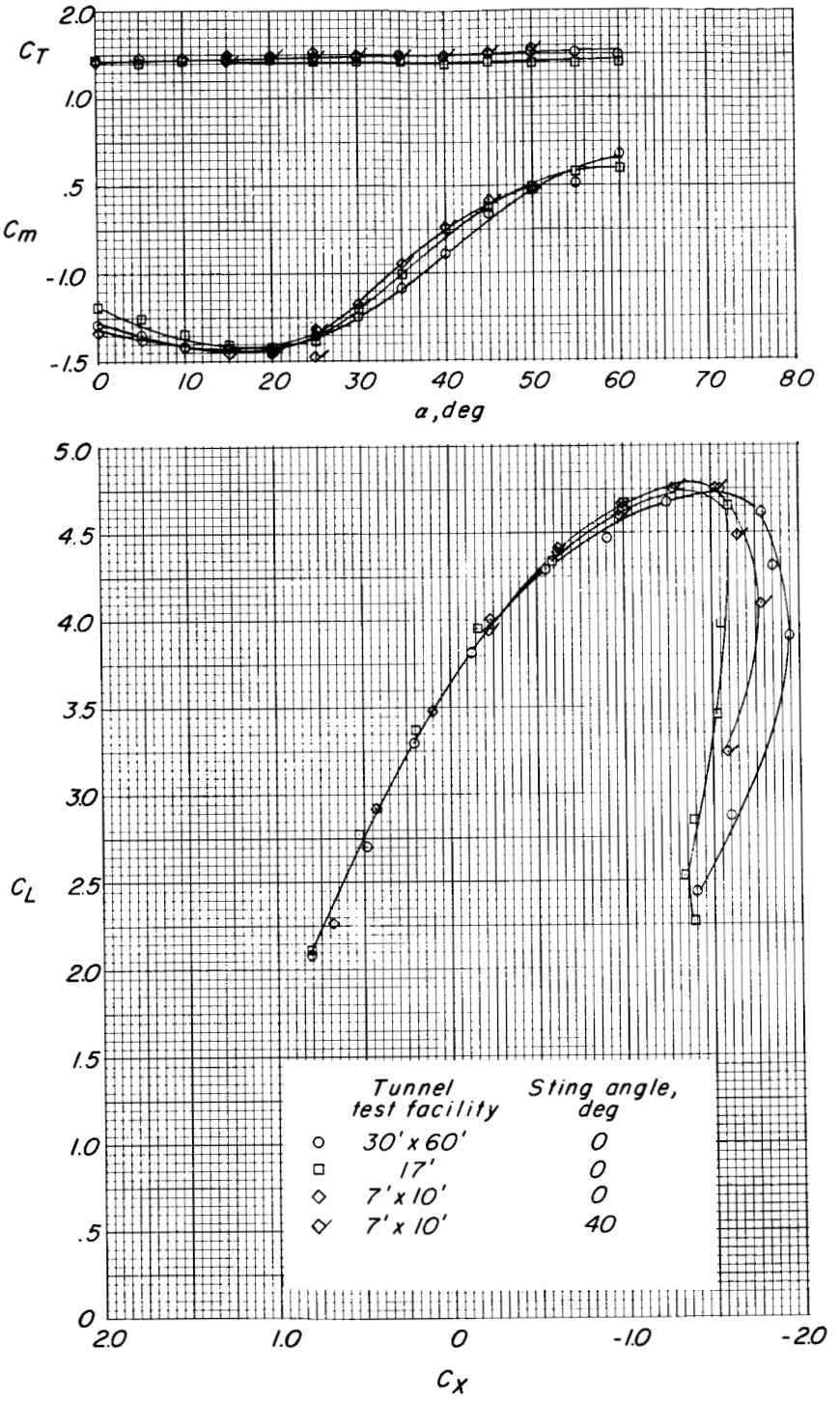

(b) $C_T \approx 1.5$; $C_{T,S} \approx 0.60$.

Figure B2.- Continued.

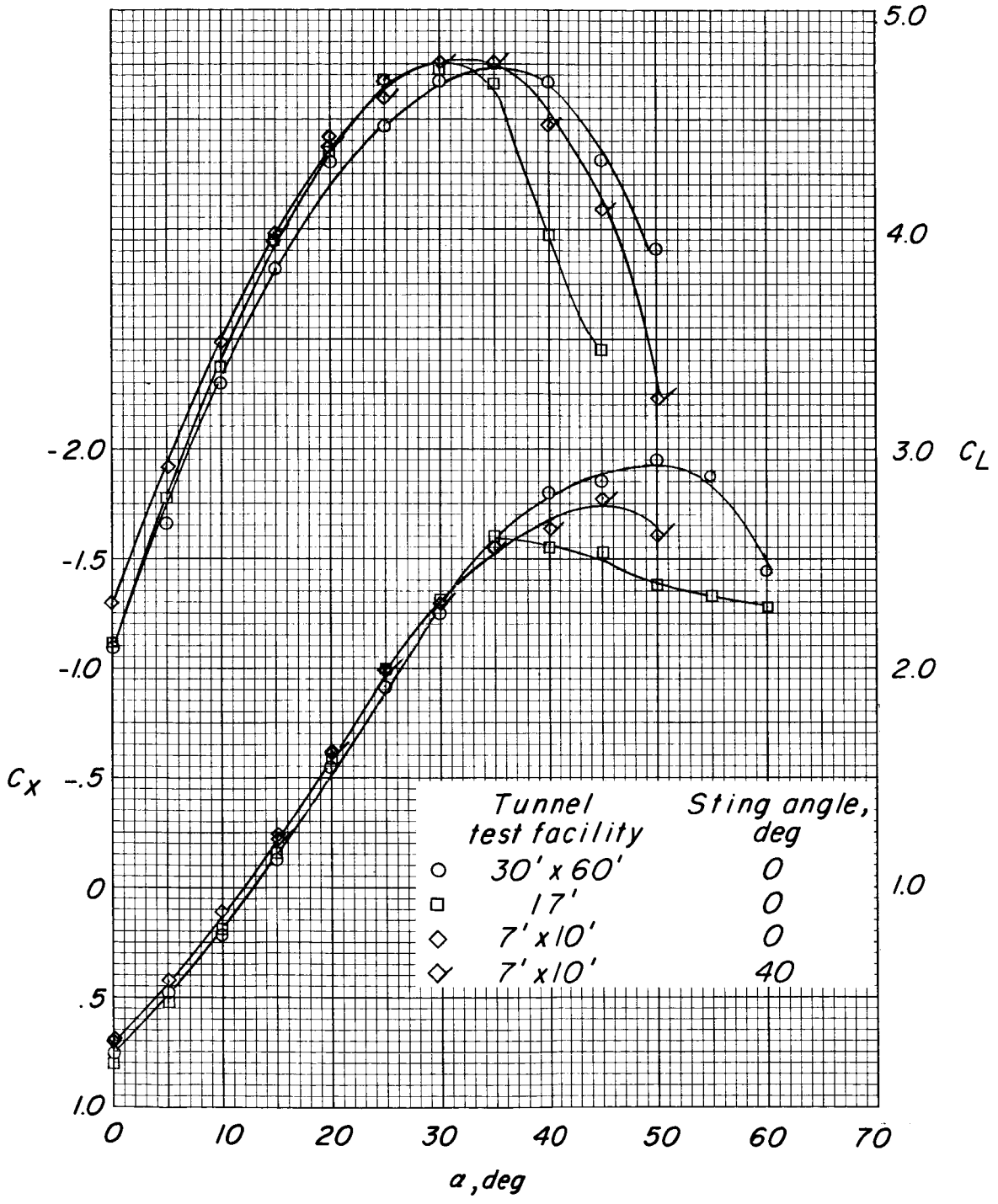

(b) Concluded.

Figure B2.- Continued.

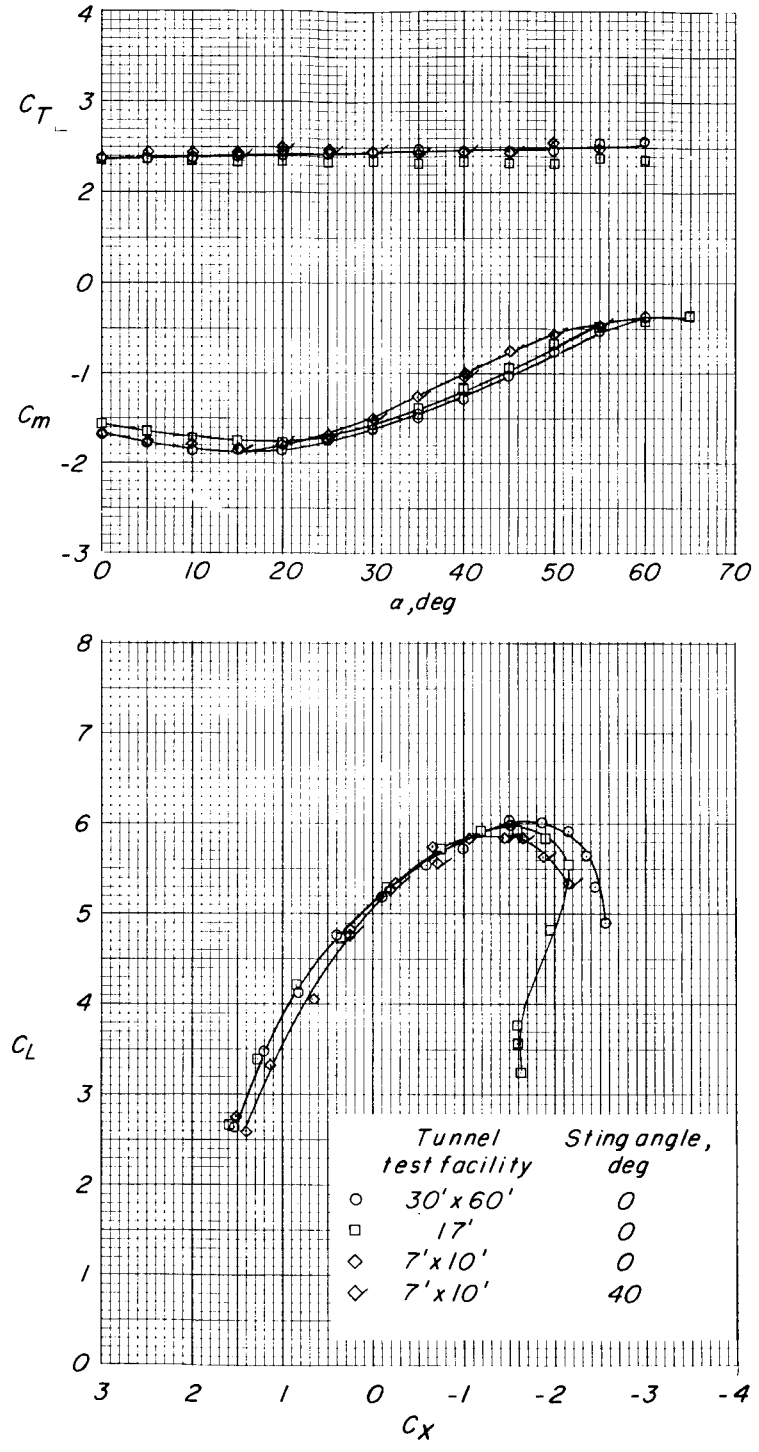

(c) $C_T \approx 2.5$; $C_{T,S} \approx 0.72$.

Figure B2.- Continued.

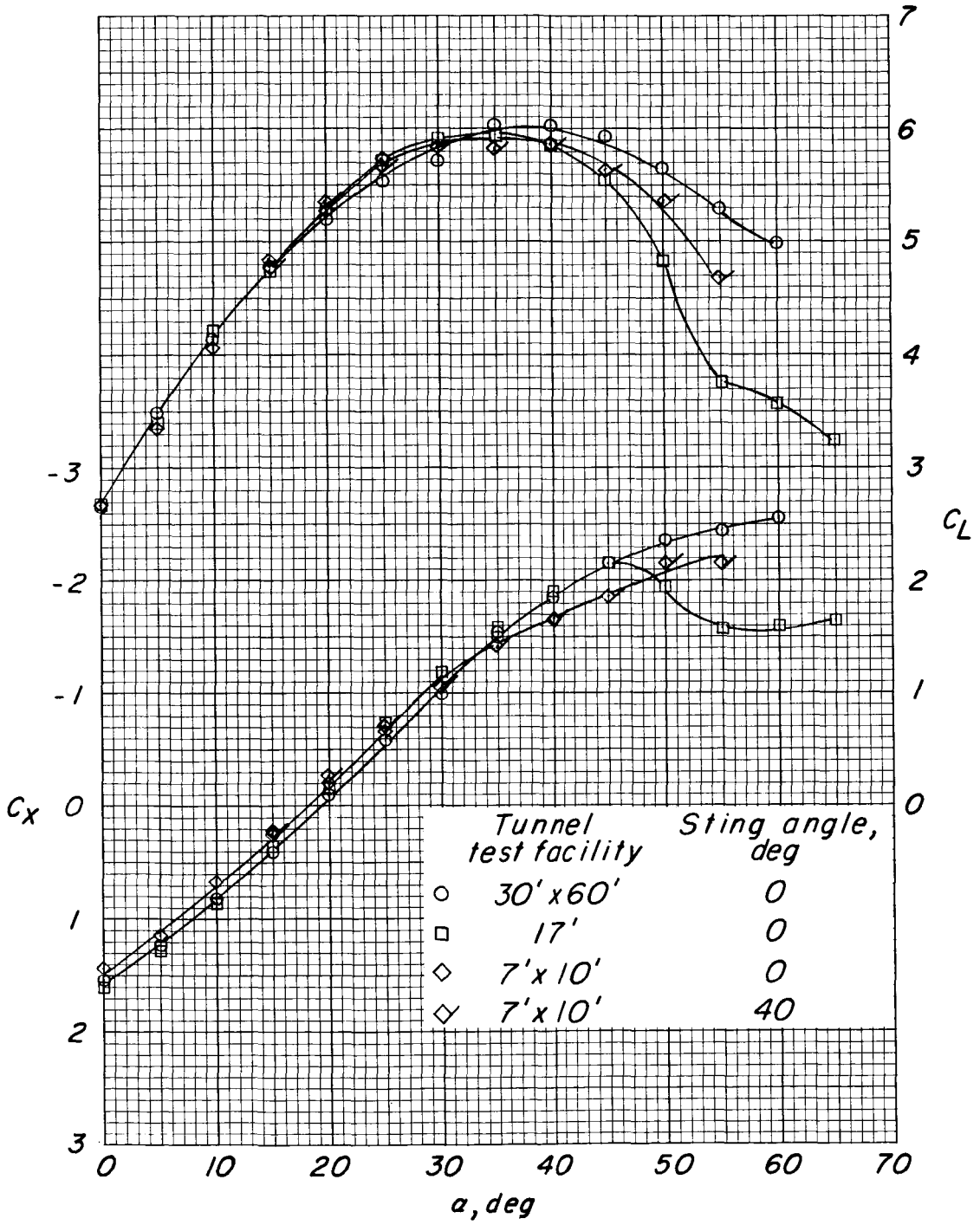

(c) Concluded.

Figure B2.- Continued.

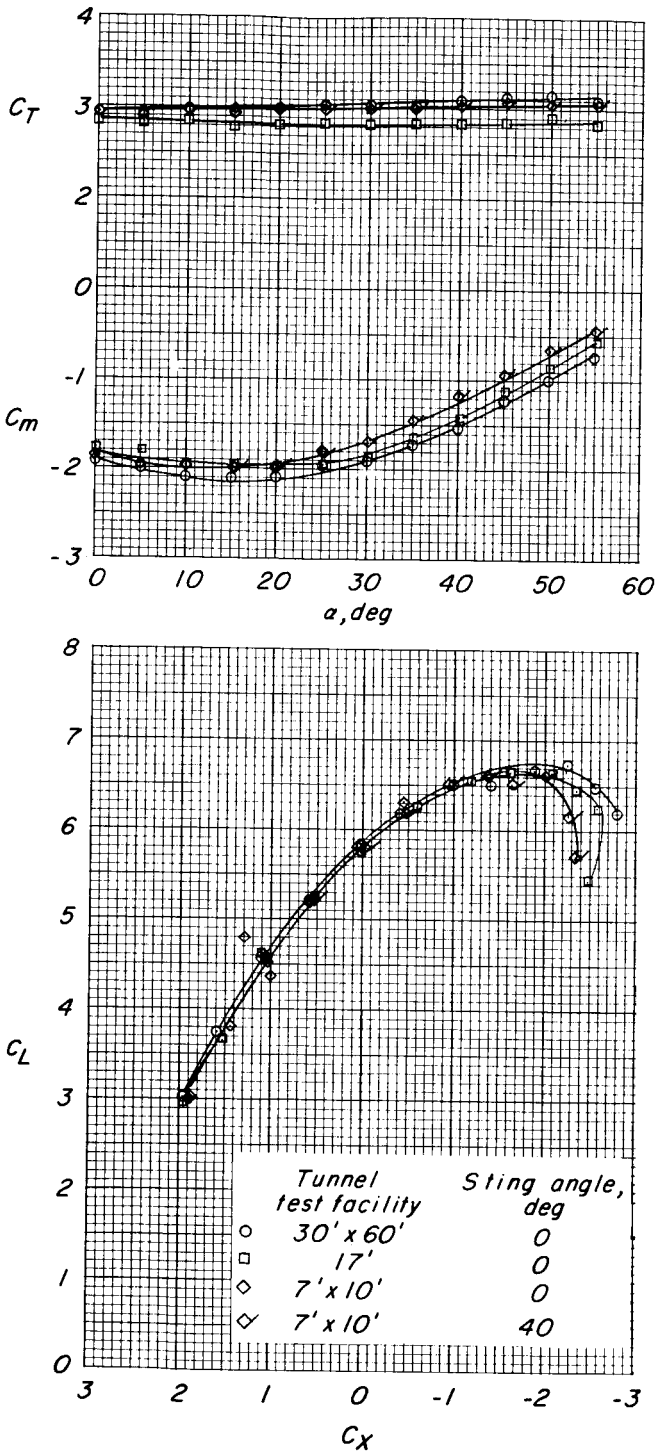

(d) $C_T \approx 3.0$; $C_{T,S} \approx 0.75$.

Figure B2.- Continued.

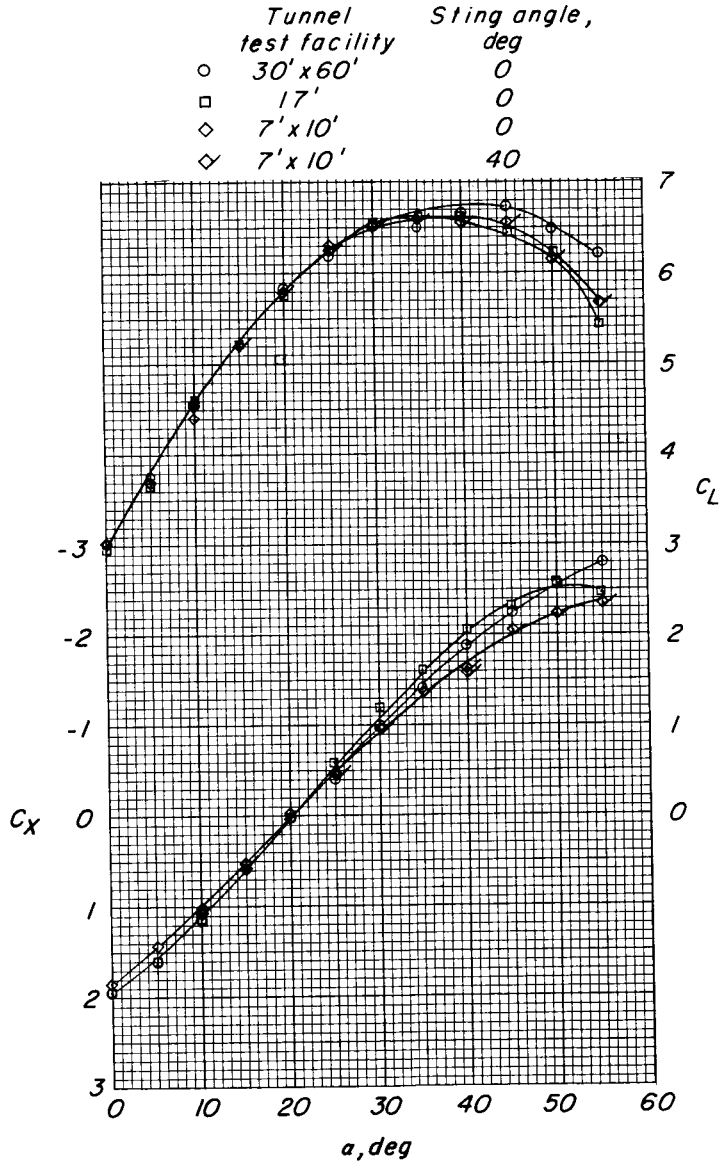

(d) Concluded.

Figure B2.- Continued.

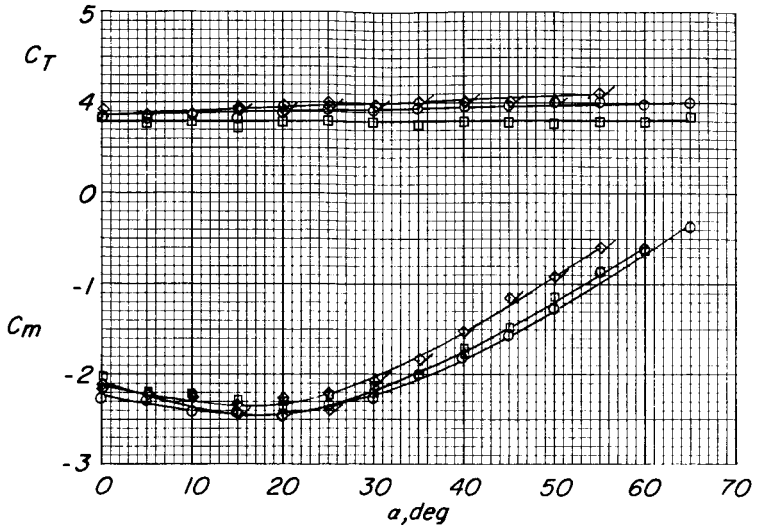

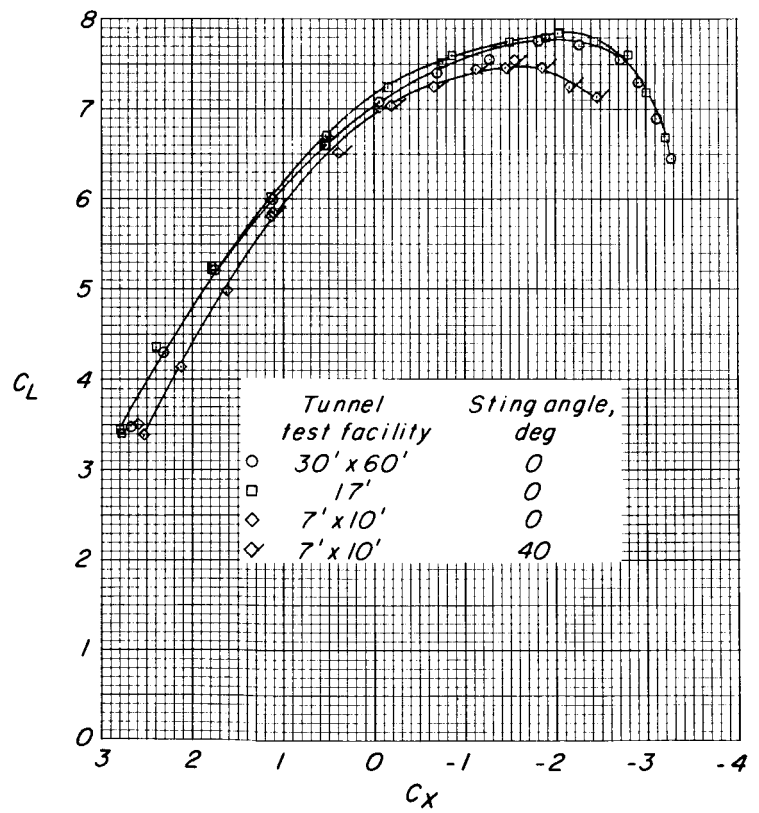

(e) $C_T \approx 4.0$; $C_{T,S} \approx 0.80$.

Figure B2.- Continued.

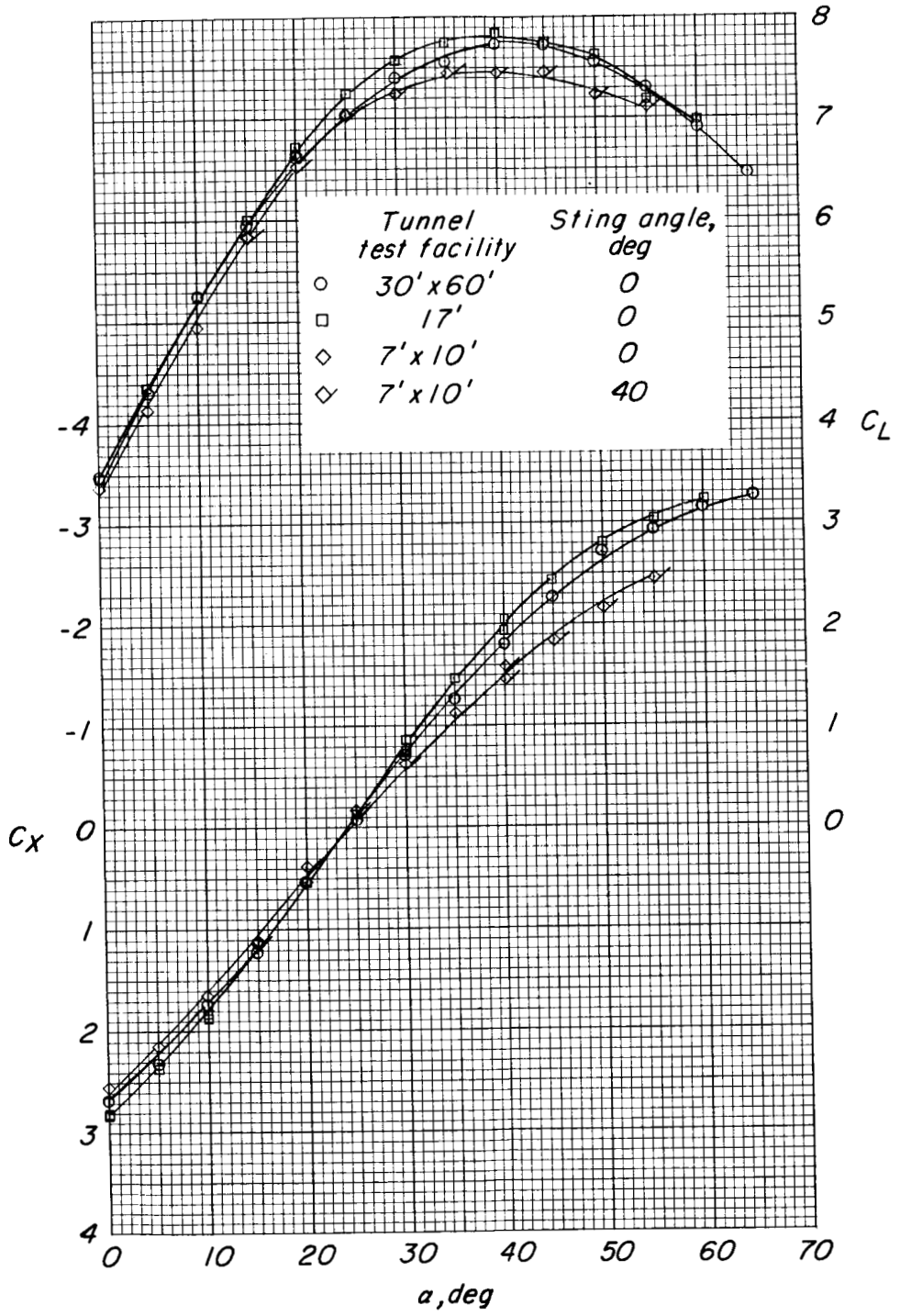

(e) Concluded.

Figure B2.- Continued.

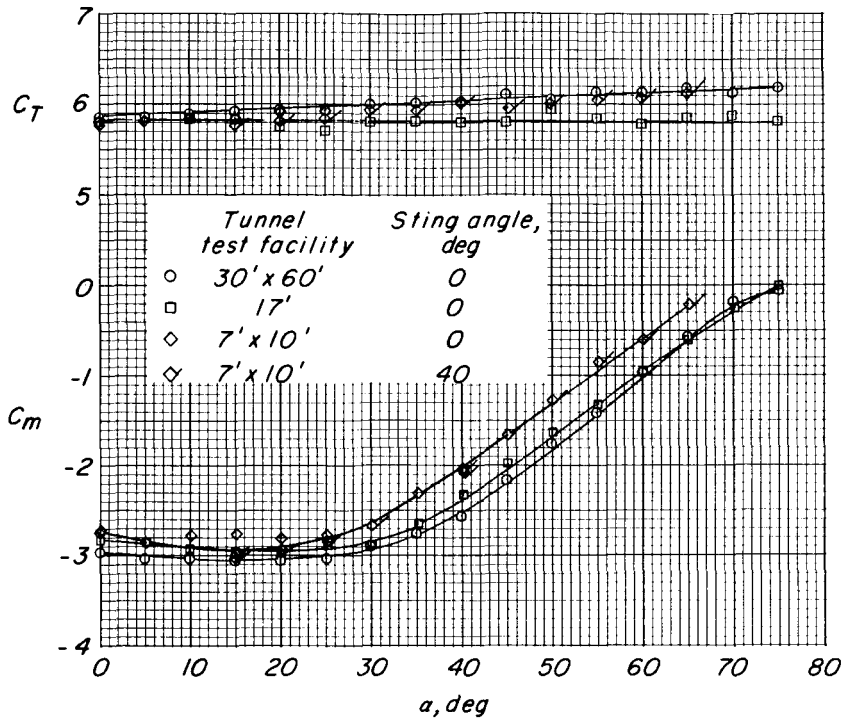

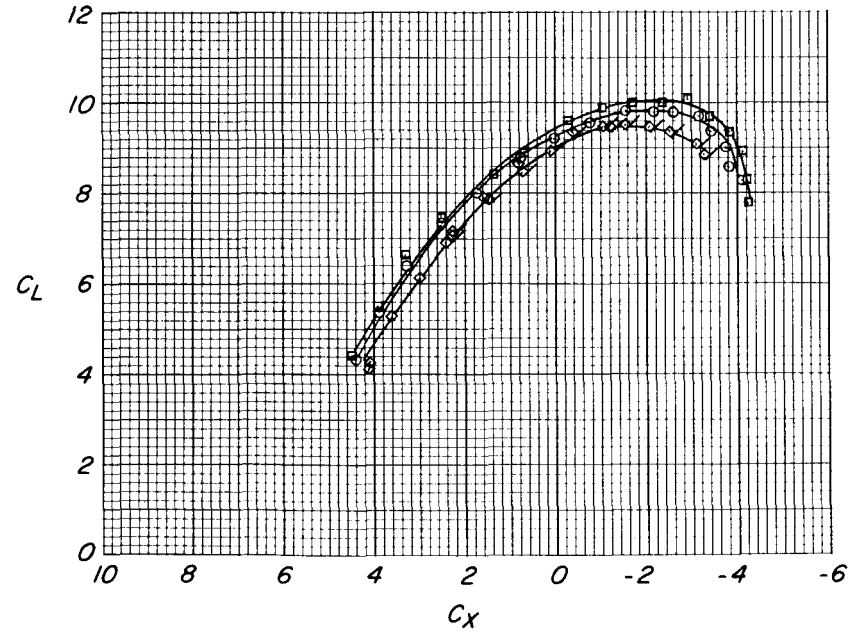

(f) $C_T \approx 6.0$; $C_{T,S} \approx 0.86$.

Figure B2.- Continued.

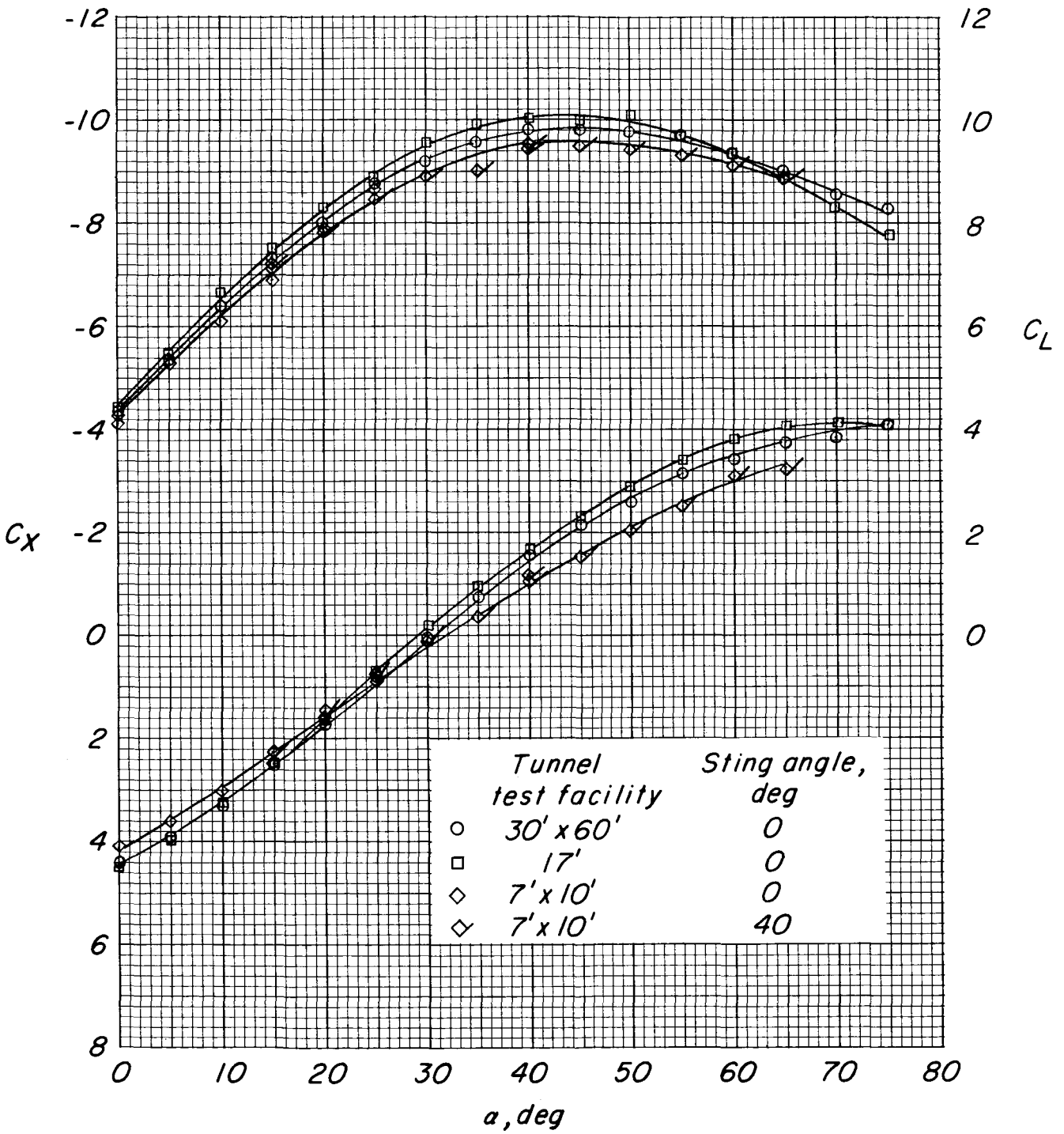

(f) Concluded.

Figure B2.- Continued.

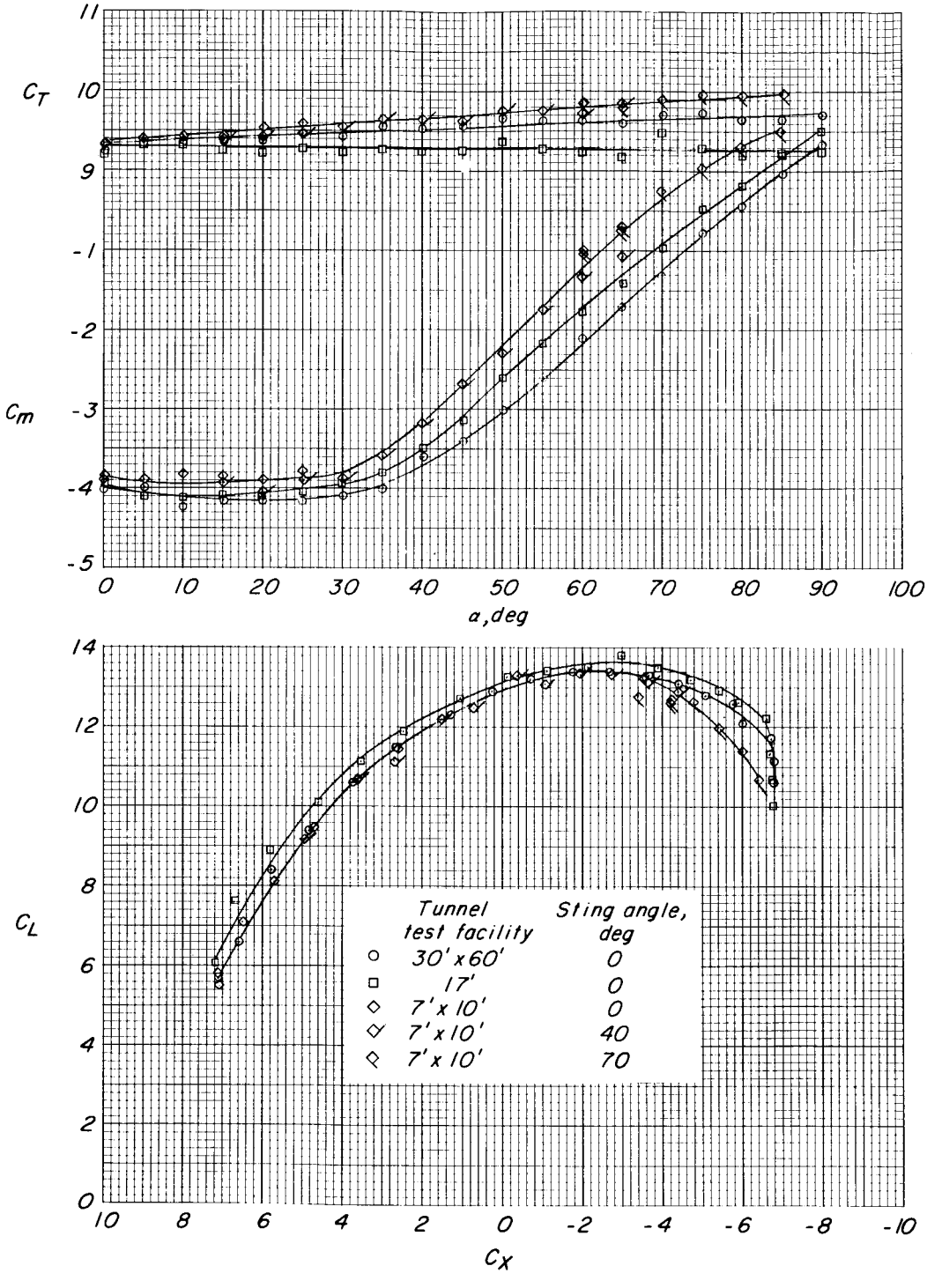

(g) $C_T \approx 9.5$; $C_{T,S} \approx 0.90$.

Figure B2.- Continued.

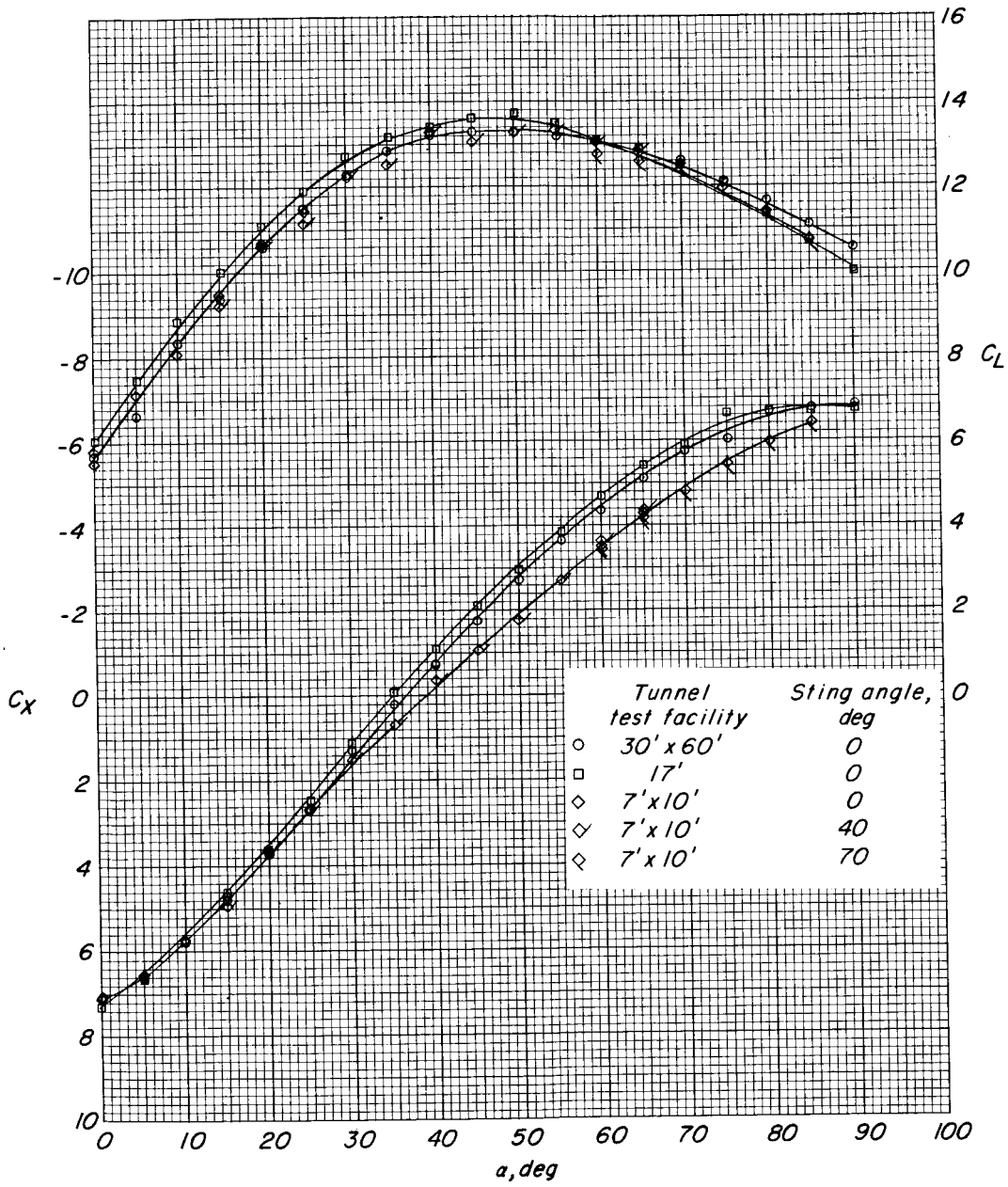

(g) Concluded.

Figure B2.- Continued.

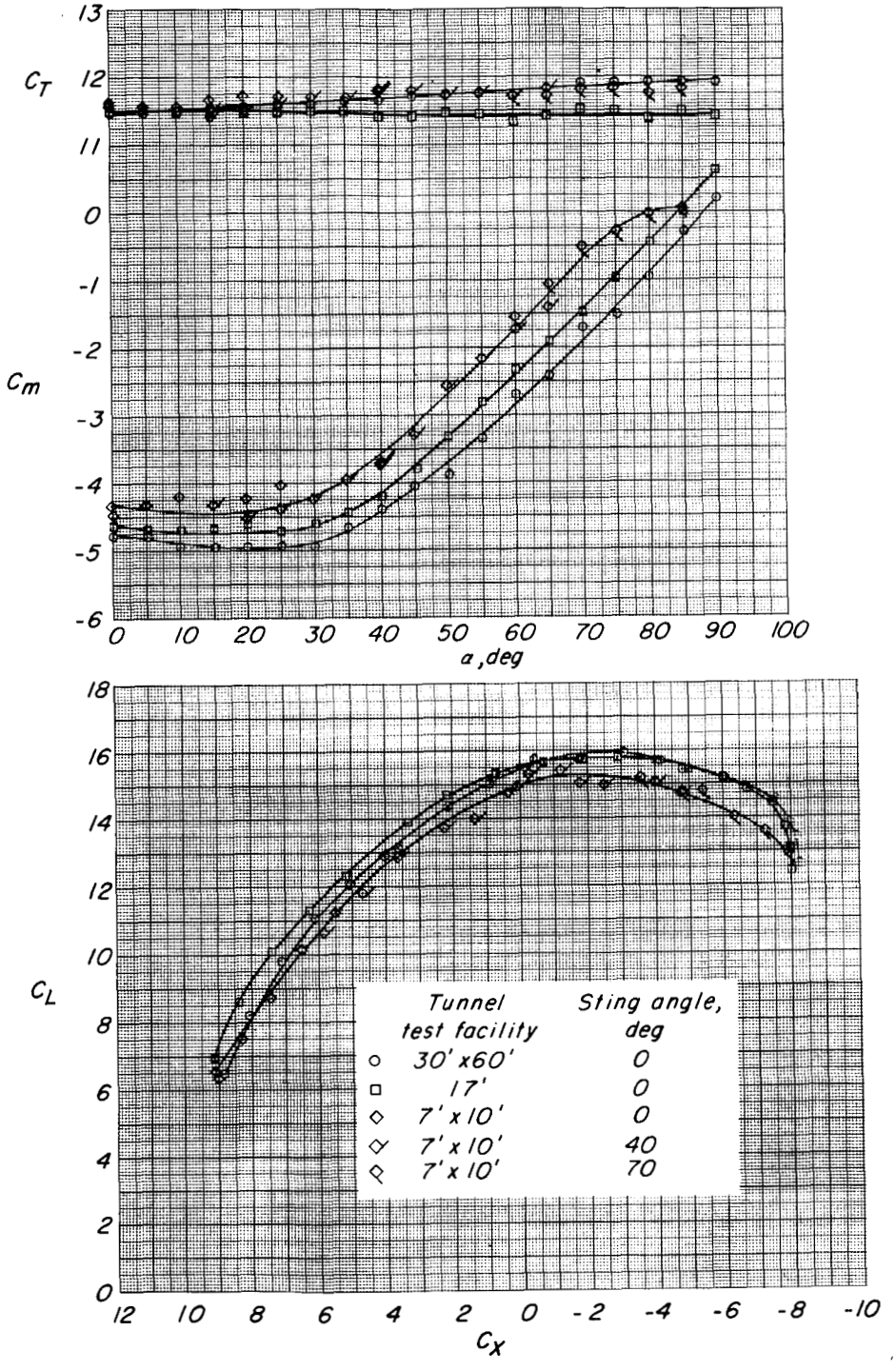

(h) $C_T \approx 11.5$; $C_{T,S} \approx 0.92$.

Figure B2.- Continued.

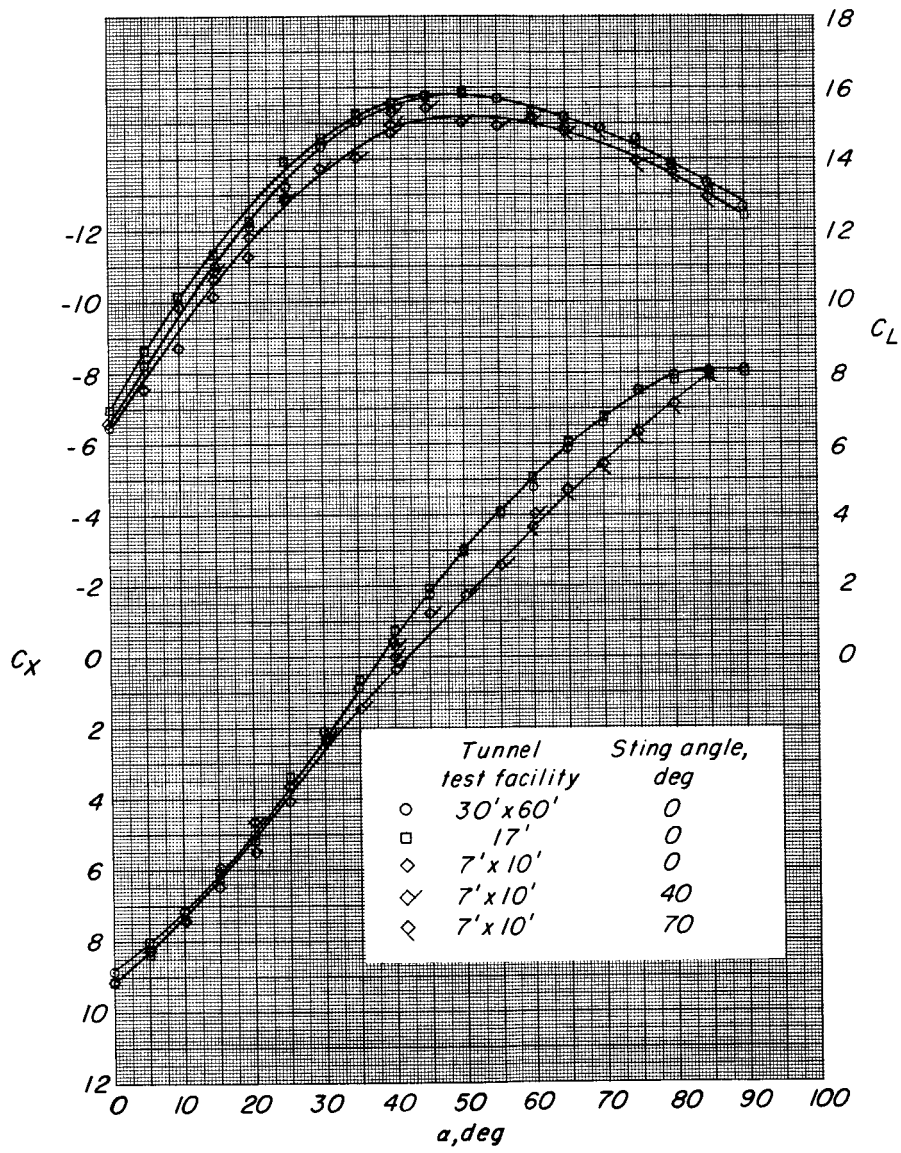

(h) Concluded.

Figure B2.- Continued.

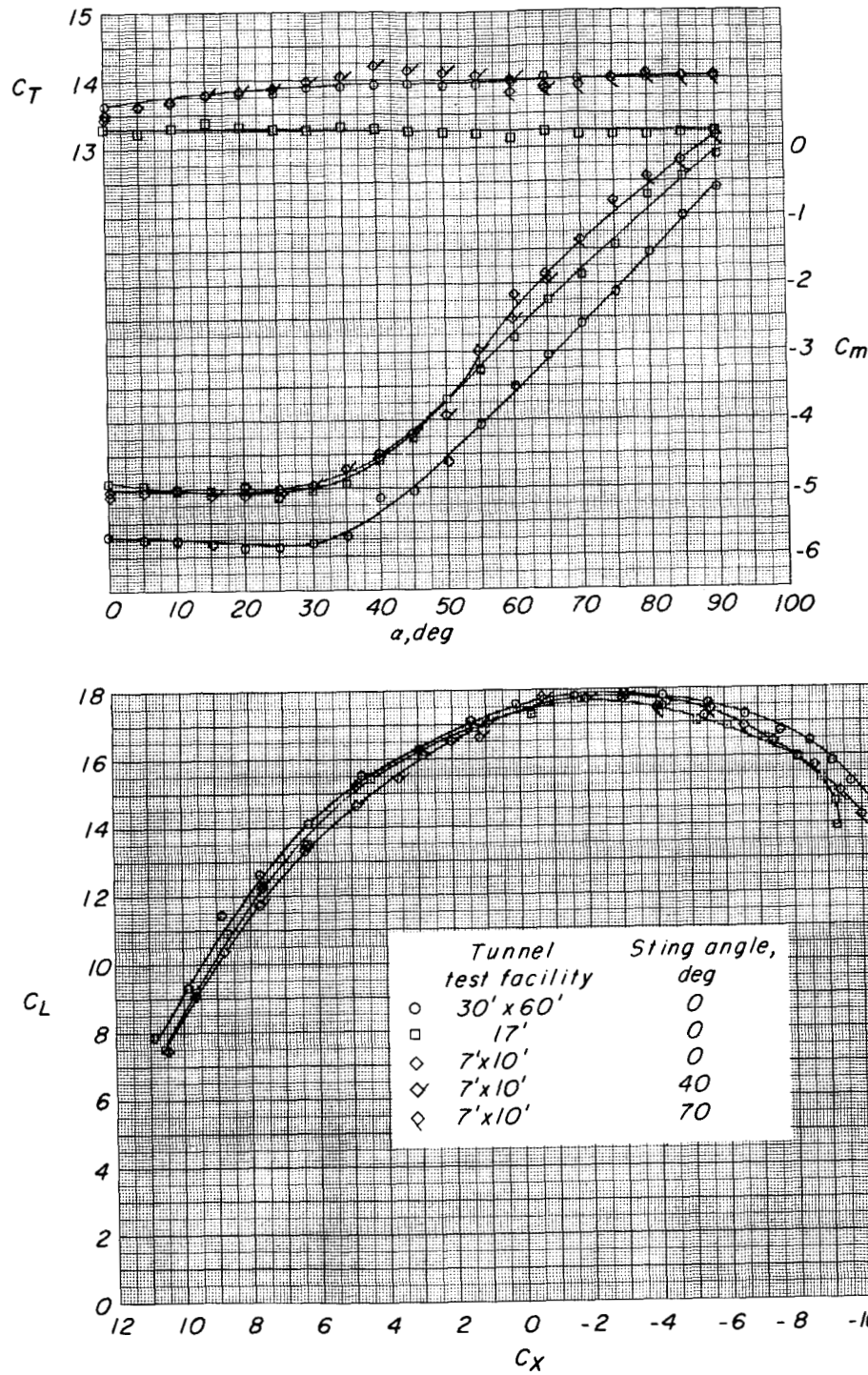

(i) $C_T \approx 13.5$; $C_{T,S} \approx 0.93$.

Figure B2.- Continued.

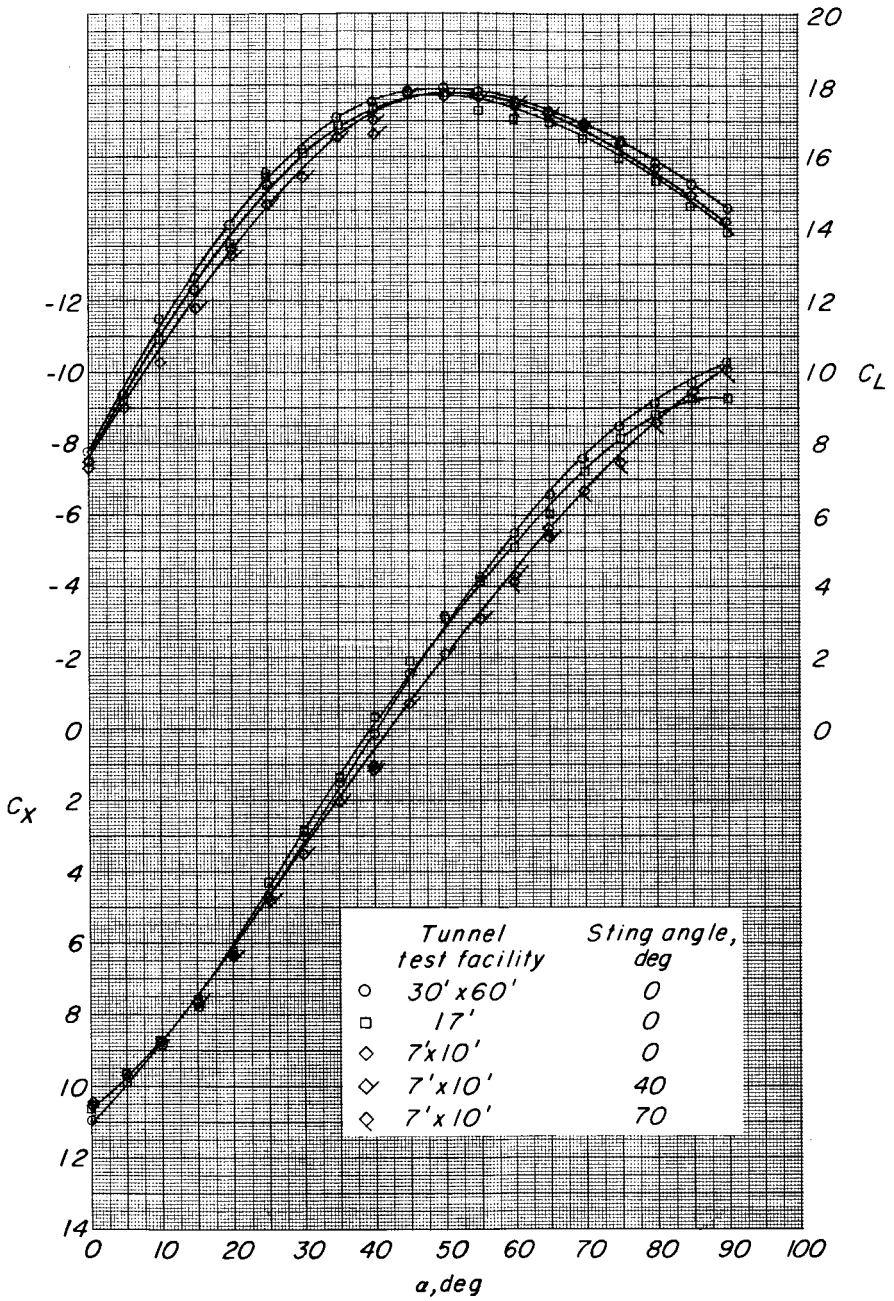

(i) Concluded.

Figure B2.- Continued.

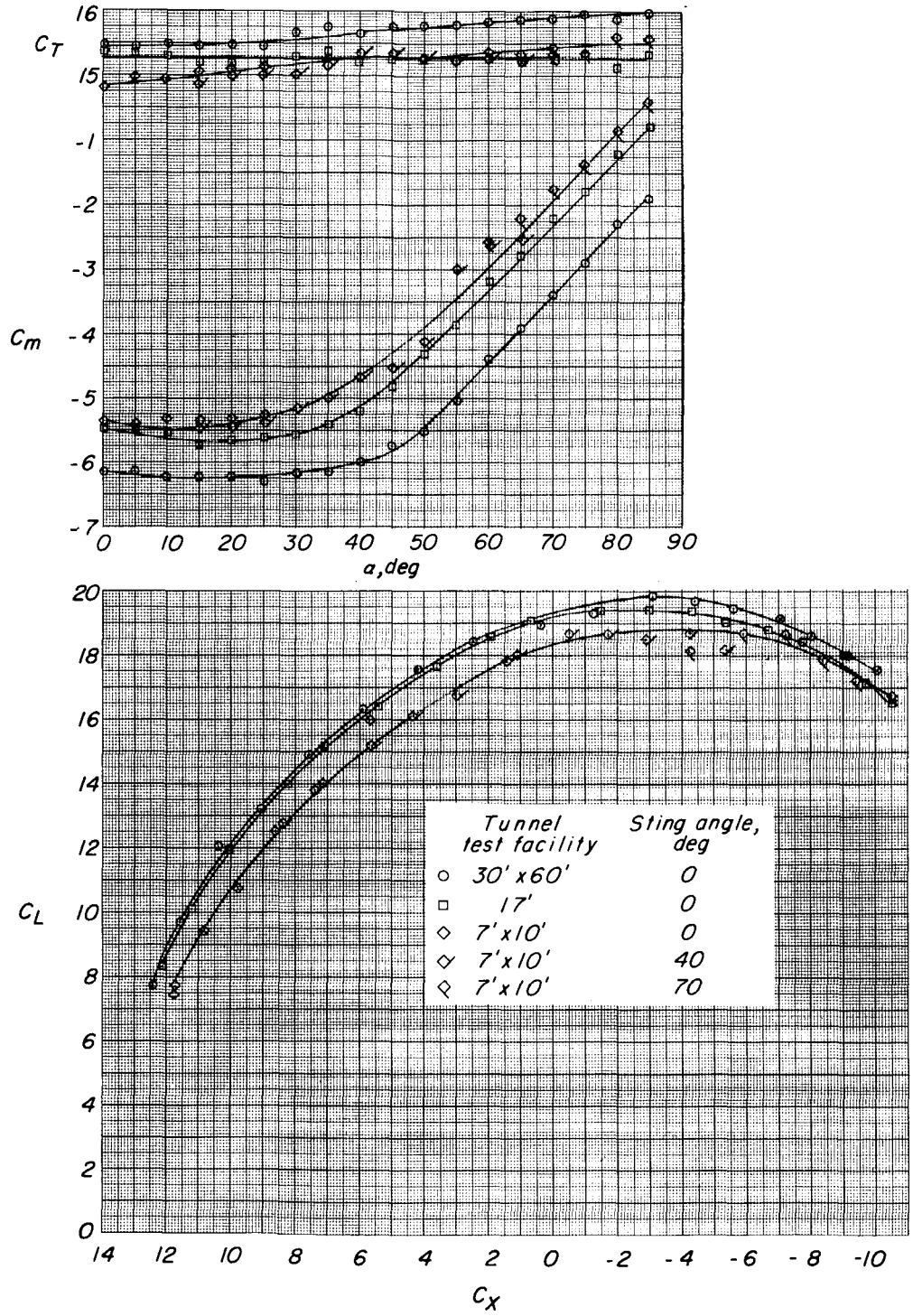

(j) $C_T \approx 15.5$; $C_{T,S} \approx 0.94$.

Figure B2.- Continued.

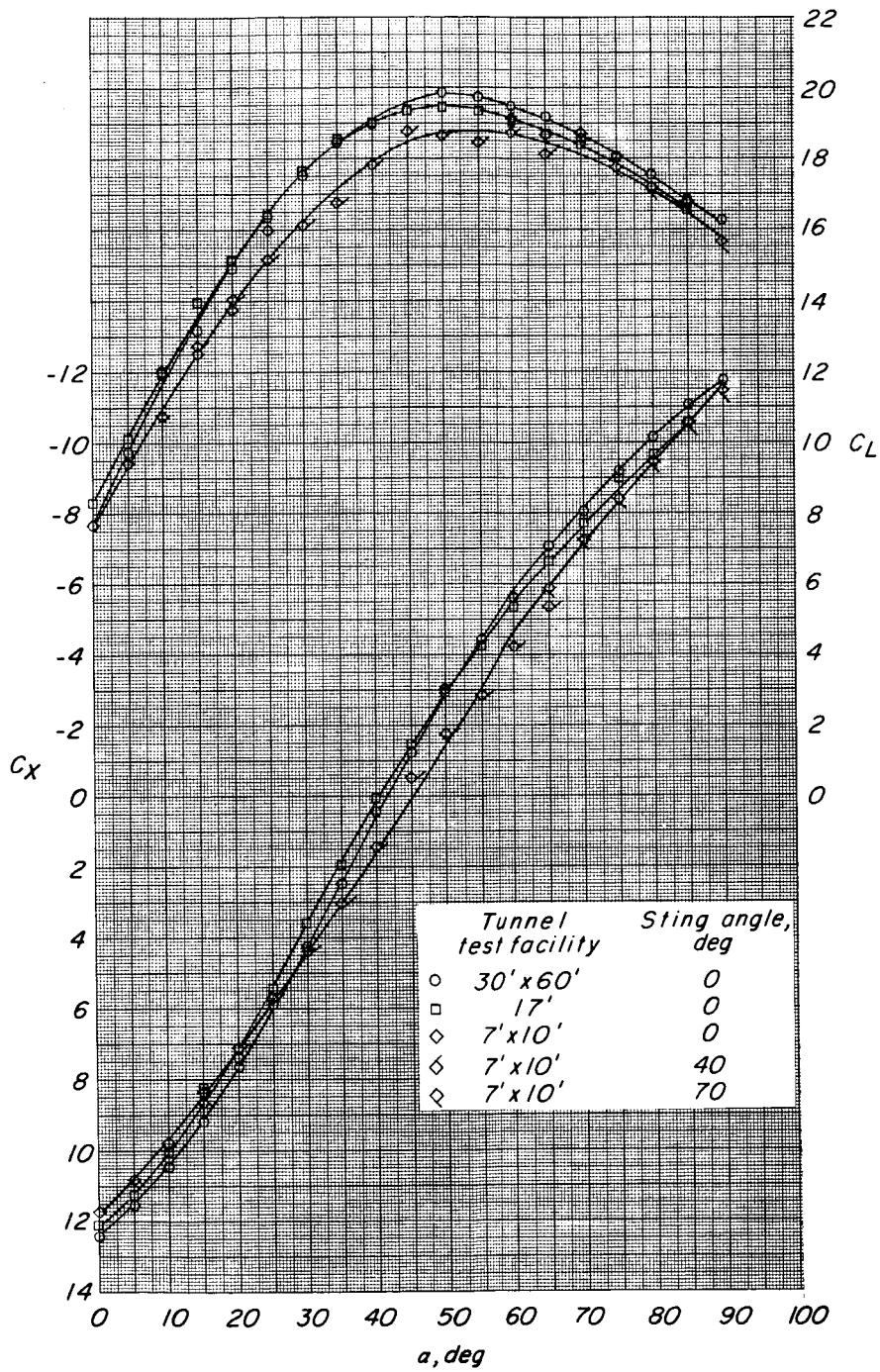

(j) Concluded.

Figure B2.- Concluded.

REFERENCES

1. Heyson, Harry H.: Linearized Theory of Wind-Tunnel Jet-Boundary Corrections and Ground Effect for VTOL-STOL Aircraft. NASA TR R-124, 1962.

2. Theodorsen, Theodore: The Theory of Wind-Tunnel Wall Interference. NACA Rept. 410, 1931.

3. Staff of Powered-Lift Aerodynamic Section, NASA Langley Res. Center: Wall Effects and Scale Effects in V/STOL Model Testing. AIAA Aerodynamic Testing Conf., Mar. 1964, pp. 8-16.

4. Davenport, Edwin E.; and Kuhn, Richard E.: Wind-Tunnel-Wall Effects and Scale Effects on a VTOL Configuration With a Fan Mounted in the Fuselage. NASA TN D-2560, 1965.

5. Lowry, John G.; and Polhamus, Edward C.: A Method for Predicting Lift Increments Due to Flap Deflection at Low Angles of Attack in Incompressible Flow. NACA TN 3911, 1957.

6. Gillis, Clarence L.; Polhamus, Edward C.; and Gray, Joseph L., Jr.: Charts for Determining Jet-Boundary Corrections for Complete Models in 7- by 10-foot Closed Rectangular Wind Tunnels. NACA WR L-123, 1945. (Formerly NACA ARR L5G31.)

7. Heyson, Harry H.: Tables of Interference Factors for Use in Wind-Tunnel and Ground-Effect Calculations for VTOL-STOL Aircraft. Part I - Wind Tunnels Having Width-Height Ratio of 20. NASA TN D-933, 1962.

8. Heyson, Harry H.: Tables of Interference Factors for Use in Wind-Tunnel and Ground-Effect Calculations for VTOL-STOL Aircraft. Part II - Wind Tunnels Having Width-Height Ratio of 1.5. NASA TN D-934, 1962.

9. Heyson, Harry H.: Tables of Interference Factors for Use in Wind-Tunnel and Ground-Effect Calculations for VTOL-STOL Aircraft. Part III - Wind Tunnels Having Width-Height Ratio of 1.0. NASA TN D-935, 1962.

10. Heyson, Harry H.: Tables of Interference Factors for Use in Wind-Tunnel and Ground-Effect Calculations for VTOL-STOL Aircraft. Part IV - Wind Tunnels Having Width-Height Ratio of 0.5. NASA TN D-936, 1962.

11. Kirkpatrick, David L. I.: Wind-Tunnel Corrections for V/STOL Model Testing. M. A. E. Thesis, Univ. of Virginia, 1962.

12. Nielsen, Kaj L.: Methods in Numerical Analysis. The Macmillan Co., c.1956.

NASA-Langley, 1965 L-4141